Title

SOME OP THE PHYSICAL PROPERTIES OF CURIUM AMD PROTACTINIUM MEDALS AND PROTACTINIUM TETRAFLUORIDE

Author

Bansal, Brij M.

Publication Date

1966-04-15

UCRL-16782

University of California
Ernest O. Lawrence
Radiation Laboratory

SOME OF THE PHYSICAL PROPERTIES OF CURIUM AND PROTACTINIUM METALS AND PROTACTINIUM TETRAFLUORIDE

DISCLAIMER

UNIVERSITY OF CALIFORNIA
Lawrence Radiation Laboratory
Berkeley, California

July 19, 1966

ERRATUM

TO: All recipients of UCRL-16782

FROM: Technical Information Division

Subject: UCRL-16782, "Some of the Physical Properties of Curium and Protactinium Metals and Protactinium Tetrafluoride," Brij M. Bansal (Ph. D. Thesis), April 15, 1966.

Please make the following corrections on subject report.

The photograph now shown on page 39 should be moved to page 64, and vice versa (the figure captions are not to be moved).

UCRL-16782

UNIVERSITY OF CALIFORNIA

Lawrence Radiation Laboratory
Berkeley, California

AEC Contract No. W-7405-eng-48

SOME OF THE PHYSICAL PROPERTIES OF CURIUM AND PROTACTINIUM METALS AND PROTACTINIUM TETRAFLUORIDE

Brij M. Bansal

(Ph.D. Thesis)

April 15, 1966

SOME OF THE PHYSICAL PROPERTIES OF CURIUM AND PROTACTINIUM METALS AND PROTACTINIUM TETRAFLUORIDE

Contents

SOME OF THE PHYSICAL PROPERTIES OF CURIUM AND PROTACTINIUM METALS AND PROTACTINIUM TETRAFLUORIDE

Brij M. Bansal

Lawrence Radiation Laboratory
University of California
Berkeley, California

April 15, 1966

ABSTRACT

The construction and operation of a semi-adiabatic microcalorimeter are discussed. The heat of solution of curium metal in 1.0 M HCl at 298.4±0.2°K has been measured and found to be -139.9±1.0 kcal/mole. This value is combined with available thermodynamic data to calculate the following standard heats of formation at 298°K: $Cm^{+3}_{(aq)}$, -140.6±1.3; $CmCl_{3(c)}$, -226.1±1.2, both in kcal/mole.

The construction and operation of a low temperature magnetic susceptibility apparatus are discussed in detail. The magnetic susceptibility of curium metal has been investigated from room temperature to about liquid helium temperature (6-8°K). The metal followed the Curie-Weiss law from room temperature to 145°K. Between 145 and 77°K the metal becomes ferromagnetic with a Curie temperature T_c = 131±10°K. At liquid hydrogen and helium temperatures the metal again seems to show paramagnetic behavior. No evidence of antiferromagnetic behavior, however, was observed. The effective magnetic moment for the metal has been found to be 8.03±0.1 Bohr magnetons, indicating the presence of a $5f^7$ configuration in the metal.

The magnetic susceptibility of protactinium metal has been measured in the temperature range 20-298°K. The molar susceptibility is found to be 268±14 × 10^{-6} c.g.s. units at room temperature, and to be virtually independent of temperature within the experimental accuracy of ±5% over the temperature region investigated.

The molar magnetic susceptibility of PaF_4 has been calculated from the available Landé g value for octahedrally coordinated Pa(IV) ($PaCl_4$-Cs_2ZrCl_6 crystal) and the J quantum number of Pa(IV) ground state; the value so calculated is 4735×10^{-6} c.g.s. units.

I. INTRODUCTION

The discovery of the transuranium elements has extended the periodic table by more than 10% and provided chemists with the opportunity to investigate the properties of the terminal members of a second series of "f" or inner transition elements analogous to the lanthanides.

As in the case of the latter series, it would seem likely that many of the more interesting problems for investigation by inorganic chemists will be concerned with properties of the solid state, especially the physical properties of the metals. The recent increase in the availability of the heavy man-made actinides[1] has made it possible to study the bulk chemical and physical properties of these elements and their compounds.

Extensive studies are being made to elucidate the nature of the metallic bond in the heavy element region. In comparison with the more common metals, the heavy metals—uranium, neptunium, and plutonium—all exhibit anomalous physical properties. For example, they have quite complex and unusual room temperature crystal structures instead of the simple ones (hexagonal close-packed, face-centered cubic, or body-centered cubic) found in most metals. Americium metal, prepared and investigated by McWhan,[2,3] appears to be the first transuranium element to exhibit a relatively simple structure.

Until very recently, almost no work concerning magnetic susceptibilities of curium metal was reported. The magnetic properties of curium metal and some of its compounds were investigated by Marei[4] in the temperature range 77 to 551°K. Marei[4] reported that at 77°K the reciprocal susceptibility ($1/\chi$) versus temperature (T) curve shows a marked displacement in the direction of the temperature axis. However, in the temperature range studied he found no conclusive evidence for ferromagnetism, in contrast to the well-known behavior of gadolinium, which becomes ferromagnetic near room temperature.

In a review of their studies of the chemistry of protactinium, published in 1954, Sellers, Fried, Elson, and Zachariasen[5] described the

preparation of protactinium metal by reduction of the tetrafluoride with barium at 1400°C. The metal so obtained was reported by Zachariasen[6] to be body-centered tetragonal, with two atoms per unit cell. The cell parameters were given as $a_1 = 3.925 \pm 0.005$ Å, $a_3 = 3.238 \pm 0.007$ Å, corresponding to a calculated density of 15.37 g/cm^3.

Until very recently no magnetic susceptibility studies have been reported on protactinium metal and its compounds. Cunningham[7] has recently reported some properties of protactinium metal including partly the work which will be described here. He reported the molar susceptibility to be $250 \pm 50 \times 10^{-6}$ c.g.s. units at room temperature based on the investigation of a single susceptibility measurement.

Very recently Fowler et al.,[8] from Los Alamos Scientific Laboratory, have reported that they have observed superconductivity in protactinium metal below 1.4°K. With this in view we thought that we might be able to see the increase in diamagnetic susceptibility of protactinium metal near liquid helium temperature.

Thermodynamic data are an essential feature of the description of the chemistry of any element. Suffice to say that one of the most compact ways of storing chemical information is in the form of tables of thermodynamic properties of substances. Thermodynamic data may be used not only to reconstruct much of the information from which the data came, but also to make predictions about unknown reactions and to get estimates or interpolation from plots of available data on the other members of the series.

Although numerous papers dealing with various aspects of the chemistry of curium have been published, none have reported experimental values for the heat or free energy of formation of any curium species. Many of the available thermodynamic data on the transuranium elements deal with the earlier members of this series. There are practically no thermochemical data available on curium and transcurium elements. Very recently Wallmann and his co-workers[9] have reported the heat of solution of curium metal and the heats of formation of $Cm^{+3}_{(aq)}$ and $CmCl_{3(c)}$, including in part the work which will be described here.

In the following work the experimental procedure followed in the determination of the heat of solution of curium metal is presented. The results are combined with available thermodynamic data to calculate the heats of formation of $CmCl_{3(c)}$ and $Cm^{+3}_{(aq)}$. The magnetic susceptibility of the curium metal has been measured from room temperature to liquid helium temperature, and its ferromagnetic transition has been investigated. The magnetic susceptibility studies on the protactinium metal and protactinium tetrafluoride have been made from room temperature to liquid hydrogen temperature. The description of a new apparatus which made it possible to make susceptibility measurements at liquid hydrogen and liquid helium temperatures is given. The results found are discussed in the light of the properties of the other actinides and rare earth elements.

II. MICROCALORIMETER

A. Construction

The microcalorimeter used to measure the heat of solution of curium metal in this work is of the semiadiabatic type, kinetically vacuum-jacketed, water-bath thermostated at 25°C, and having a heat capacity of about 9 calories per degree and a temperature sensitivity of about 1×10^{-5} degree. A general view of the apparatus is shown in Fig. 1.[10]

The calorimeter unit is shown in Fig. 2.[11] The tantalum reaction chamber (M) is suspended from the submarine support (H) by means of a tubular lucite hanger (J) vacuum sealed at both ends with neoprene O-rings. The submarine support contains five vertical holes through which a platinum resistance thermometer and calibrating heater connecting leads (K,L) and the stirring shaft (I) pass. The stirring shaft is a quartz rod about 0.042 in. in diameter and is supported at the upper end by means of a bakelite collet chuck clamped in the stirring head (D) which includes a spring and a stop screw to permit depression of the shaft a fixed distance for breaking the sample bulb which is attached to the lower end of the shaft. The stirrer is rotated at about 300 rpm by a synchronous inductor motor connected through a flexible shaft to the stirring head. The heater leads are attached to a four-prong cord connector (B) mounted in a plastic block (C). The thermometer leads are attached to massive copper binding posts (A). The stainless steel submarine chamber (O) is screwed onto the frame against a greased neoprene gasket for a vacuum seal. A thermal radiation shield (N) consisting of two concentric tantalum cylinders is placed midway between the reaction chamber and the submarine to diminish heat transfer by radiation. To reduce heat transfer by air conduction and convection, the space between the reaction chamber and the submarine is evacuated through the 1/2 in. tube (G) by means of a mercury diffusion pump and a U-shaped liquid nitrogen trap backed up by a Welch Duo-seal forepump. The value of the thermal leakage modulus, k, is about 0.005 per minute, where k is defined by the expression

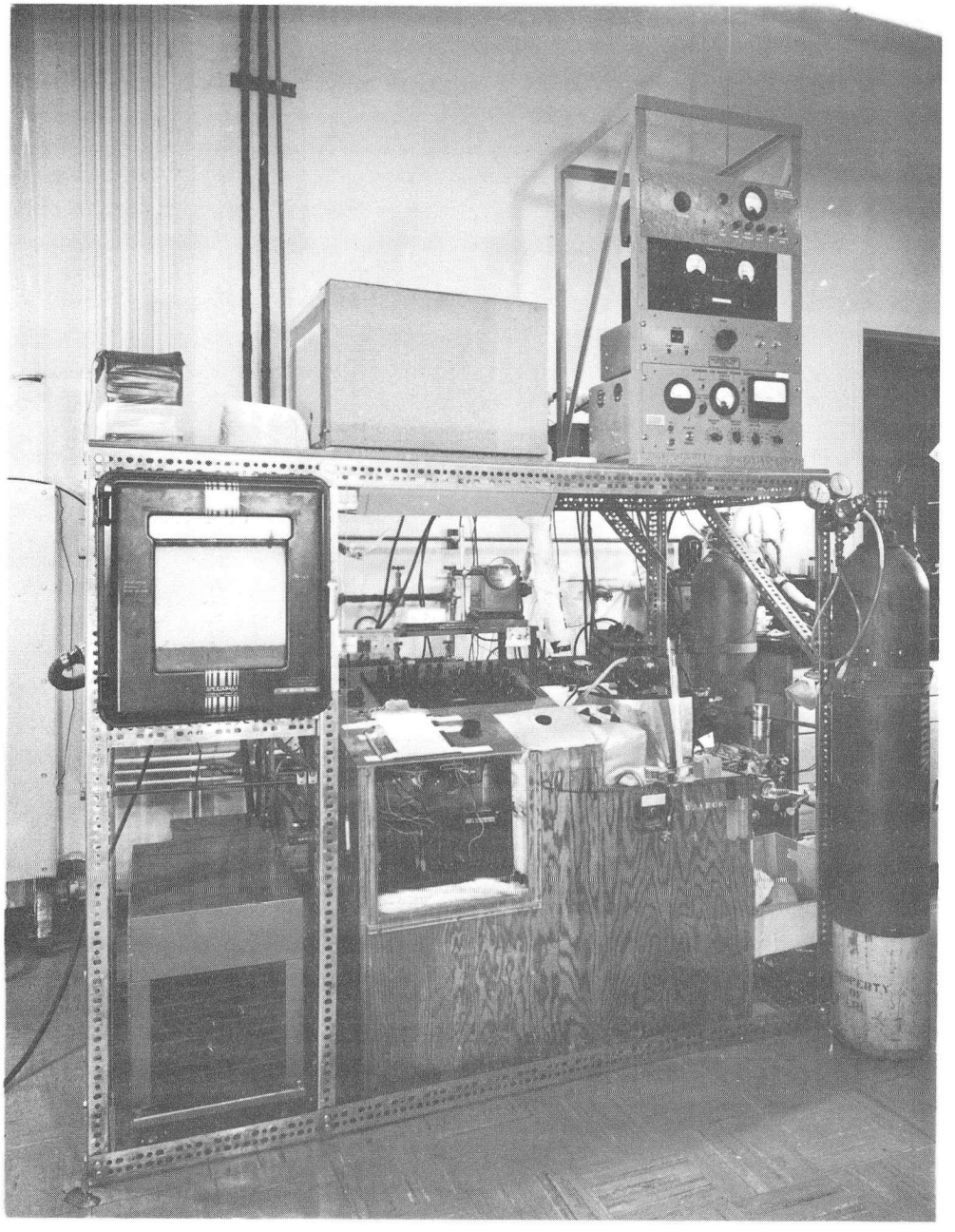

ZN-4596

Figure 1. General view of microcalorimeter.

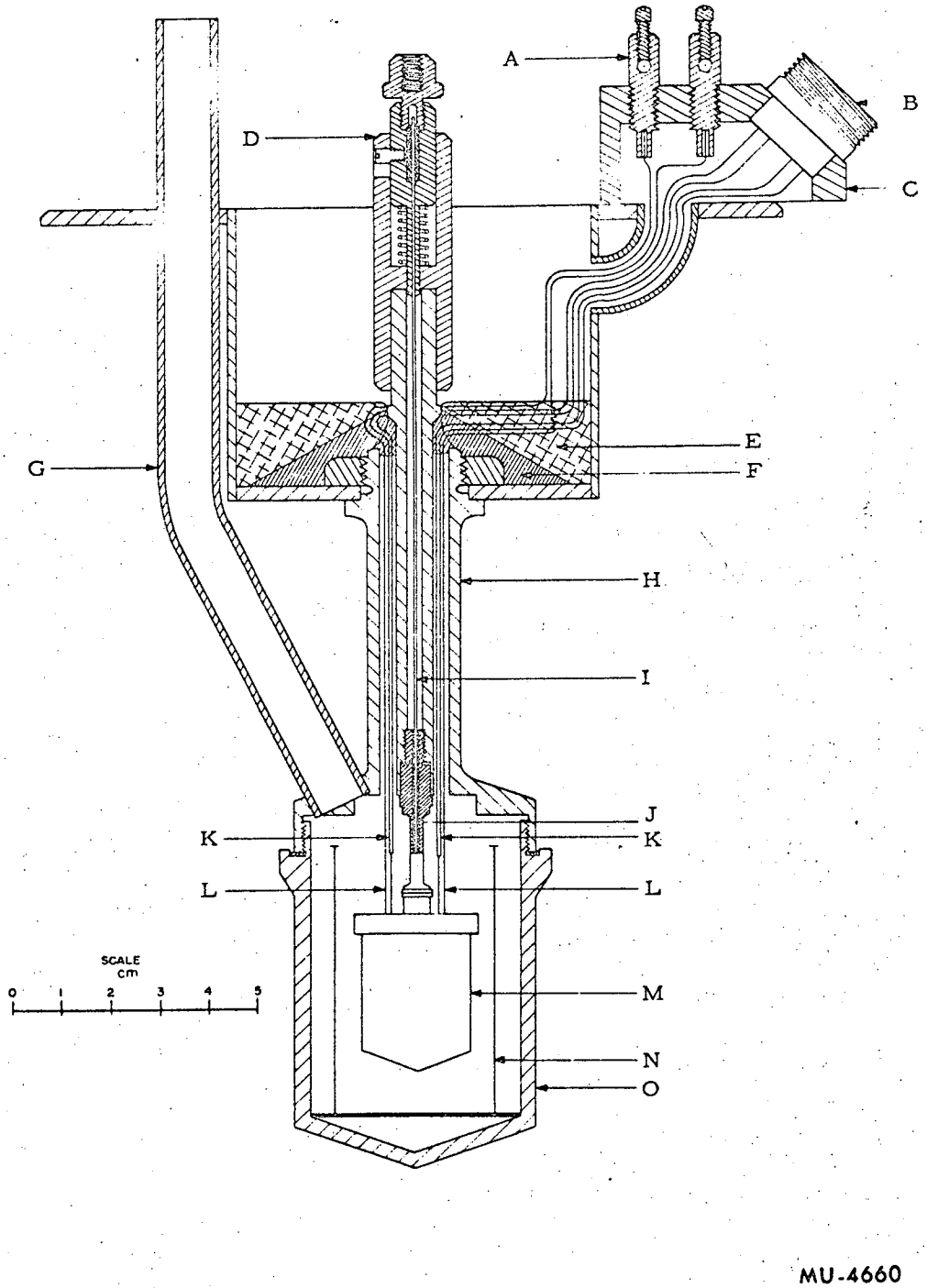

Figure 2. Microcalorimeter cross-section.

Legend for Figure 2

A. Copper binding posts
B. Four-pronged plug
C. Plastic block
D. Spring loaded screw-in-slot arrangement
E. Paraffin used to partially fill the supporting frame above the Apiezon wax for protecting the leads
F. Apiezon "W" wax used to seal the upper ends of the holes through which the electrical leads pass
G. 1/2 in. tube
H. Submarine support
I. Stirring shaft
J. Hollow lucite hanger
K. Heater leads
L. Thermometer leads
M. Tantalum reaction chamber
N. Radiation shield
O. Stainless steel submarine chamber

$$k = -\frac{1}{\theta}\frac{d\theta}{dt},$$

where θ is the difference between the temperature of the calorimeter and the temperature at which it is in equilibrium with the thermostat, and t is the time. At a pressure of 10^{-5} mm of mercury or less, generally attained during operation, the principal heat leaks are by conduction along the hangar, stirring shaft, and electrical leads.

Details of the reaction chamber are shown in Fig. 3.[11] The reaction chamber (H) which has a capacity of about 9 ml is made of tantalum. The cap (F), the four thermometer and heater conduits (G), and the spool and sleeve (I, J) are also of tantalum with gold-soldered joints where the conduits join the spool and cap. The four-bladed platinum stirring propeller (K) is attached to the stirring shaft (B) with Apiezon "W" wax, which is also used to attach the sample bulb (L). The sample is introduced into the solution by depressing the shaft to break the bottom of the bulb against the anvil (M).

Construction of a satisfactory resistance thermometer and calibrating heater of the small dimensions imposed by the scale of the work is a very delicate operation. Its construction and packaging has been described in detail by Burnett elsewhere[10]; however, for completeness, it will be described here very briefly. The thermometer is constructed of 1 mil platinum wire and the heater is either No. 44 Manganin or No. 40 Karma wire. These are wound non-inductively on a mica strip 1.45 cm × 4.50 cm × 1-2 mil thick which has been notched along the edges to hold the wires in place. The platinum wire is wound on one end and the heater on the other. This strip is then sandwiched between two more mica strips, and the combination wrapped around the tantalum spool and held in place with three lengths of 5 mil tantalum wire. The assembly must now be annealed at about 600°C under high vacuum for about 18 hr in order to relieve strains in the wires.

The thermometer circuit is shown in Fig. 4; it is a simple, modified Wheatstone bridge. The unit is mounted in a box constructed of 1/8 in.

mild steel to provide electromagnetic and electrostatic shielding. The resistors R_1, R_2, R_3, and R_4 are located in an oil-filled iron pipe extending from the bottom of this box into the thermostat. D is a calibrated Leeds and Northup 4-dial decade resistance box. A 6 V storage battery cut and wired to give 2 V provides a source of very constant current to the bridge which draws about 36 mA. The low pass filter is designed to attenuate ac frequencies much greater than 1 c.p.s. The potential dividers, R_{10}, R_{11}, may be used to reduce the sensitivity by about a factor of 10, and under these conditions the entire time temperature curve can be recorded graphically. Thus accurate corrections for thermal leakage can be computed from the curve. This procedure will be described in somewhat more detail later.

The dc breaker amplifier is a Beckman Model 14 with an input impedande of 50 Ω. The recorder is a Leeds and Northup Speedomax Type G dual range, dual speed, self-standardizing model. In order to avoid the erratic behavior of the system due to temperature sensitivity of the decade box, the breaker amplifier, and its input cable, the box and the cable are wrapped in pads of glass wool insulating material and the breaker amplifier itself is enclosed in a styrofoam box and is cooled by a stream of air.

The heater and timer circuit is shown in Fig. 5.[10] The timer circuit consists of a frequency-regulated power supply and its input is a standard 60 c.p.s. frequency which is divided down to 1 c.p.s. Current is supplied to the heater circuit by a 115 V regulated power supply. The timer circuit is coupled to the heater circuit output through on and off switches that start and stop the heater power on the full second. A bell sounds when the heating starts and when it stops; a register records the number of seconds. The accuracy of the timing and stability of the output are good to a few hundredths of a percent. The selection of the fraction of maximum power to be applied is made with the help of a multipole switch. These fractions are 0.1, 0.2, 0.3, 0.4, 0.5, 0.75, and 1.0. The current-measuring resistor, which is in series with the calorimeter heater, is of

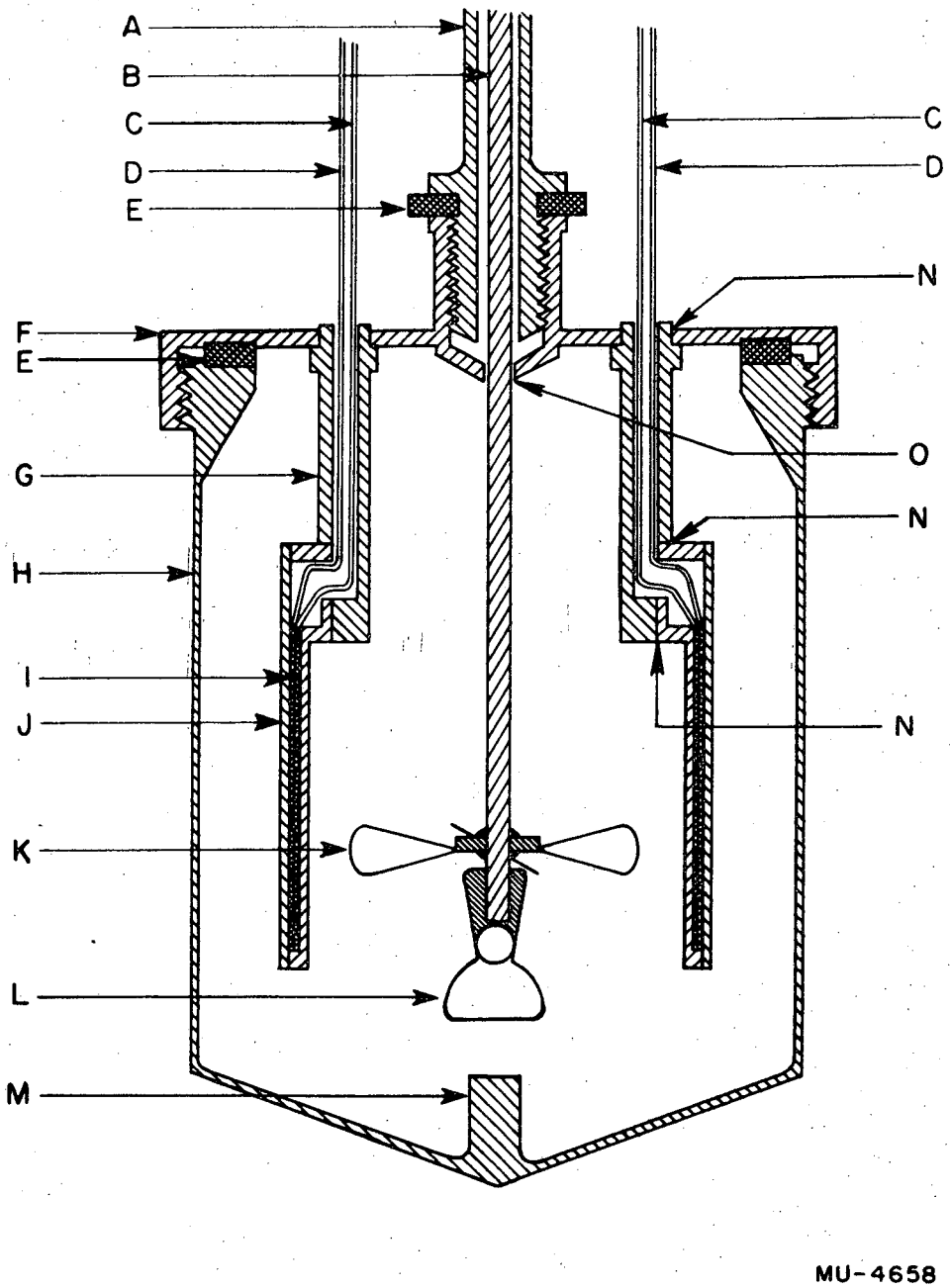

Figure 3. Cross section of microcalorimeter reaction chamber.

Legend for Figure 3

A. Fine lucite hanger
B. Quartz stirring shaft
C. Heater leads
D. Thermometer leads
E. O-ring
F. Ta cap from which spool is suspended by four posts
G. Post
H. Reaction chamber
I. Mica sandwich with thermometer and heater
J. Ta sleeve
K. Propeller for stirring solution
L. Sample bulb
M. Anvil for breaking bulb when shaft is depressed
N. Gold-soldered joints
O. Hole in cap of spool

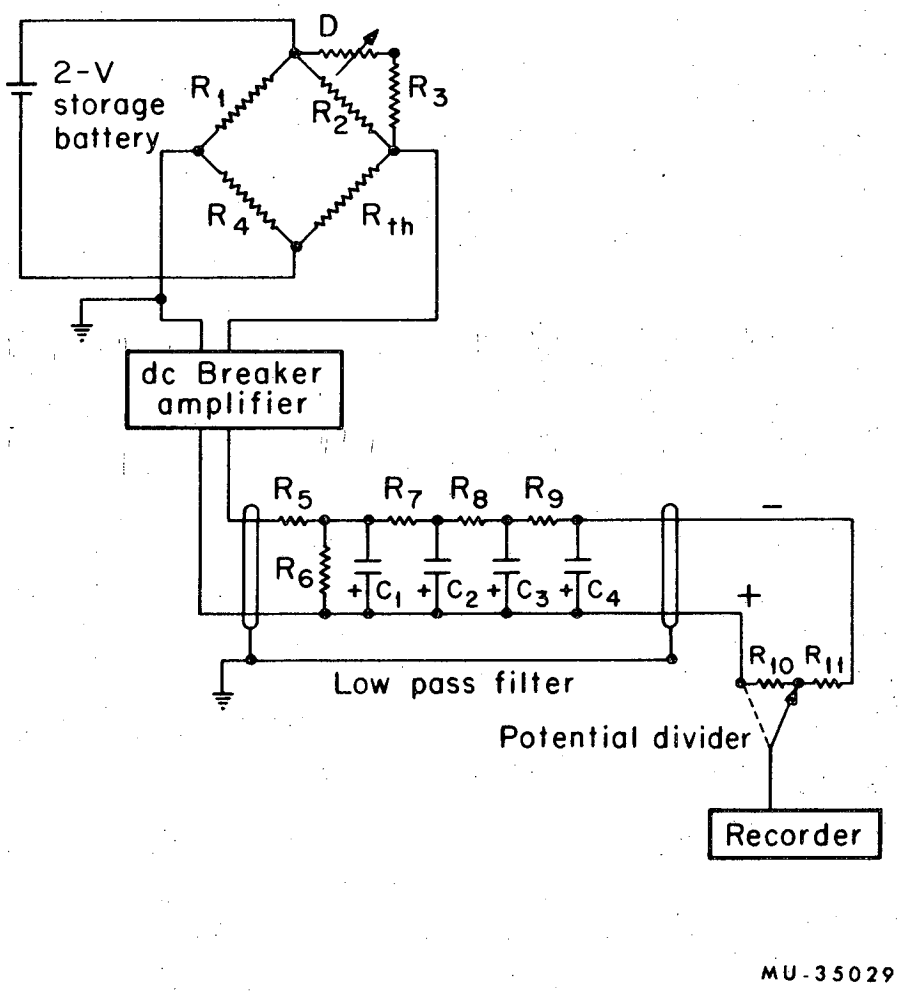

Figure 4. Thermometer circuit.

Legend for Figure 4

D. Decade resistance box ranging from 0-9999 Ω

R_1. 60 Ω
R_2. 500 Ω
R_3. 25 KΩ
R_4. 3 Ω
R_{th}. Thermometer
R_5. 1 KΩ
R_6. 200 Ω
R_7. 1.5 KΩ
R_8. 5 KΩ
R_9. 25 KΩ
R_{10}. 49 KΩ
R_{11}. 4.9 KΩ
C_1. 4000 μF
C_2. 1000 μF
C_3. 250 μF
C_4. 50 μF

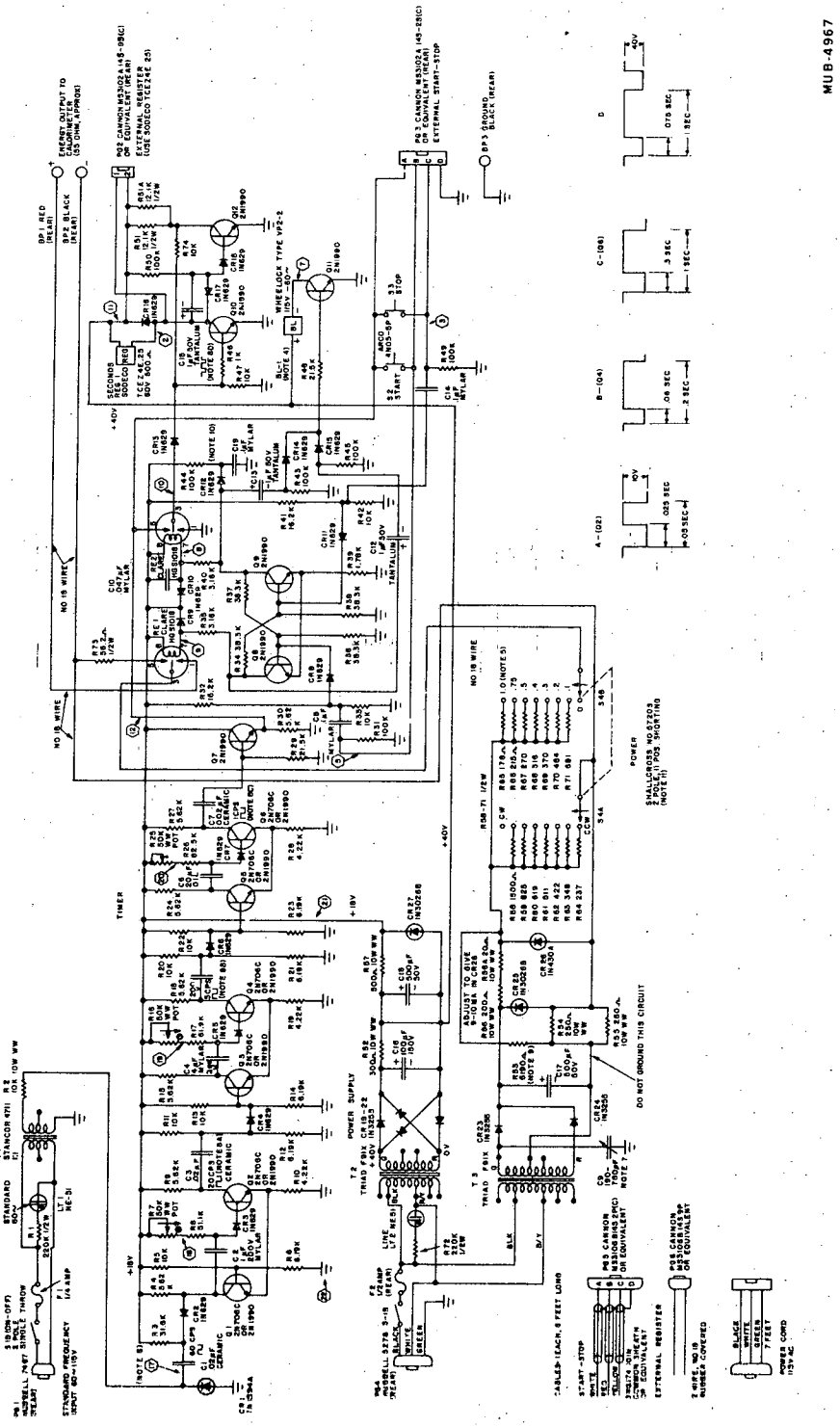

Figure 5. Heater and timer circuit.

Legend for Figure 5

1. All resistors are coated metal film types unless otherwise specified. When the wattage is not indicated, 1/8, 1/4, or 1/2 watt may be used, but 1/2 watt is preferred when space permits.
2. Overall operation of the divider network can be checked by putting on "0" and pressing "start" button. It is necessary to hold the start button down for a time not exceeding 1 sec. The register then records the elapsed time in seconds between sounds of the bell, which can be compared with any standard clock. The "stop" button turns off the counter at any integral second.
3. The timing error due to delay in operation of RE-1 can be determined by placing the "power" switch on 0.1 and using the "energy output" as a gate to control a timer operating at a frequency of 10 kc or higher. The net error should not be more than a few milliseconds, and is reproducible.
4. This bell is polarized and the polarity must be determined so that the gong sounds when current is applied.
5. These numbers indicate the fraction of maximum power being applied. The "power" switch, S-4, should be labeled with these numbers.
6. Numbers in hexagons refer to pin numbers on Plug-In board.
7. Adjust C-9 to minimize hum between floating "Energy Output" negative lead and ground.
8. R-53 is adjusted so that variation in line voltage has minimum effect on "Energy Output" voltage.
9. C-19, CR-12, and R-44 serve only to insure that when the one switch is turned on, the flip-flop Q8-Q9 always comes on in the "stop" position.
10. After turning on "power" switch, the 8.4 V regulated supply for the "Energy Output" is within 0.1% of the final value in 15 sec, within 0.05% in 90 sec, and within 0.01% in 2 hr.
11. Q-1, Q-2, Q-3, Q-4, Q-5, and Q-6 (2N706C) may be replaced by 2N1990's.

the Manganin wire-wound type immersed in an oil bath. It has proved to be stable to a few thousandths of an ohm over a period of a year's time. A Rubicon Type B High Precision Potentiometer is used with a box lamp and scale galvanometer to measure the voltage drops across the current-measuring resistor and calorimeter heater. Usually, calibration heat inputs are of the order of 0.2 to 0.4 cal and agree to a few hundredths of a percent.

The sample bulbs of about 50 μl capacity are constructed of Pyrex and have very thin flat bottoms. They weigh from 40 to 50 mg. Previously the bulbs were sealed at the neck with an Apiezon W-coated Pyrex bead, but the gas in the bulb that escapes upon sealing contributed a large uncertainty to the weight of the sample. Now a fine Pyrex capillary tube is inserted into the bulb alongside the bead (see Fig. 6). A ball of degassed Apiezon W-wax is placed in the neck on the top of the bead and the bulb is sealed as before with a hot wire, except that the capillary permits reentry of gas to the bulb as the bulb cools. A piece of 3 mil tungsten wire with a small bead of degassed wax is now inserted into the outer end of the capillary and quickly sealed with a fine hot wire. The sealing should be done at a temperature high enough to melt the wax but low enough to avoid decomposition. The resultant weight loss and uncertainty during sealing, using degassed Apiezon wax, is 0.47 ± 0.17 μg. Weighings are done on a Rodder Model E quartz fiber torsion balance sensitive to ≈0.05 μg.

B. Operation

Generally, a sample is loaded one day before the run is made. The thermostat temperature is lowered a few tenths of a degree and the submarine chamber is set in place and connected to the vacuum line. At this point, the temperature of the calorimeter rapidly approaches that of the bath because of the poor vacuum in the chamber. After pumping overnight, however, the vacuum is good and when the thermostat temperature is returned to 25°C the calorimeter temperature lags behind. Several heat inputs are now made which raise the calorimeter temperature nearer the

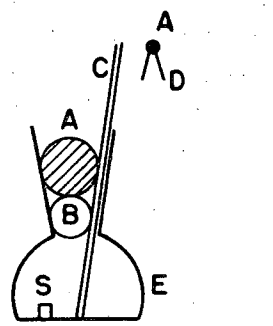

Assembled bulb

A – Degassed Apiezon W-wax
B – Glass bead
C – Pyrex capillary
S – Sample
D – 3 mil tungsten wire
E – Sample bulb

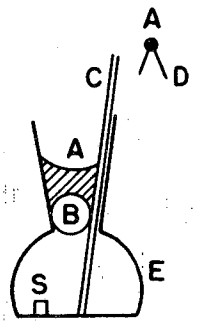

First sealing

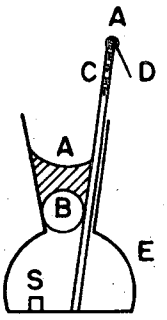

Final sealing

MUB-10581

Figure 6. Sealing sequence.

steady-state point. This point is a few tenths of a degree above the thermostat temperature due to stirring, thermometer current, and friction of the stirring shaft against the hanger.

As was previously indicated, this calorimeter is only semi-adiabatic; there is a continual drift of the calorimeter temperature towards the steady-state temperature—the drift rate being determined by the thermal leakage modulus and the temperature difference. This drift is traced on the recorder. The reaction of interest is initiated at the proper time, such that the heat evolved raises the temperature of the calorimeter from a point below the steady-state temperature to a point above. The more nearly equal the corresponding temperature differences are, the smaller the thermal leakage correction is. Now several more calibrating heat inputs are made to complete the run. A sensitivity check is made between each heat input to determine the number of recorder chart divisions per ohm change on the decade.

The performance of the calorimeter and the technique of the operation are checked by running very pure crystalline magnesium metal in 1.00 M HCl solutions and comparing the calculated value of the heat of solution of Mg metal with that obtained by Shomate and Huffman[12] on a macroscale. The magnesium metal samples are generally freshly cut and mechanically cleaned of all oxide. They are weighed on the torsion balance mentioned previously, and the weight corrected to vacuum. The observed heat of solution is corrected for the following effects:

a) The heat of breakage of the sample bulb, determined by breaking several bulbs containing a small amount of water. The applied correction is $(6\pm3) \times 10^{-6}$ calories per bulb.

b) The heat of vaporization of the water required to saturate the hydrogen evolved.

c) The heat of vaporization of the water required to saturate the dry nitrogen in the sample bulb.

Typically, corrected values for the heat of solution of Mg metal in 1.00 M HCl are found to lie in the range—111.3±0.2 kcal/mole.[10]

Shomate and Huffman's value is—111.322±0.041. The results indicate that there are no significant systematic errors in the microcalorimetric measurements and that the precision of the operation is about 0.2%.

C. Calculation

To exemplify the calculations involved, the evaluation of one calibrating heat input and the determination of one value for the heat of solution of curium metal will be presented. The preparation of pure, well-crystallized curium metal will be described in detail later.

The amount of heat put into the calorimeter can be conveniently correlated with the resistance change on the decade required to rebalance the bridge. For this to be strictly true, the position of the track on the chart paper after the heat input must be returned to exactly the same position that it had at the initiation of the heat input. However, since the heat input itself and re-equilibration of the system require a finite length of time, extrapolations of the fore-slope and after-slope to the same point—midpoint of the heating interval—are used. Also, since the decade can be changed only by integral amounts, the two extrapolated points do not usually coincide, but are separated by a certain number of chart divisions. This distance can be related to resistance imbalance by dividing it by the sensitivity in divisions per ohms. Thus the decade change required to return the bridge to the same balance point can be calculated.

If, within the temperature range of use, the heat capacity of the calorimeter is constant and the temperature coefficient of resistance of the thermometer is invariant, then the fractional change in the resistance of the thermometer will be the same for a given amount of heat added, regardless of the initial temperature. Thus, referring to Fig. 4, the fractional change in the resistance of the variable arm of the bridge (upper right arm) is equal to:

$$\text{f.c.} = \frac{\dfrac{500(25{,}000+R_2)}{500+25{,}000+R_2} - \dfrac{500(25{,}000+R_1)}{500+25{,}000+R_1}}{\dfrac{500(25{,}000+R_1)}{500+25{,}000+R_1}} ,$$

where R_1 is the decade reading at the beginning of a heat measurement and R_2 the reading at the termination of the heat process; or in other words R_1 and R_2 are just the decade values for the fore-slope and after-slope respectively. More simply,

$$\text{f.c.} = \left(\frac{25{,}000+R_2}{25{,}000+R_1}\right)\left(\frac{25{,}500+R_1}{25{,}500+R_2}\right) - 1.$$

The product term in the above equation differs from unity only in the fourth or fifth place to the right of the decimal and must, therefore, be calculated to eight or nine places.

The calculated fractional change is the same as the fractional change in the resistance of the resistance thermometer.

For a heat input, division of the observed fractional change by the calculated input in calories gives the fractional change per calorie. This figure is averaged for several heat inputs, and the average used to calculate the heat of reaction of interest from the fractional change due to the reaction.

To illustrate an example, heat input which was for 60 sec at 0.4 maximum power, and gave for the voltage drops across the standard current measuring resistor and the calorimeter heater, 0.48181 V and 0.74198 V, respectively, we calculate

$$Q = \frac{I_H^2 R_H t}{4.184} = (E_{std})(E_H)\frac{t}{R_{std}\,4.184} .$$

The value of R_{std} is 24.809 Ω; thus for this heat input,

$$Q = (E_{std})(E_H)t/103.8009$$

$$= \frac{0.48181 \times 0.74198 \times 60}{103.8009} = 0.20664 \text{ cal.}$$

The decade values for the fore-slope and after-slope were 3285 Ω and 3413 Ω respectively. Both slopes were extrapolated to the midpoint of the heat input. The extrapolation of the after-slope was 1.0 chart division down scale from that of the fore-slope, which means that the resistance change on the decade, 129 Ω, was too large to return the bridge to its former balance point. Sensitivity checks are made at intervals throughout the run, as mentioned previously, and are plotted as divisions per ohm vs average ohm on the decade. The sensitivity for this heat input was 2.643 div/Ω. Thus the decade change required to balance the bridge was:

$$129 \ \Omega - \frac{1.0 \text{ div}}{2.643 \text{ div}/\Omega} = 128.62 \ \Omega$$

The after-slope resistance, then, should be 3413.62 Ω. The fractional change can then be calculated:

$$\text{f.c.} = \left(\frac{25{,}000+3413.62}{25{,}000+3285}\right)\left(\frac{25{,}500+3285}{25{,}500+3413.62}\right) - 1$$

$$= 1.004547286 \times 0.995551577 - 1$$

$$= 0.00007863475$$

and the fractional change per calorie is then:

$$\text{f.c./cal} = \frac{0.00007863475}{0.20664}$$

$$= 3.80540 \times 10^{-4} \quad .$$

Similarly, the fractional change per calorie for the other heat inputs is calculated and the values averaged.

If the calorimeter were truly adiabatic there would be no ambiguity about the selection of values of R_1 and R_2 for the reaction at the time of break.

In reality, important quantities of adventitious heat enter and leave the calorimeter during the course of a measurement, and must be corrected for.

As was indicated previously, under operating conditions thermal equilibrium never exists between the calorimeter and its surrounding thermal environment, although a constant (steady-state) temperature will persist as long as the heat leak into the system is just balanced by the heat leak out of it.

Heat is generated by stirring, the flow of current through the thermometer and the friction of the stirring shaft with its bearing. Heat leak out of the calorimeter occurs by conduction along the stirring shaft, hanger, thermometer, and heater lead and by conduction and radiation between the calorimeter and submarine-chamber walls.

A variation in the magnitude of any one of these effects during the course of a run will change:

a) the steady-state temperature, or "balance point" of the system

and b) the slope of a temperature drift.

Under constant operating conditions the tendency of the calorimeter to exchange heat with its surroundings may be expressed in terms of a characteristic "thermal leakage modulus."

The leakage modulus usually is expressed as the rate of change of temperature of the calorimeter per unit of time per unit difference in temperature between the calorimeter and its surroundings.

Practically, for a steady-state system, the definition of the temperature difference should be changed to the difference between the actual temperature of the calorimeter and its steady-state temperature.

Thus:

$$M_T = \text{thermal leakage modulus} = \frac{dT}{dt} \Big/ (T_{actual} - T_{steady\text{-}state}) \quad ,$$

where T_{actual} and $T_{steady\text{-}state}$ are the actual temperature of the calorimeter and the steady-state temperature respectively. To a sufficiently good approximation, the resistance of the thermometer varies linearly with temperature so that the leakage modulus can be expressed as an "ohmic leakage modulus," M_Ω, where

$$M_\Omega = \frac{dR}{dt} \Big/ (R_{actual} - R_{steady\text{-}state}),$$

where R_{actual} is the actual decade setting and $R_{steady\text{-}state}$ is the decade setting at the steady-state temperature. Hereafter $R_{steady\text{-}state}$ will be represented by R_{ss}. M_Ω and R_{ss} are calculated from the fore-slope and after-slope, which are expressed as the number of chart divisions the track crosses per unit time. Since the chart movement is constant with time and the sensitivity is known, the slopes are expressed as ohms per millimeter. The fore-slope is extrapolated to the beginning of the reaction and the after-slope extrapolated to the end of the reaction. These two extrapolation points differ in time by the duration of the reaction; and also, usually by a certain number of divisions which is corrected for as it was with each heat input (see Fig. 7). For example, the difference in one case was $+1.5$ div or $0.59\ \Omega$. R_2 is then $3853+0.59$ or $3853.59\ \Omega$.

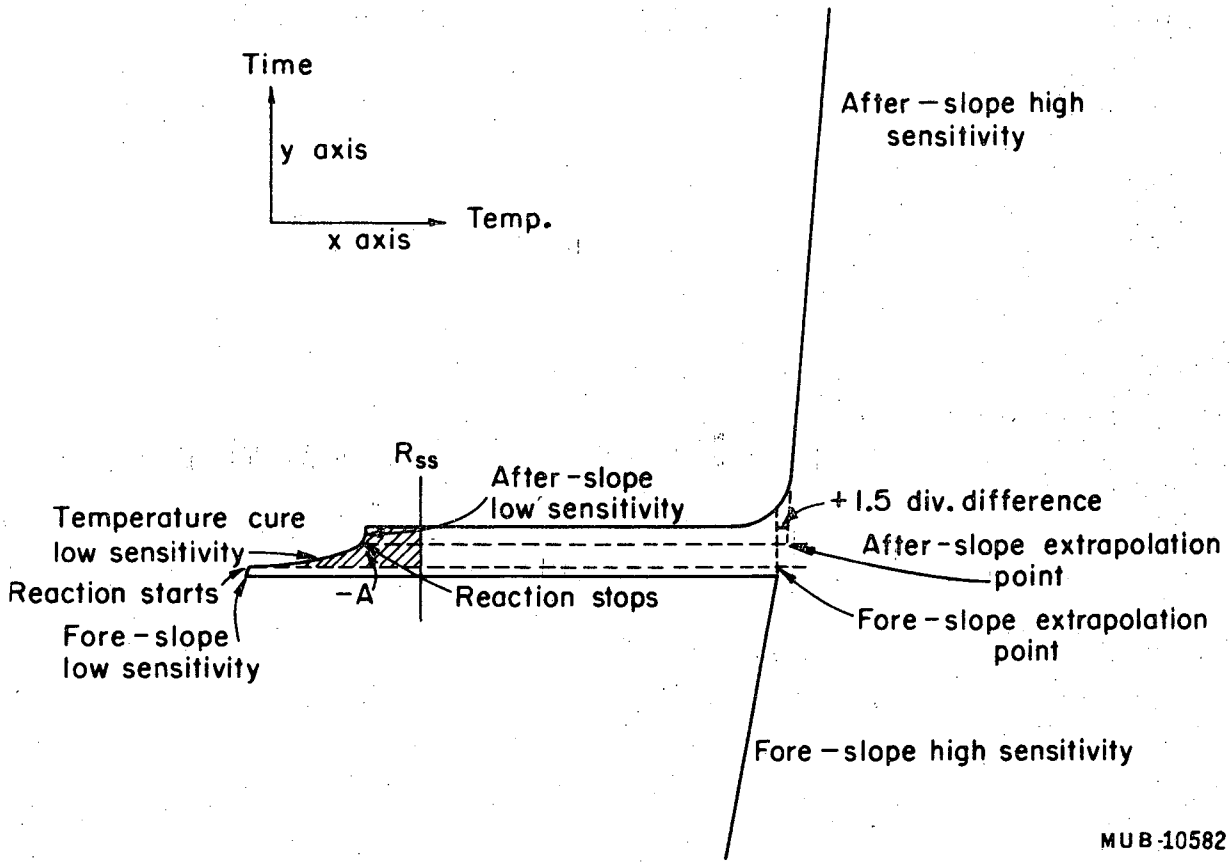

Figure 7. Recorder track for dissolution of curium metal in 1.0 M HCl.

Thus for our example

$$\text{fore-slope} = \frac{-11.0 \text{ div}}{131.6 \text{ mm} \times 2.565 \text{ div}/\Omega}$$

$$= -0.032588 \ \Omega/\text{mm} \ ,$$

$$\text{after-slope} = \frac{-5.0 \text{ div}}{176.7 \text{ mm} \times 2.557 \text{ div}/\Omega}$$

$$= -0.011066 \ \Omega/\text{mm}$$

$$M_\Omega^f = \frac{dR_1}{dt} \Big/ (R_1 - R_{ss})$$

$$= - 0.032588/(3810 - R_{ss}) \ \text{mm}^{-1} \ ,$$

$$M_\Omega^a = \frac{dR_2}{dt} \Big/ (R_2 - R_{ss})$$

$$= - 0.011066/(3853.59 - R_{ss}) \ \text{mm}^{-1} \ ,$$

$$M_\Omega^f = M_\Omega^a \ , \text{ so:}$$

$$-3.2588(3853.59-R_{ss}) = -1.1066 \ (3810 - R_{ss})$$

$$2.1522 \ R_{ss} = 8341.93$$

$$R_{ss} = 3876.00 \ \Omega$$

$$(R_1 - R_{ss}) = -66.00 \ \Omega$$

$$(R_2 - R_{ss}) = -22.41\ \Omega$$

$$M_\Omega = \frac{-0.032588\ \Omega/\text{mm}}{-66.00\ \Omega}$$

$$= 4.9376 \times 10^{-4}\ \text{mm}^{-1} .$$

As was mentioned previously, the potential divider permits monitoring the temperature curve during the reaction. The curve in this example does not go across $T_{\text{steady-state}}$ as there is no change in the sign of the slope, and the position of R_{ss} on the high sensitivity, and the sensitivity ratio. This ratio is 11. Thus:

$$\frac{\text{Sensitivity ratio}}{\text{High sensitivity, } (\text{div}/\Omega) \times (\text{mm/div})} = \text{low sensitivity, } \Omega/\text{mm} ,$$

$$\text{Low sensitivity} = \frac{11}{2.558\ \text{div}/\Omega\ 2.1\ \text{mm/div}} = 2.04773\ \Omega/\text{mm} .$$

Here $2.558\ \text{div}/\Omega$ is the average of the high sensitivities before and after the reaction.

$$(R_{ss} - R_1) = 66.00$$

and

$$\frac{66.00\ \Omega}{2.04773\ \Omega/\text{mm}} = 32.2\ \text{mm} .$$

Thus R_{ss} can be drawn across the temperature curve 32.2 mm up-scale from R_1 on the low sensitivity. This is shown in Fig. 7. The areas A and B represent the heat that leaked into and out of the calorimeter respectively. They are measured by superimposing thin mm graph paper on the chart and counting squares. Unfortunately in this particular example there is no B (heat leaked out of the calorimeter) as the after-slope did not change sign

with respect to the fore-slope. It would have been better to have made one more heat input before breaking the sample bulb or to have used a bigger sample. The low sensitivity value in Ω/mm times the leakage modulus gives the number of ohms per square millimeter. This factor times the net area, (B - A), gives us the number of ohms to be added to R_2 for the heat leak correction:

$$2.04773\ \Omega/\text{mm} \times 4.9376 \times 10^{-4}\ \text{mm}^{-1} = 1.011 \times 10^{-3}\ \Omega\ \text{mm}^{-2} \quad .$$

Since in this example B = 0, and A = 196 mm^2,

$$(B - A) = -196\ \text{mm}^2 \quad ,$$

$$\text{correction} = -1.011 \times 10^{-3}\ \Omega\ \text{mm}^{-2} \times 196\ \text{mm}^2 = -0.20\ \Omega$$

and $$R_2 = 3853.59 - 0.20$$

$$= 3853.39\ \Omega \quad .$$

The fractional change due to the reaction is 2.565373×10^{-5}. Dividing this by the average fractional change per calorie of the several heat inputs gives the net heat of the reaction:

$$\frac{2.565373 \times 10^{-5}}{3.79938 \times 10^{-4}} = 0.067521\ \text{cal} \quad .$$

As was mentioned previously, this heat value must be corrected for the heat of breakage of the sample bulb, and the heat of vaporization of water required to saturate the hydrogen evolved and the heat of vaporization of water required to saturate the dry nitrogen in the bulb.

Our calorimetric reaction is:

$$Cm^0 + 3\ H^+_{(aq)} \longrightarrow Cm^{+3}_{(aq)} + 3/2\ H_2\uparrow$$

Net heat of this reaction as calculated above	= 0.067521 cal
Heat of breakage of the bulb	= 0.000560 cal
	0.066961 cal
Correction for the heat of vaporization of water into the N_2 in the bulb and the evolved H_2	= 0.000728 cal
	0.067689 cal

Thus the heat of solution of 118.3 μg of pure curium metal in 1.0 M HCl is 0.067689 cal or ΔH_{298} = -139.6 kcal/mole.

The weight of the curium metal was corrected for:

a) weight loss during sealing

b) weight loss due to replacing the air in the bulb by dry nitrogen.

III. MAGNETIC SUSCEPTIBILITY MEASUREMENTS

Cunningham[13] has described an apparatus used to measure the magnetic susceptibility of submicrogram quantities of the plus three ions of berkelium and californium. This apparatus was modified[3] to measure the susceptibility of americium metal, curium metal, and their compounds down to liquid nitrogen temperature. Now a new apparatus has been constructed which allows the measurements to be made down to liquid hydrogen and liquid helium temperatures.

A. Principle of the Apparatus

Susceptibility measurements are made by using a pendular type magnetic susceptibility apparatus. It is essentially a modified Faraday's apparatus in which the sample, suspended on a long quartz fiber, is exposed to an inhomogeneous magnetic field. The principle of this apparatus is sketched in Fig. 8. The fiber is of uniform cross section and is assumed to be infinitely flexible. The sample is suspended midway between the pole faces of the magnet, which are shaped in such a way that the field gradient in the vicinity of the sample is large in the x-y plane and very small in the z direction. The sample experiences a magnetic force F_2 in the x direction and a gravitational force F_1, normal to F_2. An additional gravitational force F_3 acts on the center of mass of the suspended fiber. (The magnetic force on the fiber is too small to be considered.)

At equilibrium, the sum of the moments of forces acting about the pivot point P is zero. If the magnetic force acting on the sample in the z (upward) direction, as well as the magnetic force on the suspension fiber in the x direction may both be neglected in comparison with the magnetic force acting on the sample in the x direction, then we have:

$$F_1 d + F_2 d/2 = F_2 L \cos \theta \quad , \qquad (1)$$

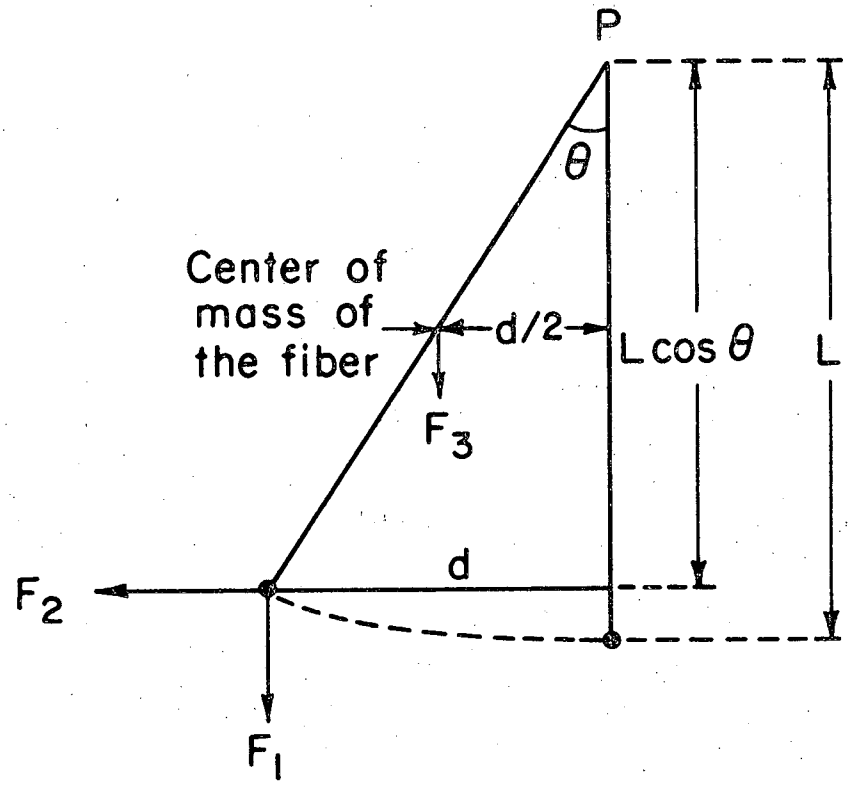

Figure 8. Principle of magnetic susceptibility apparatus.

where d is the linear displacement of the sample under the action of the force F_2 and L is the length of the fiber. But $F_1 = M_s g$; $F_2 = M_s \chi_{s(gm)} H \frac{\partial H}{\partial x}$; and $F_3 = M_f g$; where,

M_s = mass of the sample
g = acceleration due to gravity
$\chi_{s(gm)}$ = gram susceptibility of the sample
H = magnetic field at the sample
$\frac{\partial H}{\partial x}$ = field gradient in the x direction
M_f = mass of the fiber .

The magnet pole pieces are shaped to produce as large a volume of uniform $H\frac{\partial H}{\partial x}$ about the sample as possible, but in practice it is difficult to secure satisfactory constancy even in a volume as small as 1 mm^3. Hence it is customary to restore the sample with the magnet current on, to the sample position in space that it occupied with the current off, by a micrometer-controlled compensating shift of the suspension point P. Substituting for F_1, F_2, and F_3 their corresponding values in Eq. (1) gives

$$M_s\ g\ d + M_f\ g\ d/2 = M_s\ \chi_{s(gm)}\ H\frac{\partial H}{\partial x}\ L\ \cos\theta \quad ,$$

or more simply

$$(M_s + M_f/2)\ g\ d = M_s\ \chi_{s(gm)}\ H\frac{\partial H}{\partial x}\ L\ \cos\theta \quad . \tag{2}$$

If θ is small (as is usually the case experimentally), cos θ may be taken as unity (for maximum deflection obtained in these measurements θ was 0.33 deg for which cos θ = 0.99998). Then,

$$(M_s + M_f/2)\ g\ d = M_s\ \chi_{s(gm)}\ H\frac{\partial H}{\partial x}\ L \quad , \tag{3}$$

$$\therefore d = \frac{M_s\ \chi_{s(gm)}\ H\ \frac{\partial H}{\partial x}\ L}{(M_s + M_f/2)\ g} \quad . \tag{4}$$

It is convenient to rearrange Eq. (4) to give

$$\chi_{s(gm)} = \frac{(M_s + M_f/2)\, g\, d}{M_s\, H\frac{\partial H}{\partial x}\, L} \quad , \tag{5}$$

since the susceptibility of the sample is the quantity of experimental interest. Direct measurement of $H\frac{\partial H}{\partial x}$ is virtually impossible.

So for a given magnet current and suspension fiber, it is customary to lump the constants g, L, and $H\frac{\partial H}{\partial x}$ into a single apparatus constant

$$K = g/L\; H\frac{\partial H}{\partial x} \quad ,$$

so that Eq. (5) can be written as

$$\chi_{s(gm)} = \frac{(M_s + M_f/2)}{M_s}\, Kd \quad . \tag{6a}$$

A special case of Eq. (6a) is that when $M_f \ll M_s$, then we get

$$\chi_{s(gm)} = Kd \quad . \tag{6b}$$

In this case the deflection will be completely independent of the mass of the sample. This is an important advantage of this method.

It is obvious from Eq. (6a) that in order to measure the magnetic susceptibility, two quantities, namely the apparatus constant K and the mass of the fiber M_f, are to be determined. M_f can be calculated fairly accurately from the measurements of length and diameter of the fiber, using the known density of fused silica. The apparatus constant K can be evaluated by observing the deflection of a sample of known susceptibility. There are, however, several factors which complicate this evaluation.

1) The standard sample of known mass and known susceptibility is contained in a tube of known mass but unknown susceptibility. Although the tube usually consists of fused silica, for which an accurate value for the susceptibility may be found in the literature, commercially available silica seems to show considerable variation in χ_{gm}. Even tubes made of the same silica stock give different susceptibilities depending on the manner of heating during attachment of the hook for the supporting fiber. Since $\chi_{s(gm)}$ in Eqs. (6a) and (6b) is the mean susceptibility of the combination sample-plus-tube, generally it is not accurately known. The reason for getting different susceptibilities for tubes made out of the same silica stock is not clearly understood at present.

2) Although the sample may be weighed accurately, it is suspended by a hook (attached to the fiber) which also is in the magnetic field and which in effect contributes an additional mass to the sample tube.

3) L is not strictly constant because of the elastic and thermal properties of silica (change is very, very small though), nor even necessarily the same for F_1 and F_2, since for the former it refers to the center of mass of the sample plus tube combination, which will vary according to the depth of filling of the tube with the sample, while for the latter it refers to the "center of susceptibility," which may or may not be coincident with the center of mass.

However, two measurements with a sample of known susceptibility confined to approximately the same position in the same sample tube leads to an evaluation of the apparatus constant sufficiently accurate for most purposes.

B. Calibration of the Apparatus

The procedure used for calibrating the apparatus is as follows.

1) A sample tube, weighing anywhere from 900 μg to about 9 mg, depending on the requirement, is prepared from clean, thin-walled silica tubing. A fine and sharply bent hook is fused to the tube, and the tube with the hook is cleaned by repeated boiling in 6 M HCl. The tube is dried and weighed to ±5 μg on an assay balance.

2) The mass of the hook (attached to the fiber) from which the sample tube is suspended is estimated from its length and diameter and added to the mass determined in 1) above to give the effective mass of the tube ($M_{t,eff}$). (Since the tube and fiber hooks are both made of fused silica, they are assumed to have the same susceptibility.)

3) The tube is suspended in the susceptibility apparatus, and its position with reference to the filar micrometer hair line and scale in the telescope is noted and recorded.

4) The reading of the drum of the precision micrometer located near the head of the susceptibility apparatus is noted and recorded.

5) The magnet current is adjusted to the selected values of 1.0, 1.5, 2.0, 2.5, 3.0, 3.5, and 4.0 A.

6) The image of the sample tube in the filar micrometer eyepiece is restored to that noted in 3) by turning the drum of the precision micrometer, and the new micrometer reading is recorded for the various magnet current settings.

7) The deflection of the tube, d_0, is taken as the difference in the readings 4) and 6). A minimum of three readings of this deflection are usually taken and averaged. If, when the magnet current is on, the sample undergoes a rotation in the magnetic field, the threaded screw which supports the quartz nub to which the suspension fiber is attached is rotated until no rotation of the sample is induced by the magnetic field. A deflection of the tube away from the pole pieces is given a negative value.

8) Deflection measurements are made at room temperature and at liquid nitrogen temperature usually, but in some cases deflection measurements of the empty tube were made at room temperature and liquid helium temperature to get much better sensitivity. The deflection should be temperature-independent within the experimental accuracy of ±1%. This would indicate that the tube is free of paramagnetic and ferromagnetic impurities, since the diamagnetic susceptibility of the tube is independent of temperature. If the deflection at liquid nitrogen or liquid helium temperature is significantly less than that at room temperature, the tube is unloaded and boiled again in 6 M HCl and the entire procedure is repeated.

9) The tube is loaded with a known mass (M_{std}) of a paramagnetic substance of known susceptibility (χ_{std}). The sample mass is usually of the order of 100-200 μg and is weighed on a submicrogram balance within ±0.1 μg. It is the ratio of the paramagnetic susceptibility of the sample to the diamagnetic susceptibility of the tube that is important rather than M_{std}. Now the new deflection measurements d_1 and d_2 are made at two temperatures, usually liquid nitrogen temperature T_1 and liquid hydrogen temperature T_2. Nickelous ammonium sulfate [$NiSO_4(NH_4)_2SO_4 \cdot 6H_2O$] is used as a standard for susceptibility measurements.[14] Nickelous ammonium sulfate crystals from baker and Adamson lot No. 7 were vapor-equilibrated with a saturated solution of $Ni(NH_4)_2(SO_4)_2 \cdot 6H_2O$. The susceptibility is assumed to be given by the relation,[15] $\chi_{gm}[NiSO_4,(NH_4)_2SO_4 \cdot 6H_2O] = (3174/T+2.5 - 0.30) \times 10^{-6}$ c.g.s. Alternatively, freshly ignited neodymium sesquioxide (Nd_2O_3) can very well be used for calibration purposes, for which the susceptibility[16] is taken as

$$\chi_{gm} = 30.3 \times 10^{-6} \text{ erg/G}^2 \text{ at } 292^{\circ}\text{K}.$$

C. Calculation of Parameters

Taking the deflection of the empty tube to be d_0 and independent of temperature, its mass to be $M_{t,eff}$ ($M_{t,eff} = M_{tube} + M_{hook\ of\ fiber}$), its susceptibility to be χ_t, the mass of the calibrating substance to be M_{std}, its susceptibility at temperatures T_1 and T_2 to be $\chi_{std_{T_1}}$ and $\chi_{std_{T_2}}$ respectively, and finally, the deflection with the standard in the tube to be d_1 and d_2 at temperatures T_1 and T_2 respectively, then the following two equations can be written with the help of Eq. (3):

$$(M_f/2 + M_{t,eff} + M_{std})\, g\, d_1 = (M_{t,eff}\, \chi_t + M_{std}\, \chi_{std_{T_1}})\, H \frac{\partial H}{\partial x} L, \quad (7)$$

$$(M_f/2 + M_{t,eff} + M_{std})\, g\, d_2 = (M_{t,eff}\, \chi_t + M_{std}\, \chi_{std_{T_2}})\, H \frac{\partial H}{\partial x} L. \quad (8)$$

If we put $(M_f/2 + M_{t,eff} + M_{std}) = M_T$ (total mass) and $[g/H(\partial H/\partial x)L] = K$ as in Eq. (6a) we have

$$K\, M_T\, d_1 - M_{t,eff}\, \chi_t = M_{std}\, \chi_{std_{T_1}} \quad (9)$$

and

$$K\, M_T\, d_2 - M_{t,eff}\, \chi_t = M_{std}\, \chi_{std_{T_2}} . \quad (10)$$

Solving these two equations simultaneously we get

$$\chi_t = \frac{M_{std}}{M_T} \frac{\left(\chi_{std_{T_2}} d_1/d_2 - \chi_{std_{T_1}}\right)}{(1 - d_1/d_2)} , \quad (11)$$

$$K = \frac{M_{std}}{M_T} \frac{\left(\chi_{std_{T_2}} - \chi_{std_{T_1}}\right)}{(d_2 - d_1)} . \quad (12)$$

Hence by measuring the deflection of a magnetic susceptibility standard at two different temperatures and using Eqs. (11) and (12), both χ_t and K can be determined.

A different value of K will be obtained for each different current setting. If a new sample position is chosen it is necessary to redetermine K for each current at that new position. According to Eq. (6a), for the same given sample at two different positions, $K_1 d_1 = K_2 d_2$, where K_1, d_1 are the apparatus constant and deflection at position (1), and K_2, d_2 those at position (2). So the apparatus constants at various positions can be determined from the apparatus constant at one specified position and the ratio of the deflections at that specified position and other positions. The tube susceptibility χ_t is determined at different current settings and the average is taken as the susceptibility of the tube.

Once K has been evaluated, the approximate value of M_f may be checked:

$$\frac{M_f}{2} = M_{t,eff} \left(\frac{\chi_t}{K d_0} - 1 \right) \quad . \tag{13}$$

The calculation of the susceptibility of the blank tube from Eq. (11) is susceptible to an error because of the small denominator. A small experimental error in the determination of the ratio d_1/d_2 will contribute to an appreciable error in χ_t. Therefore the value of χ_t should be checked by using Eq. (6a) and the determined K values. For any tube of mass M_t and deflection d_0 (independent of temperature),

$$\chi_t = \frac{K d_0 (M_{t,eff} + M_f/2)}{M_{t,eff}} \quad . \tag{14}$$

For a known weight of sample M_s of unknown susceptibility, run in the tube of mass $M_{t,eff}$ and of susceptibility χ_t, giving deflection d (say) we have

$$\chi_s = \frac{(M_{t,eff} + M_f/2 + M_s)}{M_s} K d - \frac{M_{t,eff}}{M_s} \chi_t \quad , \tag{15}$$

or simply

$$\chi_s = \frac{M_T}{M_s} K d - \frac{M_{t,eff}}{M_s} \chi_t \quad . \tag{16}$$

D. Construction of the Low Temperature Apparatus

The apparatus is designed for the measurement of susceptibilities of solid samples in the mass range from about 1 mg to about 10^{-2} μg, over the temperature range from about $4^{\circ}K$ (liquid helium) to about $298^{\circ}K$ (room temperature). A general view of the apparatus is shown in Fig. 9.

Samples are suspended in a quartz tube, L, of the loading tube assembly, sketched in Fig. 10, by a very fine fiber, M, of fused silica of about 42 cm length. At the top of this tube assembly is screwed a heavy dural ring, A. The dural ring contains an inner, removable brass ring, C, which serves as a support for the fiber attachment. The brass ring is mounted in a micrometer, H, which allows the deflection to be measured by a null method, in which the sample is always restored to the same position in the magnetic field. In this way errors resulting from variations in $H\frac{\partial H}{\partial x}$ with sample position are minimized. The suspension fiber can also be rotated to bring an asymmetric sample to a position of zero rotational torque in the magnetic field. After the sample is in place, the opening in the dural ring is sealed (vacuum tight) by means of a quartz disk and neoprene O-ring, B. The image of the sample tube is restored to its initial position with reference to a hair line in the

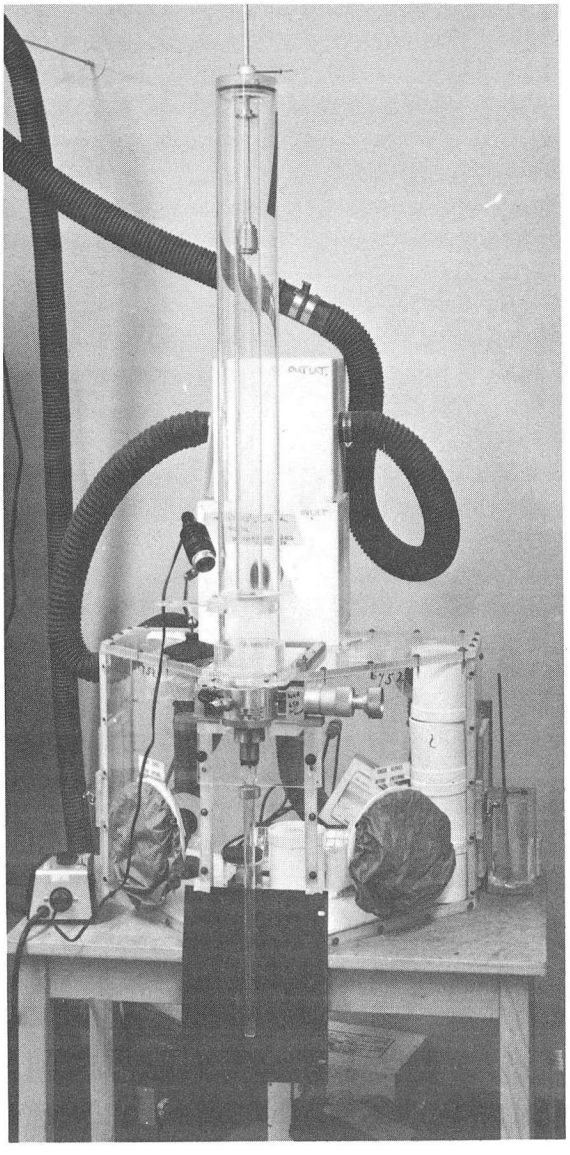

ZN-5499

Figure 9. General view of magnetic susceptibility apparatus.

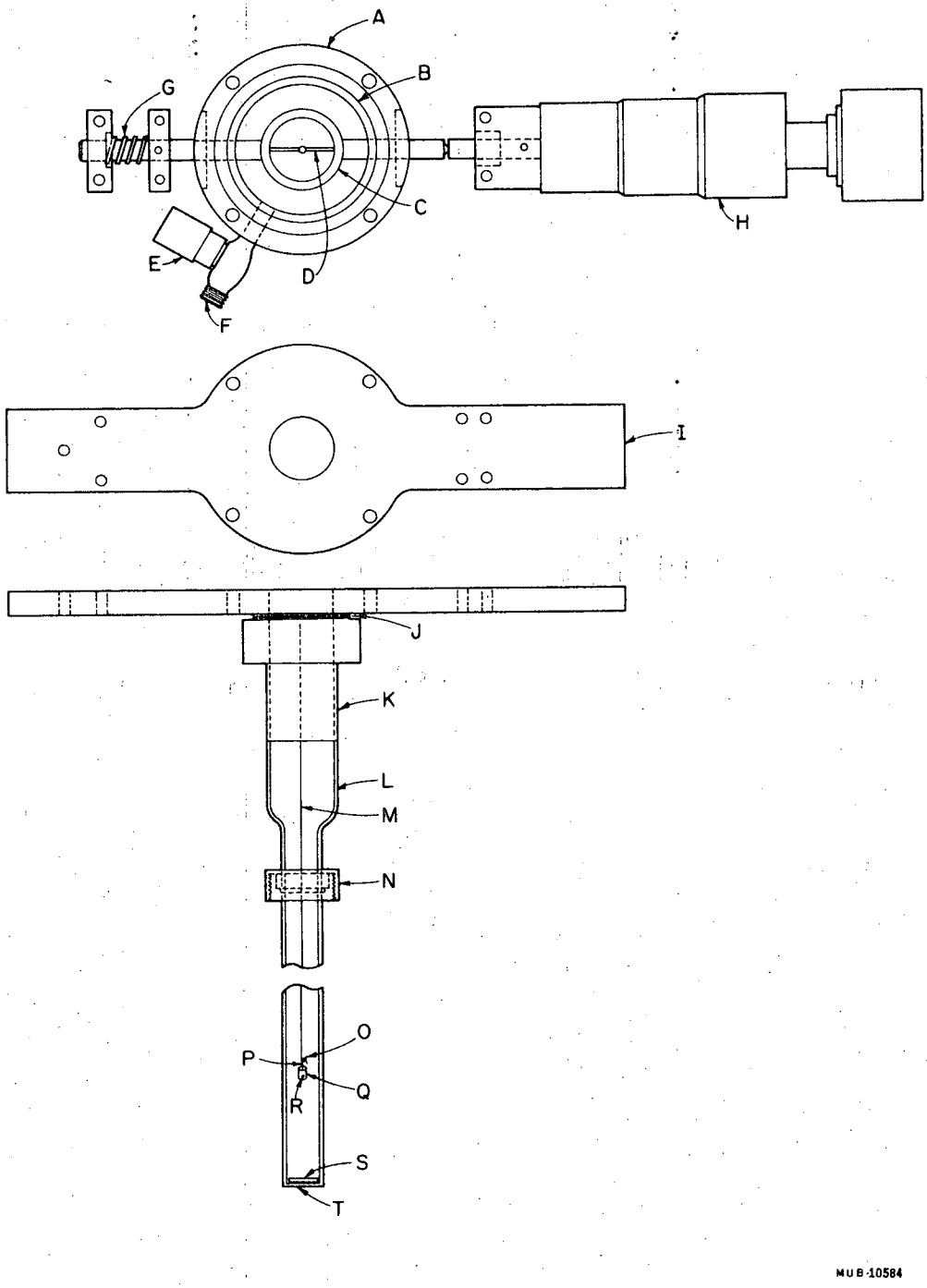

Figure 10. Loading tube assembly of the magnetic susceptibility apparatus.

Legend for Figure 10

A. Dural ring
B. Neoprene O-ring seal
C. Brass ring
D. Fiber suspension
E. Valve
F. To vacuum line
G. Spring
H. Micrometer
I. Brass plate
J. Threads
K. Brass socket
L. Quartz tube
M. Quartz fiber
N. Fitting that fits on dewar cap
O. Quartz hook attached to the fiber
P. Quartz hook fused to sample tube
Q. Sample tube
R. Sample
S. Silvered mirror
T. Optically flat quartz disk

filar micrometer of the telescopic arrangement (not shown in the figure, for simplicity of drawing) by adjusting the micrometer attached to the fiber suspension. The tube, L, in which the sample is suspended may be evacuated and flushed with helium gas. The positioning micrometer, H, can be read to within an estimated accuracy of ± 0.5 μ.

This tube assembly is suspended inside the dewar system (see Fig. 11) through the opening, A. The top head of this tube assembly is screwed to a metal frame attached to the electromagnet. The dewar system itself is suspended between the pole pieces of the magnet by a three-point suspension attached to the metal frame.

The magnet used here is a Varian 4-in. electromagnet assembly. It consists of a Model V4004 electromagnet with an air gap which can be adjusted to any value from zero to 4 in.; a Model V2300A power supply which provides unregulated dc power for driving the electromagnet; and a Model 2301A current regulator. The current regulator and power supply are interconnected to provide a stable current source. This combination regulates the dc magnet current to within $\pm 0.1\%$ for line-voltage and load resistance variations of $\pm 10\%$.

The dewar assembly is sketched in Fig. 11. Down to liquid nitrogen temperature it is possible to use a simple two-wall dewar with a quartz window at the bottom for admitting light. At liquid hydrogen and liquid helium temperatures this simple two-wall dewar cannot be used. Therefore, a three-wall dewar,[17] was used. The so-called three-wall dewar, E, is actually two-walled with a copper finger, F, acting as the third wall. The purpose of this finger is to cool the lower part of the dewar to liquid nitrogen temperature when liquid nitrogen is present in the upper part. This helps tremendously in reducing the temperature gradient between the outer and inner dewar when the latter is filled with liquid hydrogen or helium. Liquid hydrogen or helium is transferred into the inner dewar through a sealed evacuated metal tube (J, G the upper and lower section of filling tube). While liquid helium is transferred to

the dewar, the top of this filling tube is attached to a liquid helium transfer tube fitting, which has been sketched in Fig. 12. The conventional liquid helium transfer tube that connects the main liquid helium dewar to the upper part of the filling tube, J, through the above-mentioned fitting is shown in Fig. 13. The entire dewar is connected to a brass head, so-called helium dewar cap, B, which has an opening serving as an outlet for the extra hydrogen or helium in the dewar.

On the top of the quartz disk cover which seals the opening of the loading tube assembly (see Fig. 10) with the help of an O-ring (as mentioned earlier) is placed a front surface mirror with a hole in the center through which the light from a sodium lamp attached to the top of the apparatus enters the quartz loading tube. This quartz tube has a silvered mirror placed at its flat bottom which acts as a reflector, and the image of the sample tube is viewed through a telescopic system which is supported by a metal frame attached to the electromagnet.

E. Difficulties in Susceptibility Measurements on Microgram Scale

The major problem in the measurement of the magnetic susceptibility of microgram samples is the contamination of the sample with trace amounts of ferromagnetic or paramagnetic impurities. The chief sources of these undesired impurities are scalpels, tweezers, etc. with the help of which these samples are mechanically handled inside the glove box. Extra care must be taken to handle the sample tubes and samples only with gold-tipped forceps. Even with these precautions, several of the samples apparently contained ferromagnetic impurities since the susceptibility was found to exhibit slight field dependence. In the presence of these impurities the susceptibility of the sample was determined by extrapolating the apparent susceptibility against the reciprocal of the current to $1/i = 0$. This is equivalent to extrapolating to infinite magnetic field where the ferromagnetic impurity is saturated and does not contribute to the measured

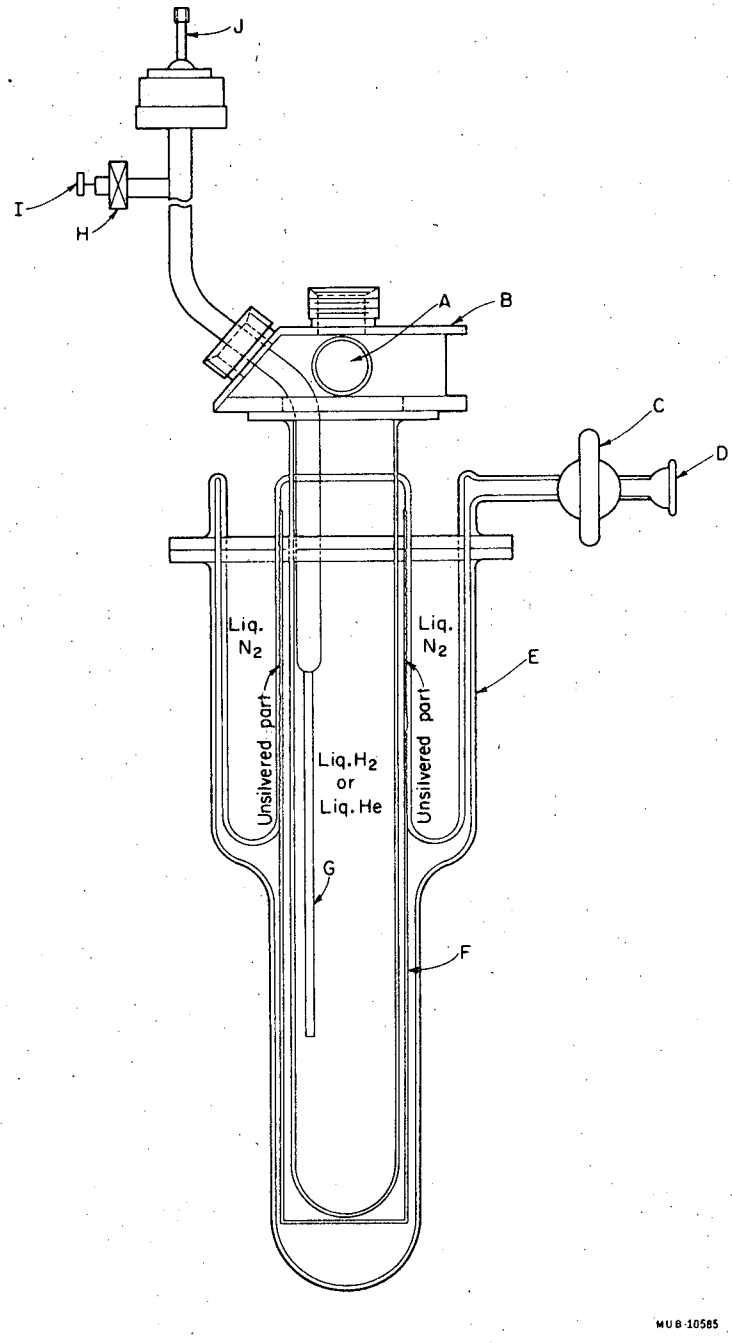

Figure 11. Dewar system of the magnetic susceptibility apparatus.

Legend for Figure 11

A. Opening through which tube assembly goes into the dewar
B. Brass cap of the dewar
C. Stopcock
D. To high vacuum
E. Three-wall dewar
F. Copper finger
G. Lower section of liquid He or liquid H_2 filling tube
H. Vacuum valve
I. To vacuum line
J. Upper section of filling tube

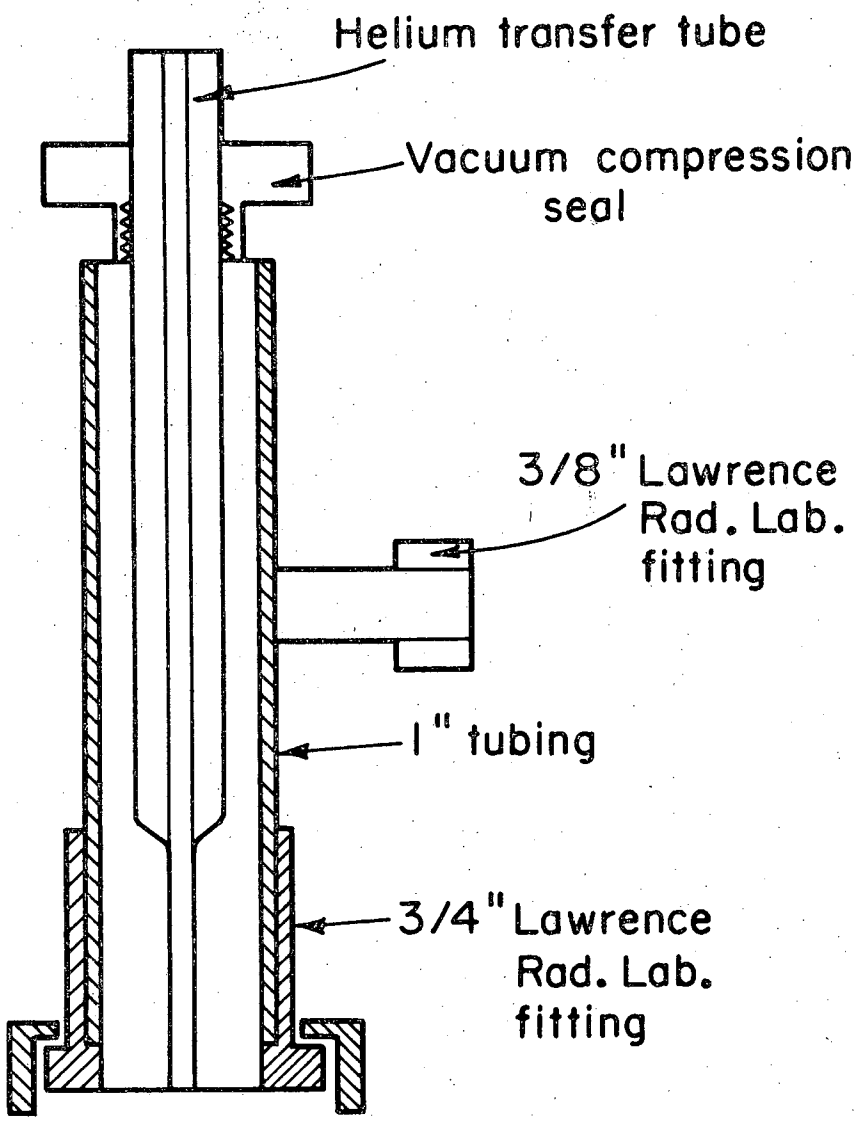

Figure 12. Liquid helium transfer tube fitting.

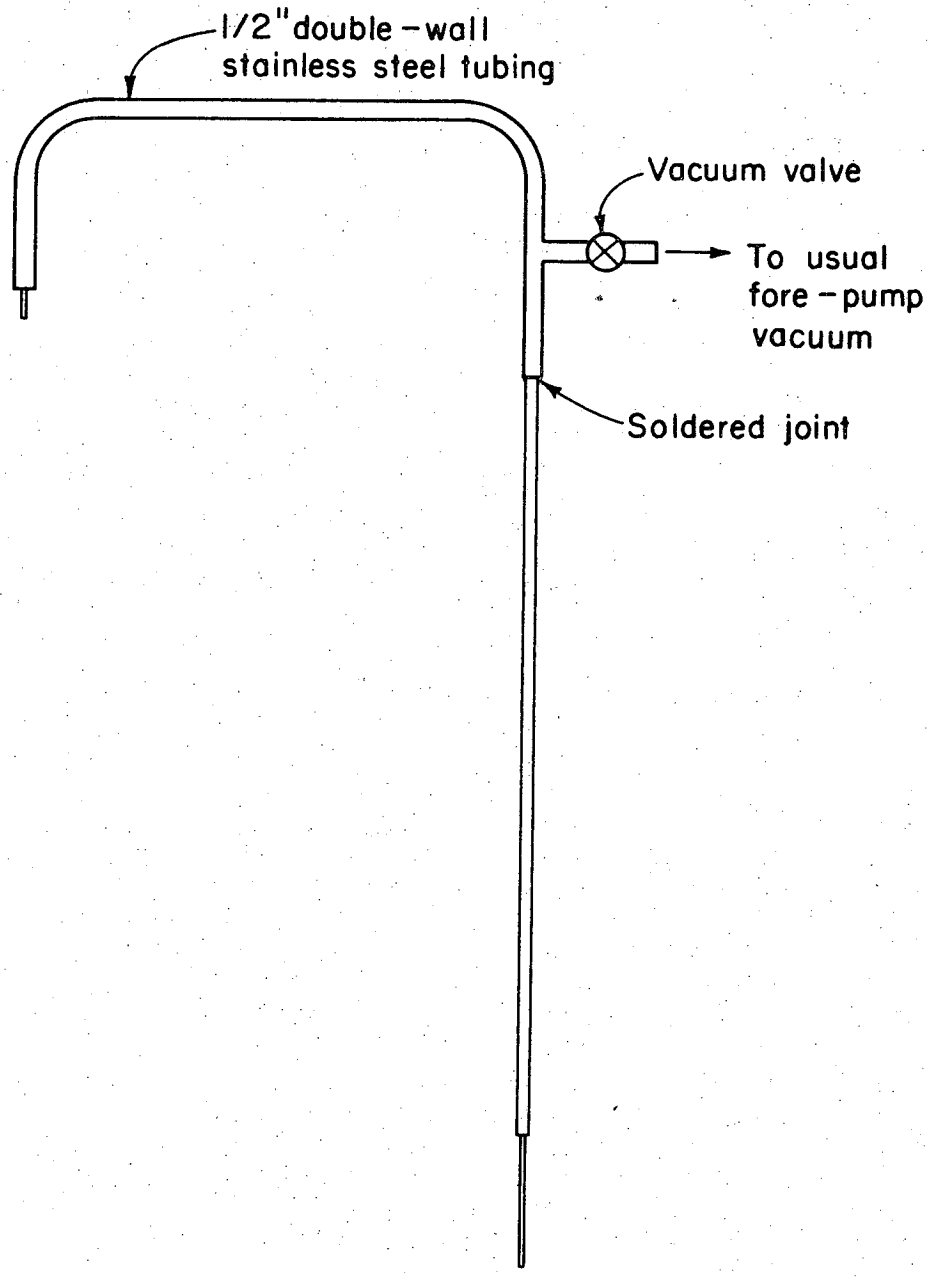

Figure 13. Liquid helium transfer tube.

susceptibility. This is the reason why all the experimental susceptibilities were determined at several different current settings (fields), if possible. This not only enabled a correction to be made for any ferromagnetic impurities present in the sample, but it also made it possible to get some evidence regarding any magnetic transitions from paramagnetic to ferro- or antiferro-states in the sample. Unlike simple paramagnetism, where the Curie or Curie-Weiss law is followed and the susceptibility shows no dependence on magnetic field strength, in the case of ferromagnetism and antiferromagnetism the susceptibility dependence on both temperature and field strength is complicated. In the case of a ferromagnetic substance, so far as field dependence is concerned, the magnetic susceptibility decreases as the magnetic field strength increases. Thus in the case of a paramagnetic substance free from ferromagnetic contamination, if one observes a decrease in magnetic susceptibility with an increase in field strength at a particular temperature, one could think that probably the paramagnetic substance has undergone a ferromagnetic transition. Although no attempt will be made to explain either ferromagnetism or antiferromagnetism in detail, either phenomenologically or theoretically, it is important to recognize their salient features, especially qualitative temperature dependence of the susceptibility. In the case of a ferromagnetic substance if we plot susceptibility (χ) vs temperature (T) it should be noted that there is a discontinuity at some temperature, T_c, called the Curie temperature. Above the Curie temperature the substance follows the Curie or Curie-Weiss law; that is, it is a simple paramagnetic. Below the Curie temperature, however, it varies in a different way with temperature and is also field-strength dependent. For antiferromagnetism there is again a characteristic temperature, T_N, called the Néel temperature. Above T_N the substance has the behavior of a simple paramagnetic, but below the Néel temperature the susceptibility drops with decreasing temperature.

These peculiarities in the behavior of ferromagnetic and antiferromagnetic substances below their Curie or Néel points are due to

interionic interactions which have magnitudes comparable to the thermal energies at the Curie or Néel temperature and thus become progressively greater than thermal energies as the temperature is further lowered. In the case of antiferromagnetism, the moments of the ions in the lattice tend to align themselves so as to cancel one another out. Above the Néel temperature thermal agitation prevents very effective alignment, and the interactions are manifested only in the form of a Weiss constant which is of the same general magnitude as the Néel temperature itself. However, below the Néel temperature this antiparallel aligning becomes effective and the susceptibility is diminished. In ferromagnetic substances the moments of the separate ions tend to align themselves parallel and thus to reinforce one another. Above the Curie temperature, thermal energies are more or less able to randomize the orientations; below T_c, however, the tendency to alignment becomes controlling, and the susceptibility increases much more rapidly with decreasing temperature than it would if the ion moments behaved independently of one another.

Presumably, even in those substances we ordinarily regard as simple paramagnetic, there are some interionic interactions, however weak, and therefore there must be some temperature, however low, below which they will show ferromagnetic or antiferromagnetic behavior, depending on the sign of the interaction. As a matter of fact, the Curie point often lies below $0^{\circ}K$, and so is imaginary. The question of why such interactions are so large in some substances that they have a Curie or Néel temperature near and even above room temperature is still something of an unsolved problem. Suffice it to say here that in many cases it is certain that the magnetic interactions cannot be direct dipole-dipole interactions, but instead the dipoles are coupled through the electrons of intervening atoms in oxides, sulfides, halides, and similar compounds.

All measurements were made under 1/3 atm of purified helium gas, to assist in the rapid attainment of thermal equilibrium.

The following temperature baths were used:

		°C	°K
1.	Ice-H_2O slush	0	273
2.	Freon-22 (monochlorodifluoromethane)	-40.8	232.2
3.	Dry ice and alcohol	-75	198
4.	Freon-14 (carbon tetrafluoride)	-128	145
5.	Liquid methane	-161.5	111.5
6.	Liquid oxygen	-182.96	90.04
7.	Liquid nitrogen	-196	77
8.	Liquid hydrogen	-253	20
9.	Liquid helium	-269	4

Since there is no convenient temperature bath between liquid hydrogen and helium range (4-20°K), an attempt was made to attain temperatures within this range by passing cold helium gas (from a helium dewar) at a very controlled rate. This general cryostating technique seems to be fairly satisfactory. In comparison to normal helium dewars our present dewar is very small (capacity ≈350-400 ml) so we were never able to see liquid helium in the dewar. As a result, we think we never attained 4°K temperature; however, by passing cold helium gas at very regulated speed, as mentioned above, we could attain fairly close to 4°K. At present we are capable of attaining about 6°K or so. The temperature was determined by measuring the resistance of a carbon-composition resistor.[18] The principal advantages of these carbon-composition thermometers are high thermometric sensitivity and very low magnetic field sensitivity. A semi-empirical equation[18] relating resistance and temperature and having three adjustable constants is

$$\log R + K/\log R = A + B/T \quad ,$$

where K, A, and B are arbitrary constants to be determine experimentally. Temperatures calculated by this equation are within ±0.5% of the measured temperature from 4-20°K. The thermometer was calibrated at the boiling points of liquid N_2, H_2, and He. The calibration curve is shown in Fig. 14.

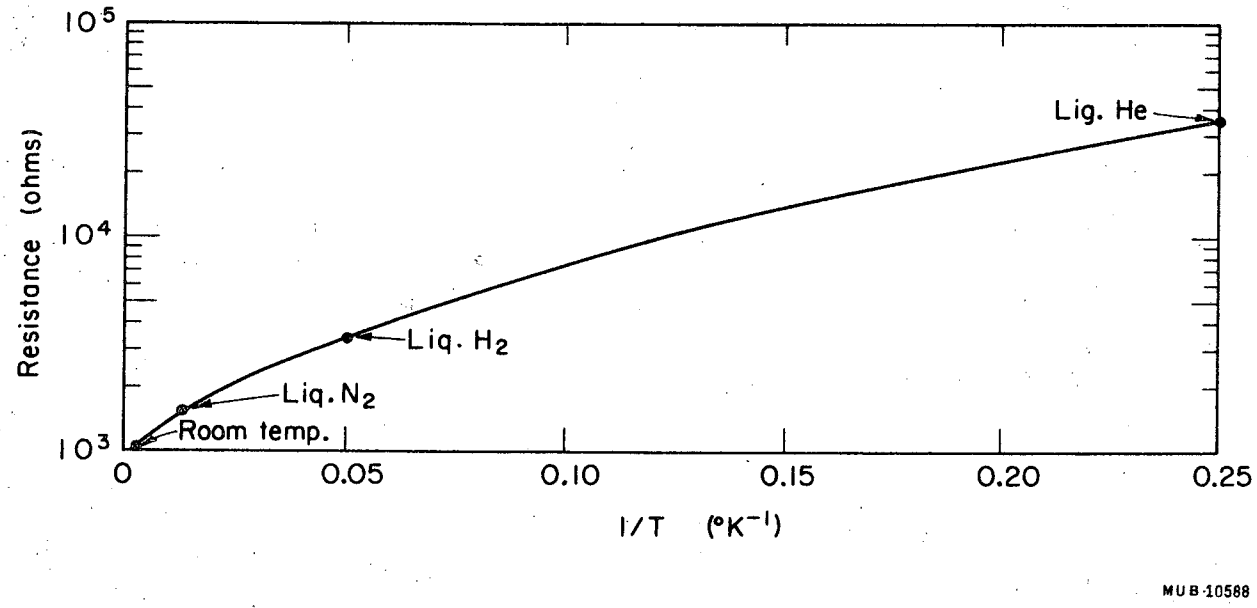

Figure 14. Calibration curve of a carbon-composition thermometer (carbon-composition resistor).

IV. OPERATION OF THE MAGNETIC SUSCEPTIBILITY APPARATUS

The principle and the construction of the apparatus and the method of calibration have already been described in the preceding section.

What is intended here is a description of the practical aspects of susceptibility measurements.

A. Preparation of Suspension Fibers

Suspension fibers are prepared as follows.

1) A 3-7 cm length of quartz rod of diameter 0.4-0.8 mm is selected and several mm of one end is cemented to a glass slide with black Apeizon wax as shown in Fig. 15(1).

2) The attached rod is wiped clean of dust particle.

3) A hook is formed at the free end by heating with a microtorch as shown in Fig. 15(2).

4) The slide is supported by means of a clamp so that the fiber projects 2-3 in. beyond the bench top [see Fig. 15(3)].

5) A platinum weight, made from 1-2 cm of 20-30 mil platinum wire bent in the form of a hook is suspended from the bottom of the fiber.

6) The fiber is heated to softening with a microtorch at a point about 1 cm above the hook, and the torch held in place until the hook has dropped about 50 cm, producing a fiber of 3-20 μ in diameter [Fig. 15(4)].

No amount of description can provide a sure guide to success in this operation. The diameter of the original quartz fiber, the mass of the weight, and the size and temperature of the flame all affect the result, which often amounts to breakage or melting of the fine fiber before the pulling is completed. However, a few practice tries usually impart sufficient experience to insure a reasonable probability of success. A fairly large hot flame seems to give the best results

7) Once success has been achieved, it is necessary to mount the fine fiber in a manner convenient for subsequent use. A satisfactory method consists of sticking the upper and lower ends to a flat backing, using small squares of sticky tape.

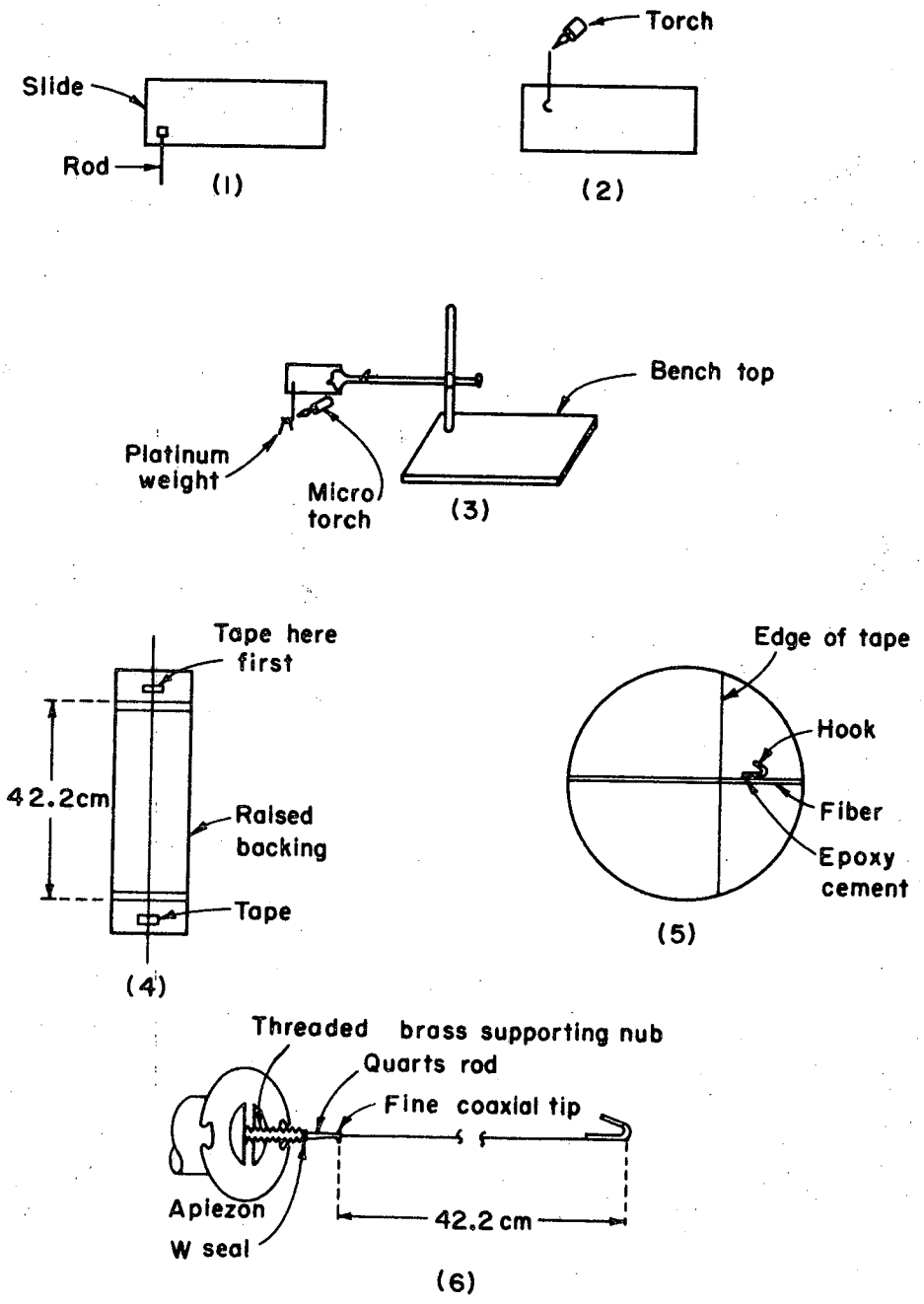

Figure 15. Preparation of the suspension fiber.

8) A sheet of dural is wrapped crosswise with cellophane tape, such that the distance between outer edges is the correct length of fiber to use in the susceptibility apparatus. The taped dural is sprayed with dull black paint, to render the fine fiber more readily visible.

The painted sheet is placed in back of the fiber and the upper end taped down as shown in Fig. 15(4). The fiber is cut with scissors above the tape. The lower end is then taped in place and the fiber cut below the tape.

9) A quartz hook for the lower end of the supporting fiber is prepared from about 6 mm of 50-100 μ diameter quartz fiber. A large hook is first formed and then cut to a short vee of about 3 mm height, by scratching with a carborundum (silicon carbide) chip or diamond-point pencil and breaking with tweezers.

10) The previously drawn fine fiber, mounted on the backing, will not have a uniform diameter, and will usually be finer at the top than at the bottom. The finer end is placed under a binocular microscope, with the backing plate properly supported. One arm of the hook is moistened with a droplet of freshly prepared epoxy cement, and the other arm is held in forceps. The sticky arm is touched to the mounted fiber just beyond the edge of the cross tape as shown in Fig. 15(5). Here a short section of the fiber is raised up out of contact with the backing. The epoxy will hold the hook firmly to the fiber and in a few hours will harden to form a permanent bond.

Care must be exercised, of course, not to cement either the fiber or the hook to the backing plate.

11) After the epoxy is set, the opposite end of the fiber is fastened to the threaded brass supporting nub, at a distance of 42.2 cm from the bottom end of the hook as shown in Fig. 15(6).

This is done as follows: A few chips of black Apiezon are dropped into the hole in the end of the brass supporting nub. A short length of quartz rod which fits snugly into the hole, and which has been drawn to a

fine coaxial tip is pushed into the hole and the nub heated until the Apiezon melts. A small amount of Apiezon is then melted onto the tip.

The upper end of the fine fiber is now cut to the appropriate length (by pressing with a scalpel) and the cut end gently laid on the apiezon-coated tip of the quartz rod.

A quick brush with a cool flame will melt the Apiezon and stick the fiber to the nub (sometimes epoxy cement has also been used to attach the fiber to the nub). The excess fiber below the hook may now be cut off, by pressing with the edge of a silicon carbide crystal. This operation should be performed under the microscope.

Before attempting to move the fiber, a light platinum weight should be fastened to the hook to keep it vertical, otherwise room air currents may literally tie it in knots.

The brass nub may now be raised so that the fiber is in a vertical position. With the lower part of the nub held firmly in forceps, the brass supporting ring is clamped onto the end of the loading rod, and the fiber carefully withdrawn into the loader unit. Before withdrawing the fiber it is cleaned of any dust particles or tiny fibers which may have accumulated on it during preparation. This is done by carefully passing a very fine quartz rod along the fiber several times.

B. Preparation of Sample Containers

Sample containers should be light, strong, and have a low susceptibility which preferably should be temperature-independent. Chemical resistance to 4-6 M HCl in ethyl alcohol is also desirable. Containers made of fused silica or of any of a number of organic polymers satisfy these requirements. Silica tubes have been used throughout the work described here. They are from 0.5-1 mm in diameter and 6-10 mm in length. Larger sizes should be avoided because of the relatively steep force gradients in the magnetic field. The normal weight of the tubes ranges from 900 μg to 8-9 mg.

The tubes are prepared from very thin wall silica tubing of appropriate diameter, previously prepared by hard pulling from clean, light wall tubing of about 1-2 cm diameter.

Before pulling the large tubing it should be cleaned with detergent and distilled water, rinsed with alcohol, and dried.

Care should be exercised to produce small diameter tubing of circular cross section, since this will minimize the problem of rotation in the magnetic field.

The prepared semicapillary is cut into lengths of about 8-10 cm by scratching with a silicon carbide crystal, and then is stored in a closed container.

Tubes are prepared from the semicapillary as follows.

1) A section of the tubing is grasped near one end with cork-tipped forceps while the other end is held by hand.

2) The tube is heated with a microtorch about 1 cm from the forceps-held end, which is merely supported while the tube is rotated within the fingers of the hand.

3) After a section of the tubing has been heated uniformly to incandescence, a quick push with the forceps and a simultaneous pull with the hand will thin the heated section to fiber thickness.

4) The fiber is scratched close to the forceps-held end and broken off. Any hole remaining is sealed by heating the bottom of the 1 cm tube with a microtorch. Heating beyond that necessary to close the hole should be avoided.

5) If the bottom closure is thin and axially symmetric it is satisfactory. If it is considerably distorted it may be rounded by closing the open end with Apiezon wax and heating the closed end with a torch. The increase in pressure inside the tube owing to the heating will suffice to expand the bottom into a hemispherical form. The Apiezon is then dissolved in carbon tetrachloride.

6) The hook for the tube is prepared from a quartz rod of 25-100 μ in diameter. This is done as follows: The tube is placed on a slide in such a manner that about 2 mm of the open end projects over the edge of the slide. About 10 cm of fine quartz rod (25-100 μ diameter as stated previously) is now placed on another glass plate, which is set parallel to the first plate and about 1 cm from it. The quartz rod is moved until it touches the side of the tube about 1 mm from the open end. The quartz rod is heated, very gently at first, then strongly till it fuses to the tube.

The tube is then held in a cork-tipped forceps, and the quartz rod is bent in the form of a vee (sharply bent hook) at a distance of about 3-5 mm from the open end. The free end of the quartz rod is broken off at a distance of about 2-4 mm from the bent place, leaving the tube with the required hook.

Sometimes the hook is made first in the proper vee shape and then fused to the tube by using a Model V water welder manufactured by Henes Manufacturing Company.

After several tubes are made, they are cleaned with 4-6 M HCl by the method of alternate boiling and cooling. Finally the tubes are boiled in conductivity water and allowed to cool. After drying they are stored in a well-cleaned small screw-capped vial.

C. Filling Sample Containers

A piece of lucite block about 2-3 cm in length and 1-2 cm in width is prepared with several holes of different sizes. The lucite block is cleaned by washing with concentrated HCl and then water.

The sample container of known tare weight is placed in one of the holes, which will keep it in a vertical position.

For filling the containers with non-radioactive samples like nickelous ammonium sulphate, a microspatula made of platinum wire is used. The transfer is usually not quantitative since some of the powder stays

on top of the opening of the tube. This is removed by shaking the tube and brushing it with a small clean camel-hair brush.

The cleaned tube is weighed on the submicrobalance to determine the weight of the material within ± 0.1 μg. After it is weighed, the tube is placed in a clean hole in the lucite block to be ready for loading in the apparatus.

For radioactive samples the following procedure is used: The lucite block is stuck firmly onto an ice-cream carton lid by using double-face tape. The sample tube is placed in a closely but gently fitting hole in the lucite block. The carton lid is covered and introduced into the Berkeley piano box. The lid with the lucite block and tube is placed on a microjack. The microscope on top of the box is adjusted so that the tube opening is clearly seen. The sample chunk is then picked up with either gold-tipped forceps or a fine tungsten needle, under a microscope. Normally the metal chunk will stay on one arm of the forceps when the jaws are released. The tip of the jaw holding the sample is introduced into the tube, and touched to the side of the tube. The sample will then fall into the tube and settle in the bottom.

A powdered radioactive substance like PaF_4 is loaded in the tube through a microfunnel which in turn is introduced into the tube with the help of a micromanipulator. (Needless to say all of this operation is done under a microscope in a glove box.)

Extra care must be taken not to touch the tube from outside at all when filling containers with radioactive substances.

Now the lid containing the lucite block is covered and transferred to the loading box to be ready for loading.

D. Loading of the Apparatus

The loader unit used is sketched in Fig. 16. It consists of an outer lucite tube of about 85 cm length and about 9-10 cm diameter, and an inner concentric tube of about 70 cm length and 4-5 cm diameter. The lucite tubes are sealed together with two lucite plates, one at the top and the other at the bottom. An aluminum rod of about 100 cm length, which is fitted with a clamping arrangement to hold the brass ring of the apparatus, can to in and out the inner tube.

For loading a cold sample the aluminum rod is lowered until the hook of the fiber is in a position which can be easily reached. The lucite block which holds the sample tube is brought underneath the hook of the suspension fiber and the hook of the sample tube is engaged to the hook of the suspension fiber. The lucite block is pulled down slowly, leaving the sample tube hooked to the fiber. The fiber is withdrawn inside the loader unit and its door is closed.

The entire loader unit is then placed on top of a specially designed glove box, which is shown in Fig. 17, having a sliding window arrangement. The loading tube assembly of the susceptibility apparatus is placed on a platform attached to the loading box. Now with the help of the sliding window arrangement the loader unit is brought onto the top of the loading tube assembly of the apparatus and the fiber is lowered slowly until the brass ring supporting the fiber settles into proper place. The brass ring is unclamped from the aluminum loading rod and finally the aluminum rod is pulled inside the loader unit. The two brass screws which hold the brass ring in place are tightened, and the opening of the loading tube assembly of the apparatus is covered with its quartz disk.

For loading an active sample, the same procedure is followed except that hooking the sample tube to the suspension fiber hook is also done inside the loading glove box. The only thing of importance here is that a blank tube or some other weight must be hung on the fiber hook before its introduction into the box, to prevent blowing of the fiber and sticking to

the side of the box. The normal high velocity air flow in the box is interrupted during loading.

Finally it is worth mentioning here the problem of electrostatic charge encountered in loading and unloading the fiber. The inner tube of the loader unit has been coated with an antielectrostatic spray. Even then it very often gets electrified and pulls the fiber to the side, creating a very unhappy situation. For the same reason the quartz tube of the loading tube assembly (L, in Fig. 10) is furst coated with tin oxide to make it conducting and then sprayed with antistatic solution. No sure way of getting rid of the electrostatic problem has so far been achieved.

E. Observing the Sample and Its Positioning with Respect to the Magnet Pole Pieces

The front surface mirror with a hole in its center is adjusted on top of the loading tube assembly of the apparatus, and the sodium lamp which illuminates the sample from above is turned on. By looking in the telescope, the image of the sample tube can be seen. The telescope is then adjusted to the best possible focus; the filar micrometer is adjusted and the zero point chosen.

While looking in the telescope, the operator turns on the magnet current, and the deflection of the sample is observed. If there is any rotation the position of the sample is changed by rotating the nub which supports the fiber, in a direction opposite to that of the sample rotation. This game is played until the sample is free of rotation in the magnetic field.

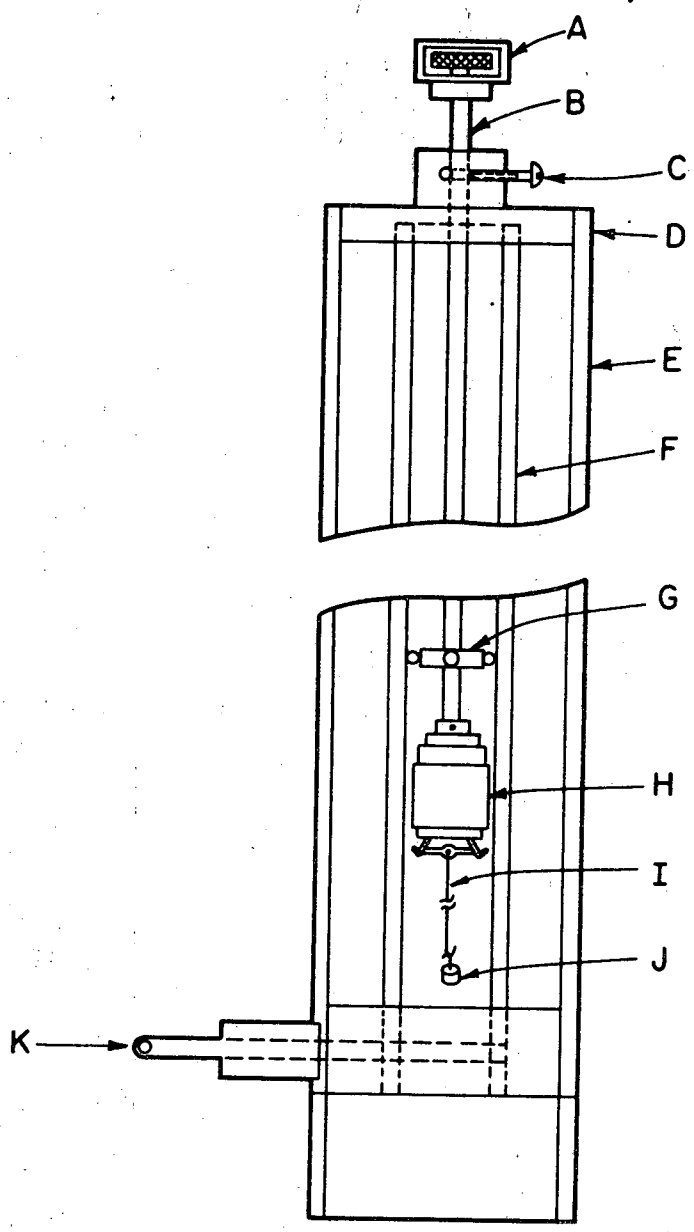

Figure 16. Loader unit of the magnetic susceptibility apparatus.

Legend for Figure 16

A. Screw for operating clamping and unclamping attachment
B. Aluminum rod
C. Screw for holding loading rod in position
D. Top plate
E. Outer tube
F. Inner concentric tube
G. Circular disk with points
H. Clamping and unclamping arrangement for support of fiber attachment
I. Suspension fiber
J. Sample tube
K. Sliding door

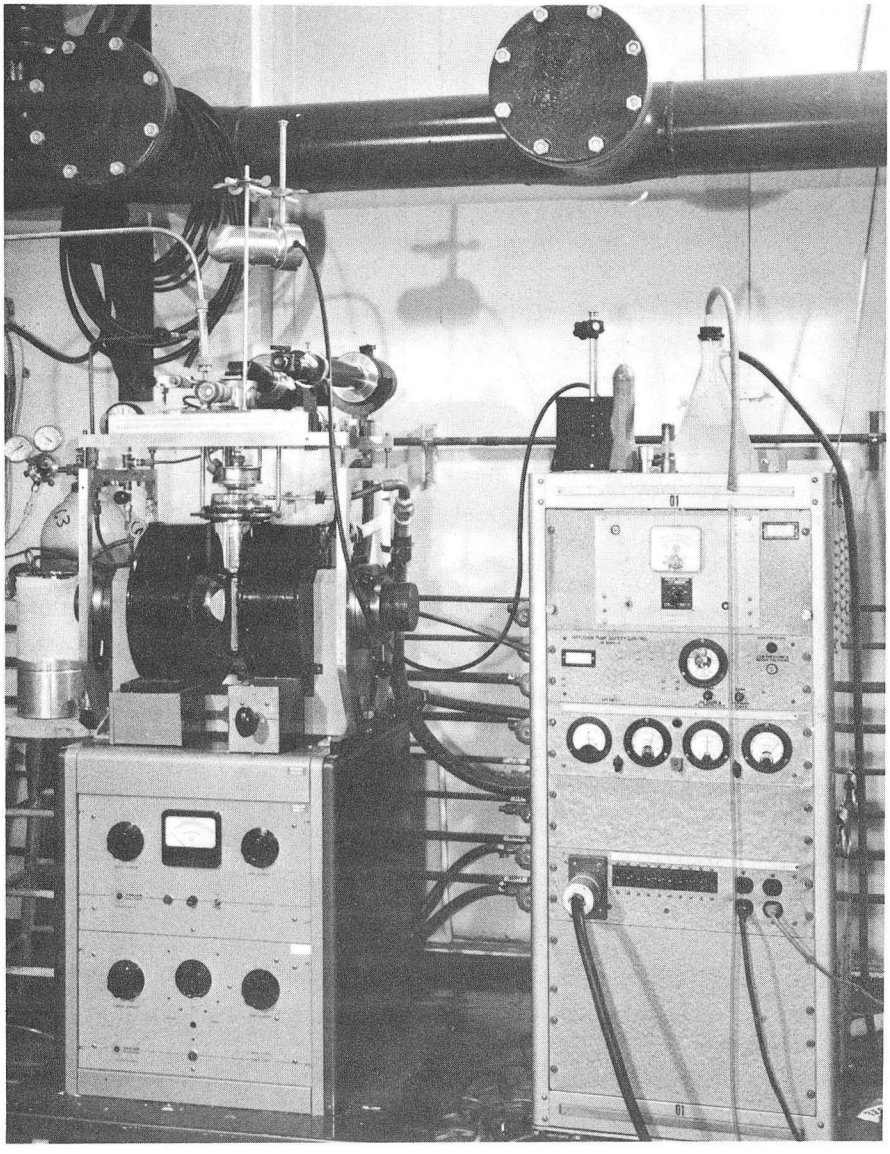

ZN-5500

Figure 17. General view of loading glove box with the loader unit and the loading tube assembly in their respective places.

F. Evacuation and Flushing of the Sample Tubes

After adjusting for rotation, the quartz disk cover of the loading tube assembly is firmly placed on its opening and the assembly is evacuated. The evacuation must proceed slowly in order not to disturb the sample. The assembly is now flushed with helium gas which has been passed through a liquid nitrogen trap. This process of evacuating and flushing is repeated three or four times. After being thoroughly flushed with helium, the assembly is filled with about 1/3 atm of helium. Now everything is all set for taking the measurements.

G. Making Deflection Measurements

The deflection is measured by a null method. First the micrometer reading is taken with the current off, and then the current is turned on and the image of the sample tube is brought to the same position that it occupied with the current off, and the new reading of the micrometer is taken. The difference between the reading with the current on and the reading with the current off gives the deflection at that particular current setting. Three or four deflection measurements are carried out at each of several current settings for each temperature. The same procedure is repeated for another set of measurements at a different temperature.

H. Unloading the Apparatus

After all the measurements at different temperatures are taken, the sample is unloaded. The unloading process is almost the reverse order of the loading. The active samples are stored in the loading box.

V. PREPARATION OF MATERIALS

A. Preparation of Curium Metal

The preparation of pure, well-crystallized lanthanide and actinide metals has proved to be a formidable task. The heats of formation of their compounds are quite high, and consequently, attempts to make the metals by classical techniques have failed. Trombe[19] has written an excellent review of the history of the rare earth metals. He points out that these metals are very reactive and that it is even difficult to find suitable materials for making the crucibles. During World War II exhaustive studies were made on the preparation of plutonium metal. The methods devised in the Metallurgical Laboratory of the Manhattan Project have been summarized by Fried et al.[20] They centered around the reduction of an actinide fluoride with an alkali or alkaline earth metal. The reductions were carried out in a double crucible system made of a refractory oxide such as beryllia or thoria, and the crucible system was heated in vacuum by resistance heating.

The preparation of curium metal (using Cm^{242} isotope) on the microgram scale was first carried out by Wallmann, Crane, and Cunningham[21] by reducing CmF_3 with barium vapor at 1275°C. They used a double crucible system in a high vacuum similar to that described by Fried and Davidson.[22] The quantities so prepared were rather small, being on the order of 4 μg or much less. However, the metal upon observation was silvery in appearance and about as malleable as plutonium prepared under the same conditions. The metal retained its bright appearance in the dry box for several hours but gradually tarnished, and on standing for about 24 hr it was rather badly corroded. Under the same conditions samples of other actinide metals, such as americium or plutonium, have shown less evidence of reaction. The greater reactivity of the curium metal may probably be attributed to self-heating by α-decay of Cm^{242} (equivalent to a power output of 1.2×10^{-4} W/μg). A sample of Cm^{242} metal, even though it is only partially isolated from its environment, may reach high temperatures, which could account for its rapid corrosion rate.

Wallmann and Cunningham[23] indicated in their work that these methods were seldom successful more than 50% of the time, because the product often soaks into the refractory oxide crucible. As a result of their experiments they suggest using an all-tantalum double crucible system and a wet-precipitated fluoride of the actinide of interest. This type of crucible system leads to more reproducible reduction conditions. They also find it more convenient to use induction heating.

McWhan, Cunningham, and Wallmann[23] described in detail the preparation of americium metal by the reduction of dry AmF_3 with barium metal, using an all-tantalum double crucible system.

Cunningham and Wallmann[24] prepared curium metal (using Cm^{244} isotope) for their crystallographic studies using barium metal as a reductant for CmF_3, which was obtained by wet precipitation of curium in 1 M HCl with vapor-equilibrated HF and then stored over P_2O_5.

Lowenhaupt and Cunningham[25] investigated the oxygen and carbon content of the rare earth metals (using mostly ytterbium metal as a stand-in) produced by reduction of their respective trifluorides with barium vapor in order to determine the ability of some drying techniques to remove oxygen and carbon from the trifluoride. They used an activation analysis technique[26,27] employing He^3-induced nuclear reactions for determining oxygen and carbon contents of these metals. They concluded that metal produced from untreated trifluoride contain about 6000 ppm oxygen, whereas the metals produced from trifluorides treated with anhydrous HF gas were found to contain as little as 300-400 ppm oxygen.

In attempting to get curium metal with low oxygen content the CmF_3 chunks were treated with anhydrous HF gas. The procedure will be described in more detail a little later. Starting from CmF_3 chunks obtained after anhydrous HF treatment, the metal was prepared by following the procedure of Cunningham and Wallmann.[24] However, a brief discussion of the variables which will affect the preparation of good metal will be given. The variables that will be considered are:

a) choice of reductant metal

b) physical form and treatment of starting materials

c) type of crucible system

d) reduction temperature and duration of reduction

e) method of heating.

a) Choice of reductant metal

The reaction used to prepare curium metal is

$$CmF_3 + (3/x)M = Cm + (3/x)\,MF_x \quad .$$

From the reaction, it is clear that the choice of the reductant metal is limited mainly by two factors.

1) The ΔF for the reaction must be thermodynamically favorable;

2) The vapor pressure of the reductant metal must be sufficiently high to permit vaporization of the excess in a reasonable time without a substantial loss of curium.

Lithium, calcium, and barium are among some of the possible reductants that satisfy these criteria in the case of curium and protactinium metals. The choice among them is somewhat arbitrary. If lithium is used, the lithium fluoride formed in the reaction vaporizes along with the excess of lithium, leaving only curium metal as the product. However, if barium or calcium is used, the barium fluoride or calcium fluoride slag provides a protective coating against surface reactions with the residual gases in the system during annealing, and tends to isolate the product from the crucible, making removal of the product easier. Moreover, even a small weight percent of light elements may constitute a high mole percent impurity [0.01 wt% Li = 0.34 mole%; 0.1 wt% Ba = 0.17 mole% (in curium)]. As the purity of the metal is of prime importance, barium is used preferentially as the reductant metal throughout all metal preparations.

b) Physical form and treatment of starting materials

The first problem in the preparation of curium trifluoride is that of insuring its freedom from cationic impurities. Because of the scale on which this work had to be done, ordinary reagents were not pure enough. The Cm^{244} used in this study was obtained from neutron irradiation of Pu^{239} and was contaminated with rare earths, other actinides, and fission products, etc. The primary separation of the actinides from reactor products was carried out in a water-shielded cave, using well established procedures.[28] Final separation of curium from other actinides (chiefly Am), rare earth elements, and common impurities such as Al, Fe, Ca, and Mg was achieved by using ion-exchange techniques, discussed in detail by Higgins.[29] The ion-exchange techniques used in this study are essentially those which have become more or less standard in actinide purification chemistry. The most significant differences that do occur are in scale and in the precautions taken to maintain high purity with respect to background contaminants. The various ion-exchange columns used and their purposes are summarized in Table I.

For the initial purification, the reagents were prepared from stock C.P. chemicals. The only exception to this were water and α-hydroxy isobutyric acid, "but". The water was the one redistilled material derived from the continuous overflow from the two-stage quartz still used for the preparation of high purity water. The "but" was prepared by dissolution in pure water, filtration, and partial recrystallization.

In the final purification the only reagents required were water and various HCl solutions. The high purity quartz distilled water used in this work was supplied by Dr. Maynard Michel of this Laboratory. The technique used for its preparation has been discussed elsewhere[30]; however, for the sake of completeness, the purification procedure will be briefly described here.

The starting material is ordinary distilled water. This is passed through a 1.5 in. diameter by 3 ft long mixed resin ion-exchange column

Table I. Summary of ion-exchange columns.

1. Alcoholic HCl column

Purpose: Actinide-lanthanide group separation.

Resin: Dowex 50 × 4; H^+ form washed with load acidity.

Temperature: Room temperature.

Load: 0.5-0.1 M HCl (load volume can be large—many FCV)

Elution behavior: First add 2-3 FCV of 2 M HCl to partially shrink the resin (this moves the transcurium elements slightly down and decreases the penetration due to the resin shrinkage). Then elute with 20 V% EtOH-HCl gassed up (12.5 M HCl) in ice until no heat is liberated and then allowed to equilibrate back to RT. Elution rate 200λ/cm^2/min. Actinides elute after 3 FCV of EtOH-HCl, well ahead of R.E., ytterbium being first to follow. The elution sequence is in the order of decreasing atomic number.

Remarks: HCl must be saturated.

2. Anion clean-up column

Purpose: Iron and Pu^{240} (daughter of Cm^{244}) clean-up.

Resin: Dowex 1 × 8, treated with 8 M HCl.

Temperature: Room temperature.

Load: 8 M HCl.

Elution behavior: Elute with 8 M HCl. The actinides and lanthanides virtually wash through but the Fe^{+3} and Pu^{+4} chloride complexes are held very tightly at the top of the column.

Remarks: Make sure that iron and Pu are present as Fe^{3+} and Pu^{4+} respectively.

(continued)

Table I. Continued.

3. $LiNO_3$ column

Purpose: Am-Cm separation.

Resin: Dowex 1 × 8, pretreated with load solution.

Temperature: Room temperature or 87°C. The column is ≈50% faster at high temperature.

Load: 10 M $LiNO_3$ - 0.005 M H^+.

Elution behavior: Elute with 4.2 M $LiNO_3$ - 0.005 M H^+. Elution order is that of decreasing atomic number.

Remarks: Low acidity is essential.

4. "but" column

Purpose: Individual actinide separation.

Resin: Dowex 50 × 12, NH_4^+ form.

Temperature: 85°C.

Load: 0.05 M HCl (minimum volume).

Elution behavior: Elute with 0.4 M α-hydroxy isobutyric acid "but" at pH 4.2-4.6.

Remarks: Very tricky to run; "but" concentration and pH are quite critical.

5. "but" clean-up column

Purpose: To remove "but".

Resin: Dowex 50 × 4.

Temperature: Room temperature.

Load: Cm fraction obtained from "but" column was brought to pH ≈3 with 1 M HCl and enough excess HCl was added to give 0.05 M free HCl.

Elution behavior: Elute with 1.5 M HCl.

(continued)

Table I. Continued

6. Clean-up column

Purpose: Separation of actinides from general inorganic crud like Ca, Sr, Al, Ba, Mg, etc.

Resin: Dowex 50 × 4.

Temperature: Room temperature.

Load: 0.5-0.1 M HCl.

Elution behavior: Elute with 2 M HCl until first indication of activity; then remove excess of 2 M HCl from the top of the column, and finally strip Cm with 6 M HCl.

Remarks: The activity should not be stripped with 6 M HCl too early; Ca, Sr, Al, and Ba elute only shortly before the actinides peak. Use of the 6 M strip will carry any Zr^{+4} in the feed into the product unless a close post-actinide cut is made.

constructed completely of polytetrafluoroethane (Teflon). The effluent from the column is continuously introduced, via polypropylene tubing, into the first stage of a two-stage continuous quartz still. Both stages operate with a continuous overflow to avoid concentration of contaminants in the boilers. The overflow from the second stage is the source of intermediate-purity water (conductivity water) mentioned above. The condensate from the second stage is piped through polypropylene to specially prepared polyethylene containers for storage. A typical spectrographic analysis of the product is shown in Table II.

High purity HCl solutions were prepared by two different techniques. Firstly, quartz distilled water was vapor-equilibrated with five-fold excess of 12 M HCl (150 ml of quartz distilled water in a specially cleaned polyethylene bottle, the so-called product vessel equilibrated with 750 ml of 12 M HCl). The spectrographic analysis of this HCl is shown in Table II. Secondly, some of the high purity HCl was supplied by Dr. Jere Green from a stock which he prepared for his californium work. The technique used for its preparation has been discussed in his thesis[31]; however, for the sake of completeness, the purification procedure will be briefly discussed here.

Room temperature saturated HCl was prepared by the treatment of quartz distilled water, contained in a specially cleaned polyethylene bottle, with purified anhydrous HCl gas. The source of the HCl gas was preparative grade tank HCl which was allowed to flow slowly through a Pyrex entrainment trap, a Pyrex prebubbler containing saturated HCl solution, and finally through a second Pyrex entrainment trap and a leached quartz wool plug filter. All lines between the quartz wool filter and the bubbler tube were made of leached quartz tubing. The spectrographic analysis of this acid is also shown in Table II. Various HCl solutions were made by dilution with quartz distilled water in specially cleaned polyethylene bottles.

Table II. Spectrographic analysis results[a] of quartz distilled water and HCl in μg per 500 λ of water and HCl.

	Al	Be	Ca	Co	Cr	Fe	Mg	Mn	Ni	K	Na	Si
Quartz distilled water	<0.01	<0.01	<0.01	<0.05	<0.01	<0.01	<0.01	<0.01	<0.01	---	---	---
HCl from vapor equilibration	<0.01	<0.01	~0.01	<0.05	<0.01	<0.01	<0.01	<0.01	<0.01	---	---	---
HCl made on bubbler system	<0.01	---	<0.01	<0.05	<0.01	---	<0.01	<0.01	<0.01	---	---	---

[a]Limits of detection by the copper spark method are given in Table III.

Table III. Limits of spectrographic detection by the copper spark method for common impurities expressed in micrograms.

0.01 μg	Al, Be, Ca, Cr, Eu, Fe, La, Mg, Mn, Mo, Nb, Si, Sr, Ti, Yb, Y, Zr.
0.05 μg	Bi, Co, Ge, In, Ni, Sm, V.
0.1 μg	Ce, Nd, Pb, Pt, Sn, U, W, Zn.
0.5 μg	Cd, Ir, Sb, Th.
1 μg	K, Li, Na, Np, Pu.

All the quartz cones, polyethylene pipettes and containers, etc. used in this work were the ones which had been leached with concentrated HCl for a long time and then rinsed with conductivity water and finally with quartz distilled water.

In this way very pure solutions of Cm were obtained.

Curium trifluoride was precipitated from the curium solution in HCl by the addition of excess aqueous hydrofluoric acid (obtained by vapor equilibration of quartz distilled water in a specially cleaned polyethylene container with five- to seven-fold excess of commercial concentrated HF solution) to make the final solution approximately 2 M in HF. The precipitation was carried out in a specially clean polystyrene centrifuge cone. After being centrifuged, the precipitate was washed two times with about 40 times its volume of quartz distilled water and two times with similar amounts of absolute ethyl alcohol. It was then allowed to air-dry by leaving the cone open to the atmosphere. Upon drying, the trifluoride compacted into a few small pieces of hard translucent material of porcelain-like appearance. It is worthy of note that the trifluoride should be obtained in the form of compact chunks rather than in the form of powder: first, because powder material will not yield a single globule of well agglomerated metal at ordinary reduction temperature; and, second, to maintain ease of loading in the crucible system. This material presumably is hydrated, since air-dried aqueous precipitates of PuF_3 have been shown[32] to contain chemically bound water.

The trifluoride chunks so obtained in the previous operation were transferred to a platinum crucible and dried for 6 to 7 hr in a stream of anhydrous HF gas at about 600°C. Pure HF was obtained by thermal decomposition of $NaHF_2$, treatment of the condensed HF with a small amount of elemental fluorine, and subsequent double distillation. Finally the fluoride chunks were transferred to a small quartz container and stored in a microdesiccator over phosphorous pentoxide.

c) Type of crucible system

Ideally, the crucible system should fulfill the following requirements:

1) be unreactive
2) yield reproducible effusion conditions
3) keep solid reductant metal from contacting the fluoride
4) be easy to load
5) permit easy removal of the product.

As mentioned previously, double crucible systems made either from refractory oxides or tantalum have been used successfully in metal preparation. Refractory oxide systems have the disadvantage that they must be fired at 1600-1800°C for several hours in order to harden and degas them. The effusion orifice is not reproducible, and it is difficult to estimate the rate of effusion of the excess reductant and consequently the reduction time. The porosity of the refractory inner crucible is variable. The metal often soaks into the crucible. As a result of these difficulties tantalum crucibles have been used in all the reductions.

Tantalum has the disadvantage that it is wet by curium metal, and molten curium dissolves appreciable amounts of tantalum. Therefore, a small conical spiral of 3 mil tungsten wire has been used to hold the chunk in the tantalum crucible in order to minimize the tantalum surface exposed.

A drawing of the entire reduction system is given in Fig. 18. It consists of an all-tantalum double crucible system [Fig. 18(b)] suspended inside a cylindrical induction shield made of 2 or 4 mil tantalum sheet. Inside this inner tantalum crucible is placed a stand made of tantalum foil fitted with a small conical spiral of 3 mil tungsten wire which receives the fluoride chunk. The use of a spiral in place of the tantalum basket employed by McWhan and co-workers[2] is a decided improvement, since much less wire is exposed for the product metal to wet. The crucible cap is pierced with a small effusion hole of about 1/3-1/2 mm

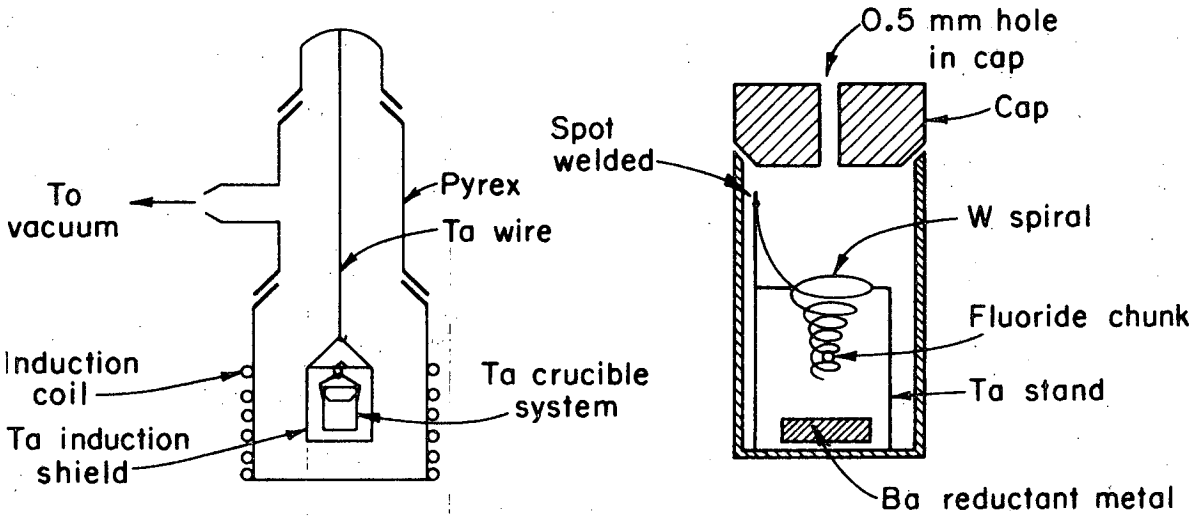

Figure 18. Fluoride reduction apparatus.

(a) Ta crucible and induction shield suspended in high vacuum line.

(b) Ta crucible and stand containing W-spiral and Ba metal.

diameter through which the barium reductant and BaF_2 effuse. An arm of a high vacuum line is surrounded with an induction coil, in the center of which are suspended the crucible and shield. The size of the hole drilled in the cap of the crucible can be adjusted to fit the desired duration of reduction at the chosen reduction temperature. The rate of effusion from a crucible can be estimated from Knudsen conditions by the equation

$$R(\text{moles/min/mm}^2) = 3.5 \times 10^{-2} P_{mm}/MT ,$$

where R is the rate of effusion of a gas from the orifice in moles per minute per mm^2 of orifice area, P is the vapor pressure of the curium or barium, M is the molecular weight, and T is the absolute temperature. (As the system does not match ideal conditions for Knudsen effusion, the actual effusion will be slower than the above estimate.) An effusion hole of about 1/2 mm is convenient for most reductions.

d) Reduction temperature and duration of reduction

The reduction temperature is critical. If it is too low, the resulting metal is powdery; if it is too high, the metal vaporizes.

The reduction time is dependent on the temperature, size of the crucible orifice, and amount and nature of excess reductant. In all the reductions of CmF_3, metal of good appearance was obtained in high yield by maintaining a reduction temperature of about 1320 to 1360°C for 2 min. Additional heating for 3 to 4 min at about 1230°C served to remove excess barium as well as the barium fluoride slag. Finally the metal was annealed for 1 min at about 1100°C in order to get well-crystallized metal.

No detectable loss of curium from the crucible system was observed under these conditions.

Elemental curium prepared as described exhibited a bright silvery surface which did not tarnish readily when exposed to air. The reductant metal Ba was not detected in any of the curium metal preparations.

e) Method of heating

Three methods of heating can be used with varying degrees of success:

1) electron bombardment

2) resistance heating

3) induction heating.

The choice among them is mainly one of convenience and reproducibility. Electron bombardment is the most efficient, but the measurement of the temperature with an optical pyrometer is uncertain because of reflection from the filament and the emissivity correction that has to be made. Far more important is the difficulty of controlling the temperature because of the arcing that occurs when excess barium effuses from the crucible.

Resistance heating is inefficient, but it provides good temperature control from the reduction temperature to room temperature. As with electron bombardment, the effusion of the excess barium can be followed by its green glow. This method has two disadvantages: first, the coil is fragile, and second, the tantalum crucible has to be insulated from the heater.

The induction heater provides accurate temperature control, permits accurate temperature measurements, and is easy to use. In all the reductions the blank tantalum assembly was degassed at >1000°C for 20-30 min or until the pressure fell to less than 10^{-6} mm Hg. (Besides degassing, this served to volatilize copper deposited during spot welding of the tantalum components.) This step is necessary since otherwise the copper condenses on the walls of the vacuum system during temperature calibration and would lead to an error in the temperature measurement if not removed beforehand. Since the power required to bring the crucible to a certain temperature varies with the orientation of the crucible, shield, and induction coil, an empirical correlation must be established between the current reading of the power generator and the temperature of the crucible, as observed under black body conditions with an optical pyrometer through a hole in the shield. This calibration was performed before each trifluoride reduction.

After cooling, a piece or several pieces of CmF_3, depending upon size, were placed in the tungsten spiral attached to the stand. Enough freshly cut barium metal (sufficient to provide about a ten-fold excess over that required for reduction) was dropped into the bottom of the crucible. The crucible, stand, cap, and induction shield were reassembled and taken as quickly as possible to the high vacuum line, in which they were calibrated, and the system was evacuated as quickly as possible to avoid reaction of the barium with the atmosphere. Pumping was continued until the pressure in the line fell to less than 10^{-6} mm Hg. Now the reduction was carried out using the following "heating sequence":

1) An initial outgassing by gradual increase of temperature to about 300°C. This was performed after the system had reached about 5×10^{-7} mm Hg or less. After outgassing, the pressure was again allowed to drop to the starting pressure.

2) Heated for about 2 min between 1320 and 1360°C for reduction.

3) Additional heating for 4 min at about 1230°C was done to remove excess barium and BaF_2.

4) Annealing for 1 min at about 1100°C was performed to get well-crystallized metal.

Finally the entire system was cooled under vacuum overnight, the stand containing the spiral and curium metal was taken out, and the metal was removed from the spiral.

Purity of curium metal: Samples of the curium metal from each reduction were analyzed by spectrographic emission analysis, using copper spark excitation. The spectrographic results for all the samples are shown in Table IV. The limits of detection by this method have already been tabulated in Table III.

A few micrograms of metal from each reduction were loaded into thin-wall quartz capillaries and the diffraction pattern was obtained with a Jarrell-Ash Model 80-010 microfucus x-ray unit, using the vertical tube, Y27 and a horizontal line filament cathode, Y37 in conjunction with a

Table IV. Purity of curium metal.[a]

Sample no.	Spectrographic results	X-ray results
1.	Nothing was detected except Ca (≈0.01 μg Ca in 40 μg of Cm). This amount of Ca is about the same as in blank (see Table II).	X-ray diffraction pattern was identified by comparing with Wallmann's dhcp structure film of Cm metal.
2.	"	X-ray film identified
3.	Nothing was detected except Ca (≈0.02 μg Ca in ≈50 μg of Cm); a little more than the amount of Ca in blank.	"
4.	"	X-ray film identified and lattice parameters calculated.
5.	Nothing was detected except Ca (≈0.01 μg Ca in ≈50 μg of Cm); same as in blank.	X-ray film identified.

[a] Ba was specially looked for in spectrographic analysis but was not detected in any sample.

Norelco 57 mm diameter camera. X-ray results are also included in Table IV. From sample no. 4 a very good diffraction pattern was obtained (including high angle lines and $K\alpha_1$, $K\alpha_2$ resolution); therefore, the lattice parameters were calculated by using a least-squares analytical treatment, programmed into a computer by Mueller and Heaton.[33] Observed intensities were compared with calculated values obtained from a 7090 computer, using the intensity program of Smith.[34] Curium metal showed a double hexagonal close-packed structure similar to α-lanthanum and the lattice parameters so obtained are:

$$a = 3.497 \pm 0.003 \text{ Å}$$
$$c = 11.335 \pm 0.005 \text{ Å} \quad .$$

These lattice parameters agree very well with those published by Cunningham and Wallmann.[24] We were able to index all the lines as dhcp except one which could not be identified with certainty. Most probably it may be indexed as fcc due to CmO.

Mass analysis showed the isotopic composition of the curium used in this work to be: Cm^{244}, 96.59%; Cm^{245}, 1.59%; Cm^{246}, 1.82%.

B. Preparation of Protactinium Metal

Grosse and Arguss[35] obtained protactinium in its elemental state for the first time by: 1) bombarding the pentoxide with 35 kV electrons and 2) decomposition of the pentachloride on a hot filament. The preparation of protactinium metal by reduction of the tetrafluoride (PaF_4) with barium at 1400°C was later described by Sellers, Fried, Elson, and Zachariasen[5] in 1954.

The protactinium metal used in this work was the one prepared by Professor B. B. Cunningham for his crystallographic studies and melting point determination. Some of the properties of protactinium metal, like crystal structure, melting point, and magnetic susceptibility have been

reported by Cunningham.[7] The protactinium metal was prepared as follows. Purification of Pa_2O_5: The starting material for the various preparations of protactinium metal was the impure oxide stock. The purification of the impure oxide was achieved by two separate schemes. The first batch of Pa_2O_5 was known to contain several weight percent of niobium. The procedure used to remove niobium is described as follows.

The pentoxide was dissolved in hydrofluoric acid and the protactinium was precipitated as K_2PaF_7 by the addition of two moles of potassium fluoride per mole of protactinium. The precipitate was collected by centrifugation, and after removing the supernatant liquid the compound was dissolved in a minimum volume of hot (85°C) 5% hydrofluoric acid. Needle-like crystals of dipotassium protactinium hepta-fluoride were obtained on cooling. This step of crystallization from 5% hydrofluoric acid was repeated. The recrystallized heptafluoride so obtained was then dissolved in hot concentrated sulfuric acid. The concentrated sulfuric acid solution was diluted to 6 N and protactinium iodate precipitated by the addition of a slight excess of iodic acid. The iodate precipitate was collected by centrifugation and then dissolved in 12 M hydrochloric acid. On heating the hydrochloric acid solution, the protactinium oxide precipitated slowly. The oxide was washed with 6 M HCl and then dried slowly under an infra-red lamp, to form a few hard coherent flakes. Spectrographic analysis of a portion of this oxide showed niobium to be below the limit of spectrographic detection (less than 0.2%).

Subsequently, another batch of Pa_2O_5 (≈40 mg) was purified by double precipitation as K_2PaF_7, dissolution of the double fluoride in 2.5 M HF, precipitation of the hydroxide by exposure of the HF solution to excess NH_3 gas, washing with dilute ammonia, and slow drying of the hydroxide in a polyethylene cone at 85°C.

On drying, the hydroxide shrank to form a single hard pellet, which was readily detached from the walls of the cone.

Spectrographic analysis of the solution of protactinium in 2.5 M HF had shown the niobium to be below the limit of detection. The only impurity detected was 0.3% Ca.

Protactinium tetrafluoride: Protactinium tetrafluoride was prepared essentially according to the method of Stein,[36] by treating the purified oxide first in a stream of hydrogen for 15 min at 600°C, and then with an equimolar mixture of pure hydrogen and HF gases for 30 min at the same temperature. Pure HF was obtained as mentioned previously by thermal decomposition of $NaHF_2$, treatment of the condensed HF with fluorine, and subsequent double distillation.

The tetrafluoride obtained from the first batch (≈10 mg) of oxide was a deep chocolate brown in color. Coherence of the original oxide flakes had been largely maintained, so that the tetrafluoride could be readily handled with forceps.

Hydrofluorination of the 40 mg oxide lump yielded a product of quite different physical appearance. The dark brown fluoride was disposed in the form of a continuous layer adhering to the sides and bottom of the platinium crucible. Unfortunately, the recovery of the bulk of the material in the form of sizeable chunks (as desired) could not be effected because of its strong adherence to the crucible surface. It was removed essentially as a fine powder.

PaF_4 gave an extremely complex x-ray diffraction pattern, which seems to resemble closely that of ThF_4. Therefore the PaF_4 so obtained was isostructural with ThF_4.

Protactinium metal preparation: Chunks of PaF_4 as obtained by the hydrofluorination of the first batch of oxide were reduced with barium metal vapor at temperatures between 1300-1400°C. The reductions were carried out in an all-tantalum double crucible system, using a 3 mil tungsten wire spiral for holding the chunk, exactly of the same type as used for the preparation of Cm metal described in detail in the previous section. Good protactinium metal was obtained under these conditions.

The compact metal was quite soft and its surface could be cleaned readily by scraping with a scalpel blade. The freshly exposed surface was silvery in appearance, but became darker rather quickly on being exposed to air. Subsequent oxidation proceeded slowly, however, and pieces of metal exposed to air for a period of a week showed only superficial oxidation.

Two attempts were made to prepare protactinium metal from the powdered fluoride at a reduction temperature of ≈1400°C; small thoria crucibles were used to contain the powder.

The first attempt was successful, yielding about 2 mg of Pa metal in the form of a thin sheet extending across the bottom of the crucible. The product was soft and malleable, similar to the metal produced previously. Spectrographic analysis of a 10 μg sample from this metal detected no impurities.

Another attempt was made to reduce the PaF_4 powder in a very tightly wound 3 mil tungsten wire spiral, but unfortunately the metal was found to spread over and between the tungsten coils, and was not recoverable in any useful form.

Finally, in an attempt to make a pellet from the powdered PaF_4, a pellet press was made by drilling 1/16-in. holes in 1/4-in. tungsten plate; a tungsten plug (1/8 in.) and plunger (3/4 in.) were made from a tungsten rod. A fairly good pellet was obtained by pressing PaF_4 powder in the above mentioned press, using a small vise. Ninety percent of the powder (estimated only) was recovered in pellet form. The pellet was crumbling somewhat on one side and the excess powder material was stored in a capillary under vacuum. Reduction of this PaF_4 pellet gave good results, but unfortunately the tungsten wires seemed quite well imbedded in the Pa metal.

The excess of the powdered PaF_4 recovered during pellet formation was loaded for susceptibility measurements but was found to be highly contaminated with ferromagnetic impurities. These impurities were obviously picked up during pelleting. Therefore another batch of protactinium was

cleaned for making some more PaF_4; we hoped it would be in the form of chunk, for susceptibility measurements. This purification will be described shortly.

The protactinium metals so obtained, as reported by Cunningham,[7] gave good x-ray diffraction patterns. He observed diffraction lines from both PaO and PaO_2, but the remaining lines he was able to index according to a body-centered tetragonal structure, in agreement with the earlier work of Zachariasen.[37] The lattice parameters, derived from a least-squares fit of the diffraction data are $a = 3.929 \pm 0.003$ Å and $c = 3.241 \pm 0.004$ Å at room temperature.

Finally another batch of about 50 mg of protactinium, which was known to contain several grams of cerium, was purified as follows.

The solid cake containing Ce, Pa, and other common impurities was dissolved partly in 10 M HNO_3 and 0.01 M HF, and the remaining solid residue was cooked with concentrated H_2SO_4 to dryness and picked up in 10 M HNO_3 + 0.01 M HF solution. From the solution so obtained, Ce and Pa both were precipitated as hydroxides by using concentrated aqueous ammonia. It may be worthy of mention that protactinium polymerizes around pH 7 (neutral solution), so first the acid was neutralized slowly by adding small amounts of ammonia at a time and then immediately a large excess of ammonia was added in order to avoid neutral medium as far as possible. The hydroxide precipitate was collected by centrifugation, the supernatant liquid removed, and the precipitate washed with conductivity water.

The hydroxide precipitate was then dissolved in 10 M HNO_3 containing 0.1 M $KBrO_3$. From this solution (in oxidizing medium) Ce(IV) and protactinium (presumably pentavalent) both were extracted[38] in 0.15 M HDEHP [hydrogen di(2-ethylhexyl)orthophosphoric acid] $(C_8H_{17}O)_2$ PH(OH) in heptane. Three to four such solvent extractions were carried out, using equal volumes of HDEHP. All the cerium and most of the protactinium came in the organic phase. From this organic phase the cerium was stripped by using 8 M HNO_3 and 1.5 M H_2O_2; along with the cerium and most of the decay products of

protactinium, only a negligible amount of protactinium came down in aqueous solution. From the organic solution free from cerium the "goodies" were stripped by using 5% HF. In this way we obtained about 49 mg of protactinium in 5% HF. Spectrographic analysis of a portion of this solution showed cerium to be below the limit of spectrographic detection (less than 0.1%). The only impurities present were: Al, 21.4; Ti, 1.7; Fe, 0.1; Zr, 0.09; Nb, 0.05; Mg, 0.05; Ca, 0.03—all in mole %.

It is well known that hydrofluoric acid prevents the extensive hydrolysis of protactinium in aqueous solution and is the preferred solvent for this element. Therefore, the solution so obtained in the previous operation was loaded on a 10 cm long column of Dowex 1 × 10, -400 mesh size anion exchange resin[39] in a 1.5 cm diameter polystyrene tube closed at the bottom with a cotton plug. After loading, the resin bed was washed with about four free column volumes of 2.5-3 M vapor-equilibrated HF. The protactinium was then eluted partly with 14 M vapor-equilibrated HF and some with 18 M vapor-equilibrated HF. Spectrographic analysis of a portion of this solution showed Al, Ti, Fe, Zr, Nb, Mg, and Ca to be below the limit of spectrographic detection. The only impurity detected was 0.2% Si.

Finally, in order to reduce the volume, the protactinium solution was evaporated and a hydroxide precipitation carried out by exposing the HF solution to excess NH_3 gas, washing with dilute ammonia, and slow drying of the hydroxide in a polyethylene cone at 85°C.

On drying, the hydroxide shrank to form a hard pellet, and starting from this the PaF_4 was prepared essentially in the same way as mentioned earlier in this section.

VI. RESULTS AND DISCUSSION

A. Calorimetric Measurements of the Heat of Solution of Curium Metal

The experimentally observed heats of solution of curium metal in 1.0 M HCl at 298.4±0.2°K are tabulated in Table V. The sample numbers refer to the preparations listed in Table IV.

Sample no. 2 had a tungsten wire imbedded in the curium metal (weight of Cm + W-wire = 220.8 μg). The weight of the tungsten wire (28.8 μg) was estimated from its diameter (3 mil) and length (13.5 mil), taking the density of tungsten to be 19.3 g/cc.

Sample no. 3 also had a tungsten wire (3 mil diameter) imbedded in it (weight of Cm + W-wire = 94.6 μg) and its weight (41.9 μg) also estimated in the same way. After the calorimeter run, the W-wire was picked up from the spool, dried overnight (by leaving it in an open petri dish), and weighed on the microbalance. It weighed 42.7 μg. The 0.8 μg difference between this weight and the estimated one is ascribed to some of the curium oxide sticking on it. After picking up the tungsten wire from the curium solution in the spool, unfortunately, it was not cleaned but just dried and weighed. Its estimated weight was incorporated into the calculations in order to be consistent with sample no. 2.

The weight of sample no. 4 was determined by radiometric assay after the calorimeter run, taking the half life of the mixture (Cm^{244}, 95.64%; Cm^{245}, 1.59%; Cm^{246}, 1.82%; Pu^{240}, 0.95%) to be 18.9337 yr and the geometry of the counter to be 51.9%. The half-life of the above-mentioned mixture was calculated from the half-lives of various isotopes present ($t_{1/2}$ Cm^{244} = 18.11 yr[40]; $t_{1/2}$ Cm^{245} = 9320 yr[41]; $t_{1/2}$ Cm^{246} = 5480 yr[37]; and $t_{1/2}$ Pu^{240} = 6600 yr.[41] The geometry of the counter was experimentally determined by counting a curium plate in our counter and then counting the same plate in another counter of accurately known geometry. Even so the weight of the sample may be good within ±1%. The weight of this sample as obtained by normal weighing on the microbalance before

Table V. Heat of solution of curium metal in 1.0 M HCl.

Sample no.	Weight of sample (μg)	Micromoles of curium	Heat evolved (cal)	$\Delta H_{298.4}$ (kcal/mole)
1	118.3	0.4848	0.0677	-139.6±0.5
2	192.0	0.7869	0.1101	-139.9±0.5
3	52.7	0.2160	0.0302	-139.8±1.0
4	70.3	0.2881	0.0404	-140.2±1.0
			Average	-139.9±1.0

loading in the microcalorimeter showed it to be 67.1 μg. The difference (3.2 μg) between this weight and the one determined by radiometric assay is attributed to two factors:

a) During the operations of loading and sealing the bulb some of the wax (previously tare weighed) chipped off.

b) The heating wire may be too hot and thereby result in considerable evaporation of the Apiezon wax.

With all this in view and because of the small weights of samples no. 3 and no. 4, the experimental uncertainty in the results of these two samples is given as ±1 kcal/mole. In order to know the heat of solution of curium metal accurate to within a few tenths of a kcal, it will be worthwhile to make some more Cm runs in the future on a large scale (400-600 μg). This size sample will give much more heat and thereby push the number on the heat of solution of Cm metal to within a few tenths of a kcal.

It may not be out of the place here to say a few words about units, auxiliary thermodynamic data, etc. In our thermochemical calculations we have taken the calorie to be equal to 4.1840 absolute joules.

All auxiliary thermodynamic data for which no reference is given have been taken from "Selected Values of Chemical Thermodynamic Properties," U. S. Bureau of Standards Circular 500 (1952).

The calorimetric measurements of the heat of solution of curium metal in 1.0 M HCl permit the calculation of the heats of formation of $CmCl_{3(c)}$ and $Cm^{+3}_{(aq)}$.

Westrum and Robinson[42] measured the heat of solution of $PuCl_{3(c)}$ in various concentrations of hydrochloric acid, obtaining -22.15±0.1, -29.5±0.1, and -31.76±0.1 kcal/mole in 6 M, 1.5 M, and 0.1 M acid respectively.

Fuger and Cunningham[43] reported -31.60±0.35 kcal/mole for the heat of solution of $PuCl_{3(c)}$ in 0.001 M $HClO_4$, 0.099 M NH_4ClO_4. They also reported -30.60±0.2 and -33.36±0.25 kcal/mole for the heat of solution of $AmCl_{3(c)}$ in 1.5 and 0.001 M HCl respectively.

One may use the data given above to arrive at an estimate for the heat of formation of $CmCl_{3(c)}$ and $Cm^{+3}_{(aq)}$.

The heat of solution of $AmCl_{3(c)}$ in 1.5 M HCl is more negative than that of $PuCl_{3(c)}$ in acid of the same concentration [ΔH solution of $AmCl_{3(c)}$ - ΔH solution of $PuCl_{3(c)}$ = -30.6±0.2 - (-29.5±0.1) = 1.1±0.3] by 1.1±0.3 kcal. For (HCl) ≦0.1 M to 0.001 M, the corresponding difference is 1.4±0.3 kcal. This difference is obtained by taking the heat of solution of $AmCl_{3(c)}$ in 0.001 M HCl to be -33.36±0.25 kcal/mole and the corresponding heat of solution of $PuCl_{3(c)}$ in 0.001 M HCl to be -31.92 kcal/mole, equivalent to that obtained by extrapolation of Westrum and Robinson data for the heat of solution of $PuCl_{3(c)}$ to infinite dilution (see Fig. 19). Hence, therefore ΔH solution of $AmCl_{3(c)}$ in 0.001 M HCl - ΔH solution of $PuCl_{3(c)}$ in 0.001 M HCl = -33.36 ± 0.25 - (-31.92±0.2) = -1.4±0.3 kcal.

By extrapolating the above heat of solution data to $CmCl_{3(c)}$ we can predict the heat of solution of $CmCl_{3(c)}$ in dilute HCl of a specified concentration to be more negative by 1.2±0.4 kcal than that of $AmCl_{3(c)}$ in acid solution of the same concentration.

Thus the predicted heat of solution of $CmCl_{3(c)}$ in 1.5 M HCl is (-30.60±0.2) + (-1.2±0.4) = -31.8±0.5 kcal/mole.

From a plot of the $PuCl_3$ heat of solution data of Westrum and Robinson[42] vs HCl concentration (see Fig. 19), the interpolated difference between 1.5 M and 1 M HCl is 0.8 kcal/mole.

Applying this same correction to $CmCl_{3(c)}$, the heat of solution in 1.0 M HCl is predicted to be (-31.8±0.5) + (-0.8) = -32.6±0.5 kcal/mole.

The experimentally observed heat of solution of curium metal in 1.0 M HCl corresponds to the reaction

$$Cm_{(c)} + (3000 \text{ to } 16000)\,[HCl \cdot 54.2\ H_2O] \longrightarrow$$

$$(CmCl_3 \text{ in } (3000\text{-}3 \text{ to } 16000\text{-}3)\,[HCl \cdot 54.2\ H_2O]) + 3/2\ H_{2(g)}.$$

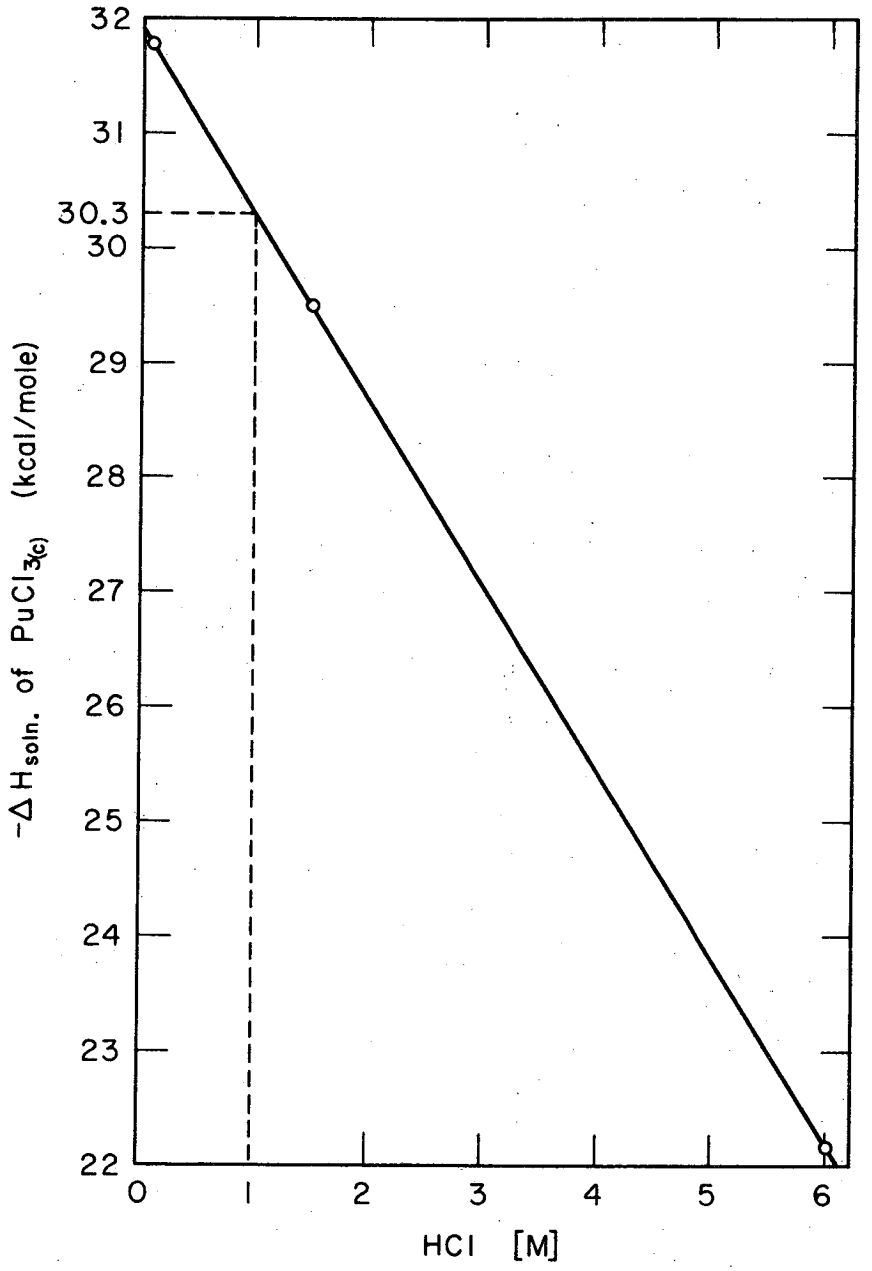

Figure 19. Plot of $PuCl_3$ heat-of-solution data vs HCl concentration.

Neglecting the slight change in composition of the 1 M HCl due to consumption of HCl in the dissolution of the metal, and taking the relative heat content of HCl in 1 M HCl ($HCl \cdot 54.2\ H_2O$) to be -39.6 kcal/mole, we calculate the heat of formation of $CmCl_3$ dissolved in [(3000 to 16000) $HCl \cdot 54.2\ H_2O$] to be $(-139.9 \pm 1.0) + (-39.6 \times 3) = -258.7 \pm 1.0$ kcal/mole. The calculation also ignores the influence of very low concentrations of $CmCl_3$ on the HCl heat content.

Accordingly, the heat of formation of $CmCl_{3(c)} = (-258.7 \pm 1.0) - (-32.6 \pm 0.5) = -226.1 \pm 1.2$ kcal/mole.

Taking -33.36 ± 0.25 kcal/mole for the heat of solution of $AmCl_{3(c)}$ in 0.001 M HCl to be equivalent to that at infinite dilution, and adding to it -1.2 ± 0.4 (predicted difference as already mentioned by extrapolating the $PuCl_{3(c)}$ and $AmCl_{3(c)}$ data to $CmCl_{3(c)}$), we estimate the heat of solution of $CmCl_{3(c)}$ in infinitely dilute HCl to be $-33.36 \pm 0.25 + (-1.2 \pm 0.4) = -34.6 \pm 0.4$ kcal/mole, whence

$$\Delta H_f^o\ Cm^{+3}{}_{(aq)} = -226.1 \pm 1.2 + 3(40.02) - 34.6 \pm 0.4$$

$$= -140.6 \pm 1.3 \text{ kcal/mole} \quad .$$

taking the heat of formation of $Cl^-{}_{(aq)}$ to be -40.02 kcal/mole.

The heat of solution of curium metal in 1 M HCl (-139.9 ± 1 kcal/mole), is similar to that of plutonium[43] (-138.65 ± 0.7 kcal/mole in 1.5 M HCl) but some 22 kcal more positive than that of americium[44] (-162.3 ± 2.7 kcal/mole in 1.5 M HCl), although americium and curium metals have similar crystal structures and similar lattice parameters. A contributing factor to this difference may be the larger heat of vaporization of curium. In other words, the more electropositive nature of americium relative to curium may be associated with its low heat of vaporization.

On the basis of present knowledge of the actinide elements, it would appear probable that the thermodynamic properties of the transcurium

elements probably will be rather similar to those of curium with a more or less regular variation of atomic number, as observed in the lanthanide elements.

B. Magnetic Susceptibility of Curium Metal

The magnetic susceptibility of a few samples of curium metal has been investigated with a special emphasis on ferromagnetic transition and behavior at low temperatures, and the results are listed in the following tables. The sample numbers, again, refer to the preparations listed in Table IV. Sample no. 4 showed field dependence which is attributed to contamination with some ferromagnetic impurities due to much handling of the sample. Therefore, the measured susceptibility was corrected for ferromagnetic impurities by plotting the measured susceptibility vs 1/i and extrapolating to 1/i = 0 to get the corrected value, as shown in Fig. 20.

The apparatus constants were determined experimentally by calibrating the apparatus with nickelous ammonium sulfate, and the susceptibility of the empty quartz tube (χ_t) was calculated from the measured deflection of the quartz tube and the known apparatus constants. The uncertainty in the apparatus constants varied from 2.2 to 3.0% depending on the current setting. The absolute error in the susceptibility of the standard material used in the standardization was assumed to be 2%, and this assumption accounts for most of the error in the apparatus constants.

Tables VI to IX give the gram susceptibility of different samples of curium metal at different temperatures. Table VI gives the susceptibility of sample no. 4 at different fields together with the corrected susceptibility which is given in the last column of the table (χ_∞). Table VIII gives the susceptibility of sample no. 5 at various fields in and near the ferromagnetic region.

The plots of the inverse of the gram susceptibility of different samples vs the absolute temperature are shown in Figs. 21-23.

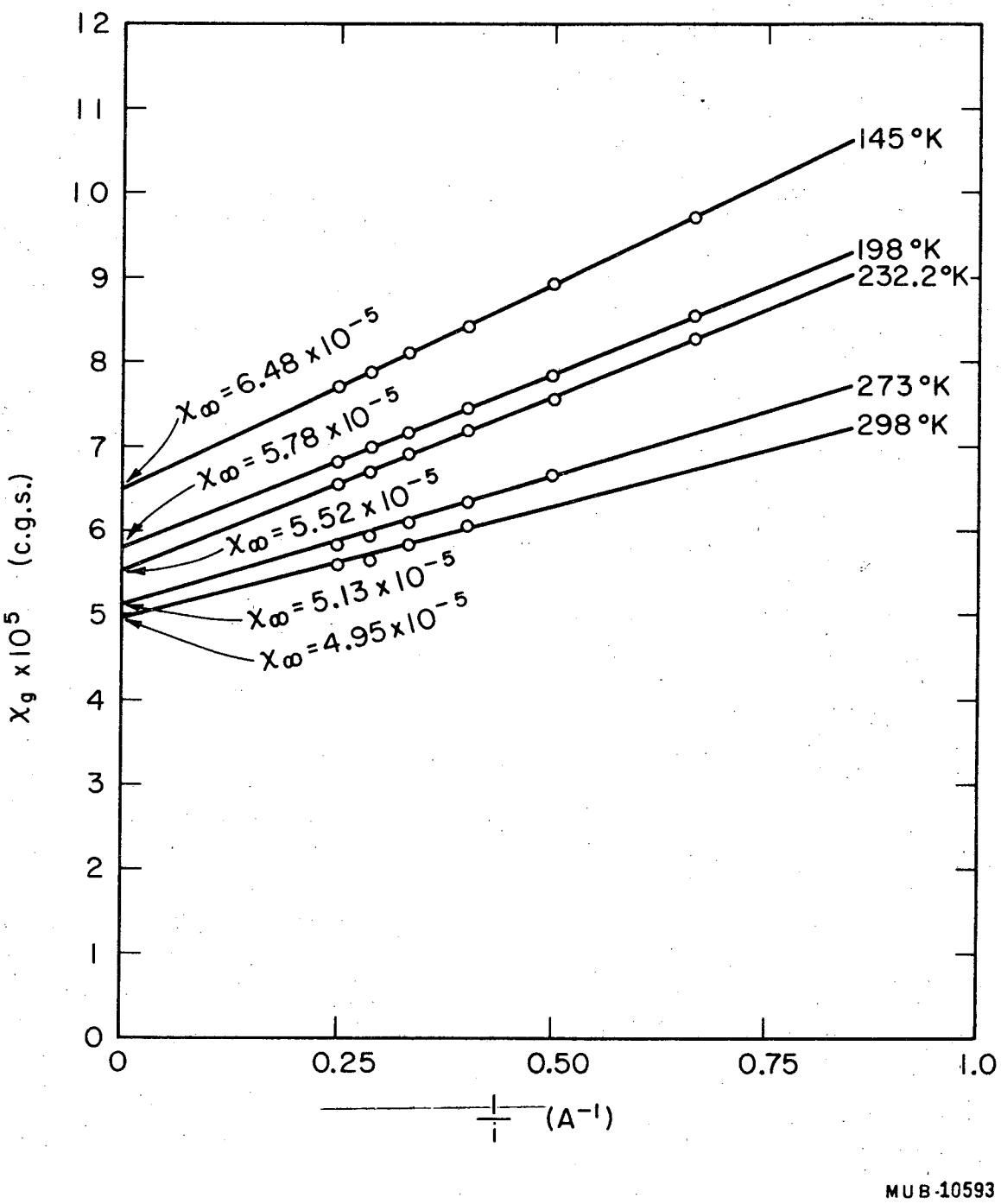

Figure 20. Correction for ferromagnetic impurities (sample no. 4).

Table VI. Magnetic susceptibility of curium metal (sample no. 4).

T(°K)	$\chi_g \times 10^6$						χ_∞	$1/\chi_g \times 10^{-4}$
	1.5 A	2.0 A	2.5 A	3.0 A	3.5 A	4.0 A		
298	-	-	60.50	58.01	56.30	55.78	49.50±0.9	2.02
273	-	66.63	63.12	60.99_7	58.91	58.24	51.30±1.0	1.95
232.2	83.06	75.41	71.84	69.13	66.93	65.50	55.20±1.0	1.81
198	85.51	78.53	74.56	71.52	68.54	68.12	57.80±1.1	1.73
145	97.09_6	88.01	84.13	81.00	78.60	77.00	64.80±1.2	1.54

$\Delta = 356 \pm 18^\circ K$ $\mu_{eff} = 7.97 \pm 0.1$ B.M.

Table VII. Magnetic susceptibility of curium metal (sample no. 5).

T(^{o}K)	$\chi_g \times 10^6$	$1/\chi_g \times 10^{-4}$
298	49.91±0.9	2.004
273	51.53±1.0	1.941
232.2	55.10±1.0	1.815
198	57.78±1.1	1.731
145	64.51±1.2	1.550
111.5	84.03±1.3	1.190
90.04	120.59±2.0	0.829
77	138.42±2.5	0.722
20	182.45±3.0	0.548
6-8	207.86±4.0	0.481

$\Delta = 384 \pm 19^{o}K$ $\mu_{eff} = 8.10 \pm 0.1$ B.M.

Table VIII. Field dependence of sample no. 5.

T(°K)	$\chi_g \times 10^6$			
	3.0 A	2.5 A	2.0 A	1.5 A
111.5	85.34	84.86	84.03	88.23
90.04	117.97	119.78	120.59	125.99
77	131.82	135.51	138.42	147.12
20	176.04	179.73	182.45	193.55
6-8	-	-	207.86	-

Table IX. Magnetic susceptibility of curium metal (sample no. 5 after mechanical deformation).

T(°K)	$\chi_g \times 10^6$	$1/\chi_g \times 10^{-4}$
298	49.76±0.9	2.009_6
273	51.33±1.0	1.948
232.2	55.10±1.0	1.815
198	57.97±1.1	1.725
145	65.15±1.3	1.535

Δ = 354±20°K; μ_{eff} = 8.02±0.1 B.M.

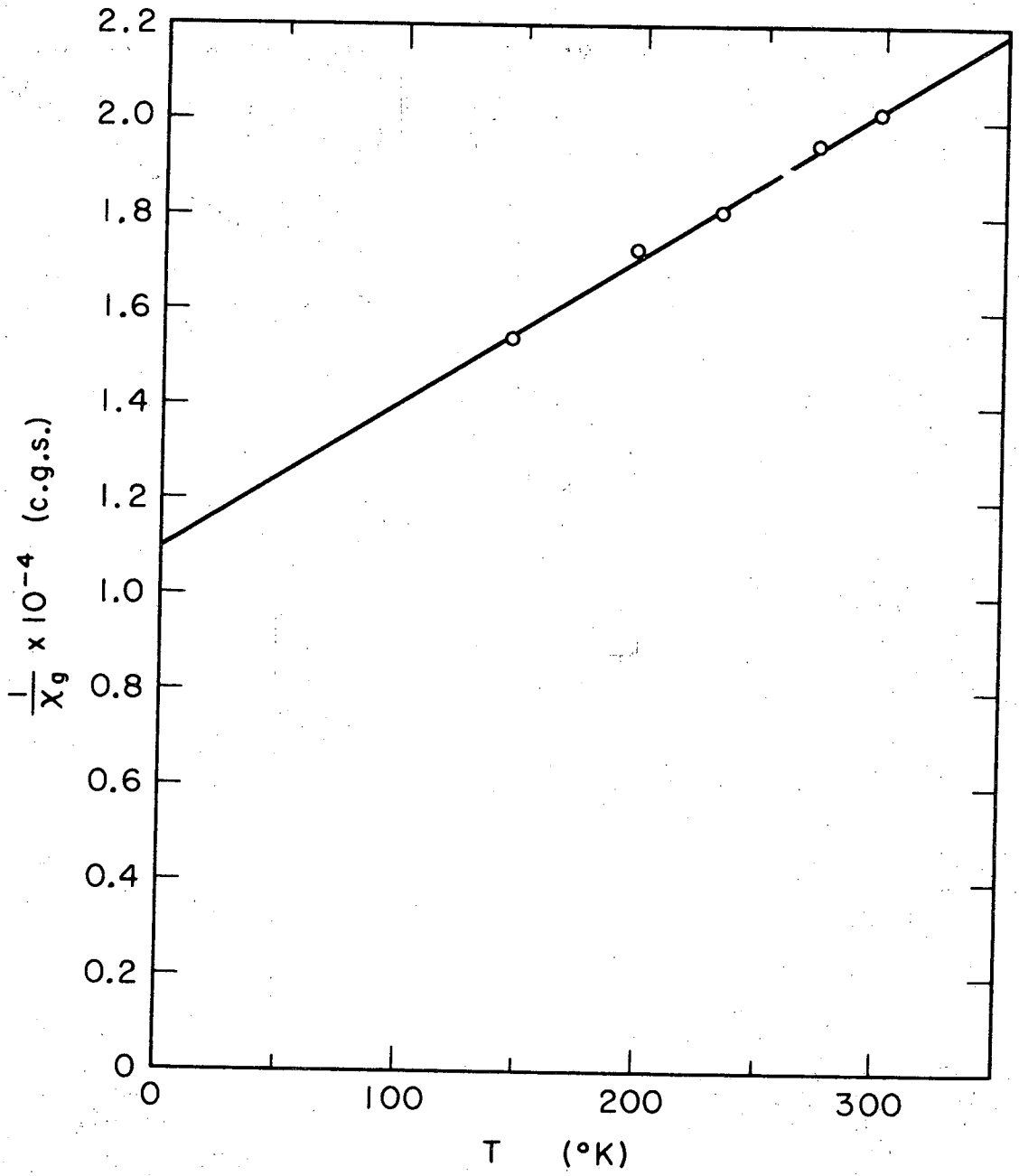

Figure 21. Plot of $1/\chi_g$ vs T(^{o}K) for curium metal (sample no. 4).

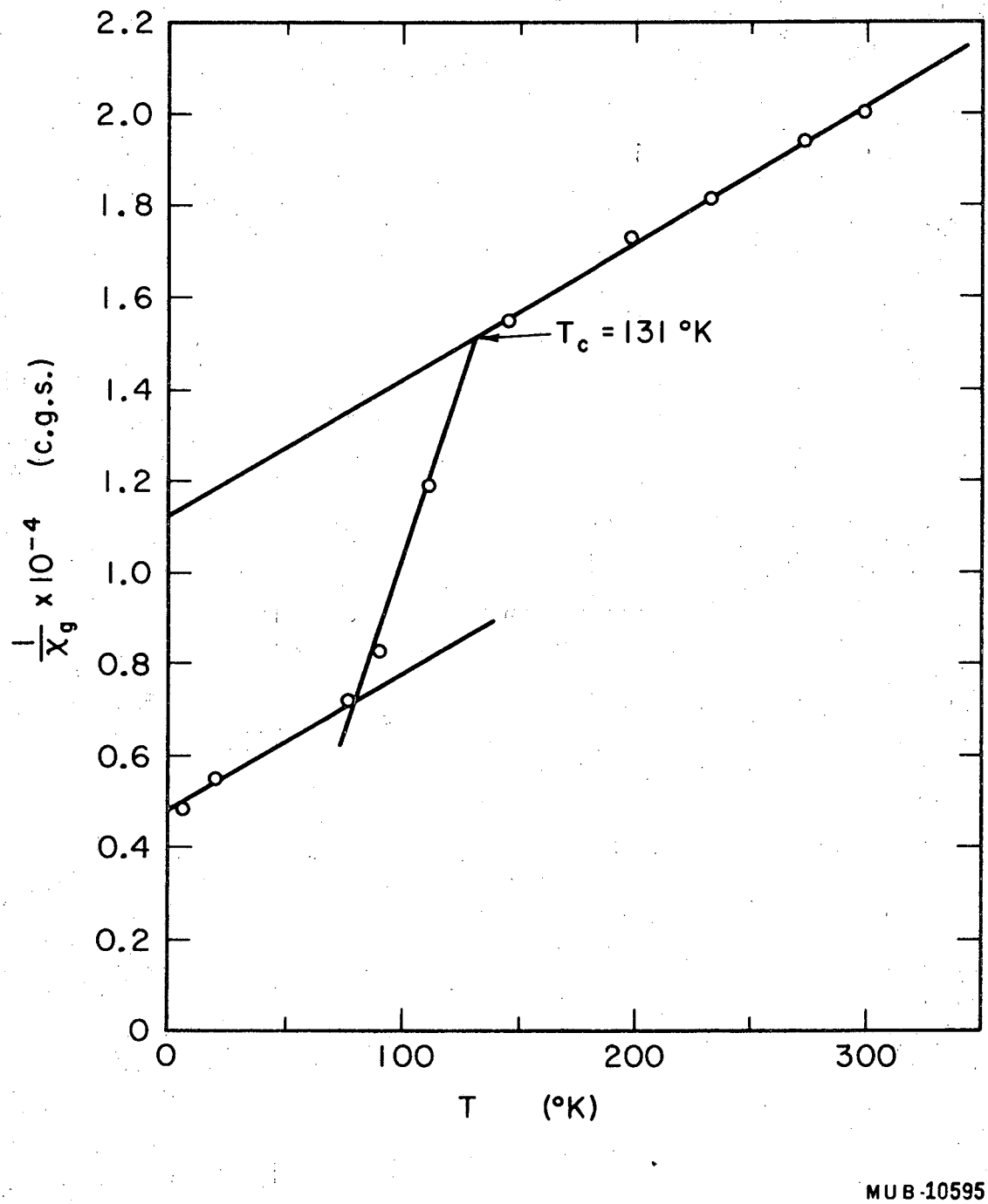

Figure 22. Plot of $1/\chi_g$ vs T($^{\circ}$K) for curium metal (sample no. 5).

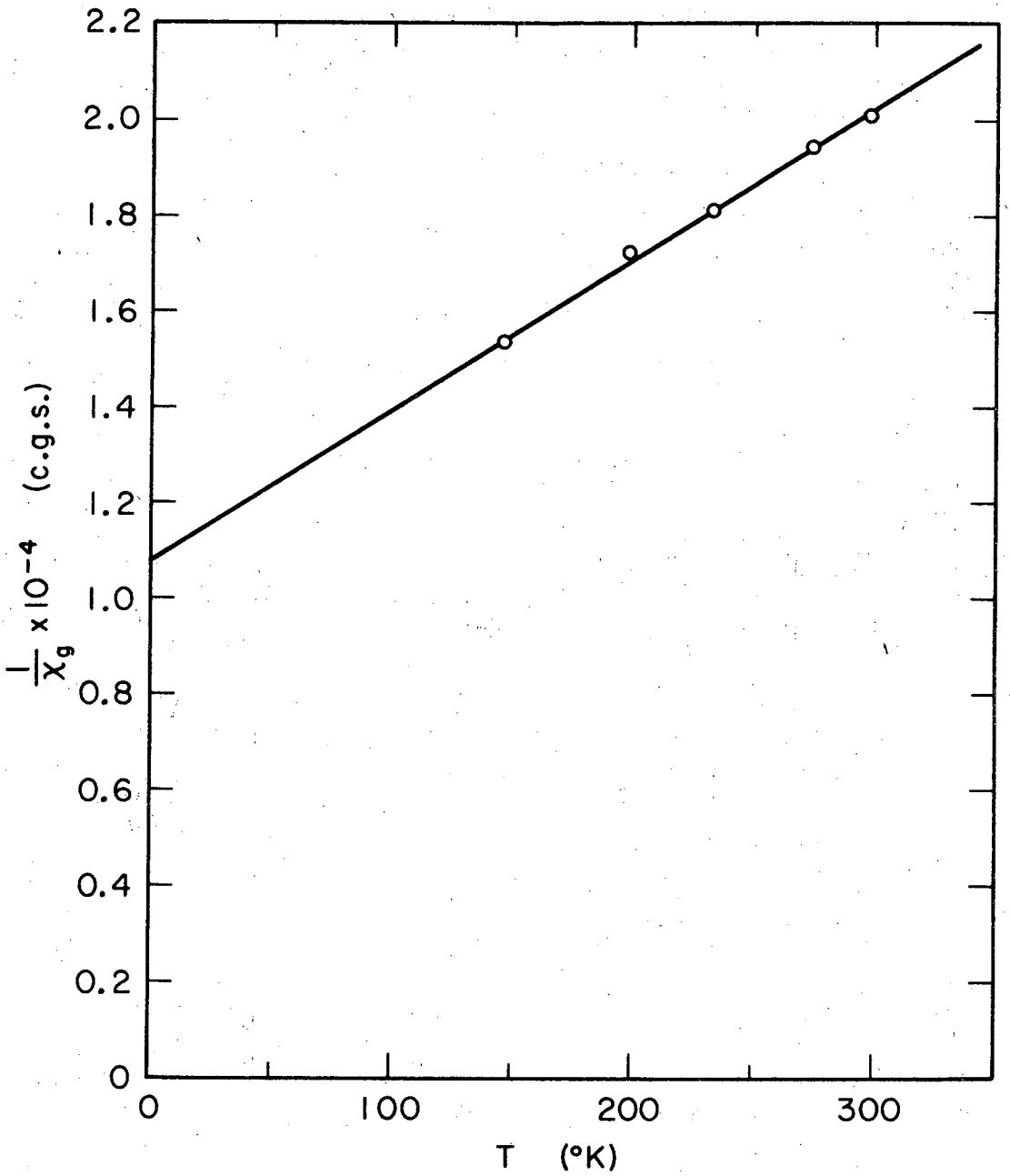

Figure 23. Plot of $1/\chi_g$ vs T($^{\circ}$K) for curium metal (sample no. 5 after mechanical deformation).

From the plot in Fig. 22 it is clear that the metal follows the Curie-Weiss law in the temperature range from 298-145°K. The same behavior was observed by Marei[4] in five of his samples. This law can be expressed in the form

$$\chi_M = \frac{C}{(T+\Delta)} ,$$

where

χ_M = the molar magnetic susceptibility,

T = absolute temperature,

Δ = molecular field constant or Weiss constant,

C = proportionality constant.

The molecular field constant was calculated for the different samples from the plot of $1/\chi_g$ vs T by using an IBM 7094 computer least-squares-fit program. This program essentially uses the equation

$$\Delta = \frac{\chi_g^{-1}}{S} - T , \qquad (17)$$

where S is the slope of the best straight line passing through the points.

The Δ value for each of the samples is given at the end of the corresponding table.

The effective moments (in Bohr magnetons) were calculated for the different samples from the measured susceptibility and the calculated Δ values as follows.

Paramagnetic susceptibility per mole corrected for the diamagnetism due to closed shell (χ_M^{corr}) is given by the Curie-Weiss law as mentioned earlier:

$$\chi_M^{corr} = \frac{C}{T+\Delta} . \qquad (18)$$

The molar susceptibility of a substance containing independent atoms, ions or molecules each of magnetic moment μ (in B.M.) is given by

$$\chi_M^{corr} = \frac{N\mu^2/3k}{T} \quad , \tag{19}$$

where

N = Avogadro's number,

k = Boltzmann's constant.

Assuming that the magnetic dipoles in various ions, atoms, or molecules of a solid are not completely independent but that the orientation of each one is influenced by the orientation of its neighbors as well as by the field to which it is subjected, χ_M^{corr} will be given by

$$\chi_M^{corr} = \frac{N\mu^2/3k}{T+\Delta} \quad . \tag{20}$$

Combining Eqs. (18) and (20) we get

$$C = N\mu^2/3k \quad .$$

From Eq. (20) we have

$$\chi_M^{corr}(T+\Delta) = N\mu^2/3k$$

$$\sqrt{3k/N} \cdot \sqrt{\chi_M^{corr}(T+\Delta)} = \mu \quad .$$

Numerical evaluation of $\sqrt{3k/N}$ gives 2.84.

$$\mu_{eff} \text{ in B.M.} = 2.84 \sqrt{\chi_M^{corr}(T+\Delta)} \quad .$$

For the derivations of Eqs. (19) and (20) one can refer to any of the standard books on magnetism.[45,46] The effective moment of each sample so

calculated is given at the end of the appropriate table (Tables VI, VII, and IX). The effective moment for the metal agrees very well with the theoretical value of 7.94 B.M. calculated from the configuration of $5f^7$, assuming Russell-Saunders coupling. The value agrees also with the recently determined value for the gadolinium metal of 8.07±0.05 B.M. with the Δ value of -310°K.[47]

The effective moment of 8.03±0.1 B.M. obtained in the case of curium metal is very close to that to be expected for the +3 ion having a $^8S_{7/2}$ ground state with Russell-Saunders coupling. Therefore the magnetic evidence mentioned above suggests that there are 3.0 electrons per curium atom used in bonding. The slightly smaller radius of americium suggests about 3.2 bonding electrons per atom for the lighter element. However, due to the large Δ values found and used in the calculation of μ_{eff}, no final statement about the exact coupling obeyed in the case of the curium metal can be made.

It is clear from Fig. 22 that the metal deviates from the Curie-Weiss law below 145°K. This is in agreement with the observation made by Marei[4] based on the results of five different samples. Obviously the metal becomes ferromagnetic in the temperature region (77-145°K). The Curie temperature T_c so calculated is 131±10°K. In order to determine a more accurate value for T_c, more measurements below 145°K should be made in the future at smaller intervals of temperature. At liquid hydrogen and helium temperatures the metal again seems to show paramagnetic behavior. No evidence of antiferromagnetic behavior, however, was observed. Table VIII shows the field dependence of curium metal below 145°K (in and near the ferromagnetic region).

The correlation between the crystal structure of the trivalent transition metals and the presence or absence of ferromagnetism (the term used in the restricted sense, that is, where there is a net spontaneous polarization) is surprisingly good. Scandium, yttrium, lanthanum, ytterbium, and lutetium are not expected to be ferromagnetic, because they do

not have any unpaired 4f electrons, while all of the other metals do. The light rare earths—all of which have complex structures—are not ferromagnetic, but the heavy rare earths—which have the normal hexagonal close-packed structure—are ferromagnetic (see Fig. 24, taken from Gschneidner and Matthias[48]). The ferromagnetic Curie temperatures have been shown by de Gennes[49] (see Figs. 24 and 25) to be proportional to $J(J+1)(g-1)^2$, where J is equal to L+S for the rare earths beyond gadolinium and g is the spectroscopic splitting factor, defined as

$$g = 1 + \frac{S(S+1) + J(J+1) - L(L+1)}{2J(J+1)} .$$

Figure 25 has been taken from the original paper of de Gennes,[49] and is more or less the same as Fig. 24 except that it is drawn on a bigger scale and therefore reveals much better the correlation between experimentally determined Curie points and those predicted by de Gennes on the basis of proportionality to $J(J+1)(g-1)^2$.

Before any such correlation can be attempted in the case of the actinides, one has to wait till some experimental data about the ferromagnetic behavior of heavy transuranium elements is obtained. The presence of ferromagnetism in double hexagonal close-packed curium is inconsistent with its absence in all of the rare earth metals which crystallize in this same structure. Suffice to say that at present the relation between ferromagnetic behavior and the crystal structure in the actinide metals is not understood.

Marei[4] found the Δ values for different curium metal samples ranging from 135-348°K. In order to determine the effect of mechanical deformation on the Δ value the sample no. 5 was remeasured after mechanically deforming the curium metal piece. The uncertainty in Δ value is such that it is very hard to draw any conclusion regarding the effect of mechanical deformation. The Δ values before and after deformation are 384±19°K and 354±20°K respectively. Nothing can be said conclusively as

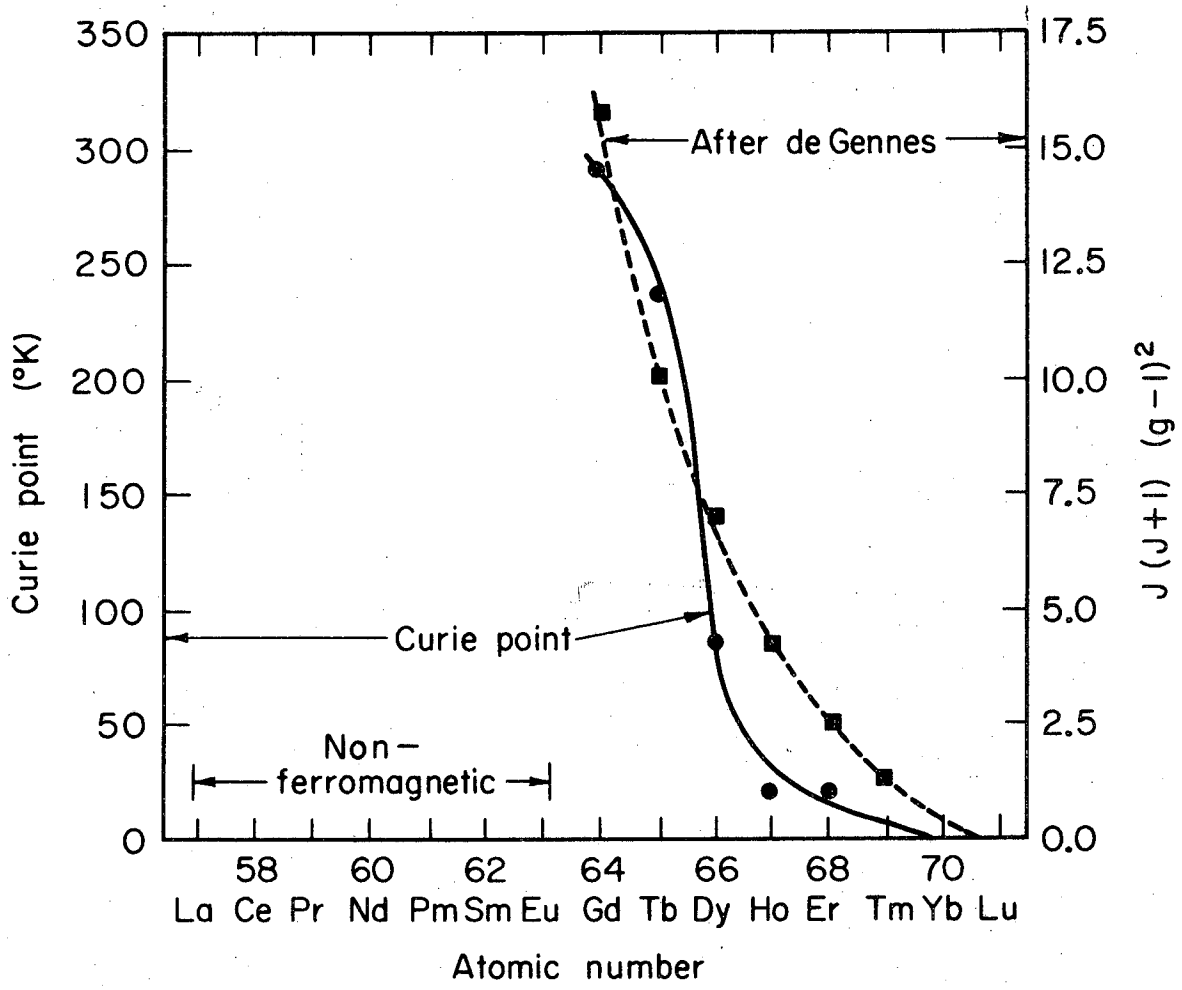

MUB-10597

Figure 24. Ferromagnetic transition temperatures of the rare-earth metals, and their proportionality to the de Gennes factor, $J(J+1)(g-1)^2$.

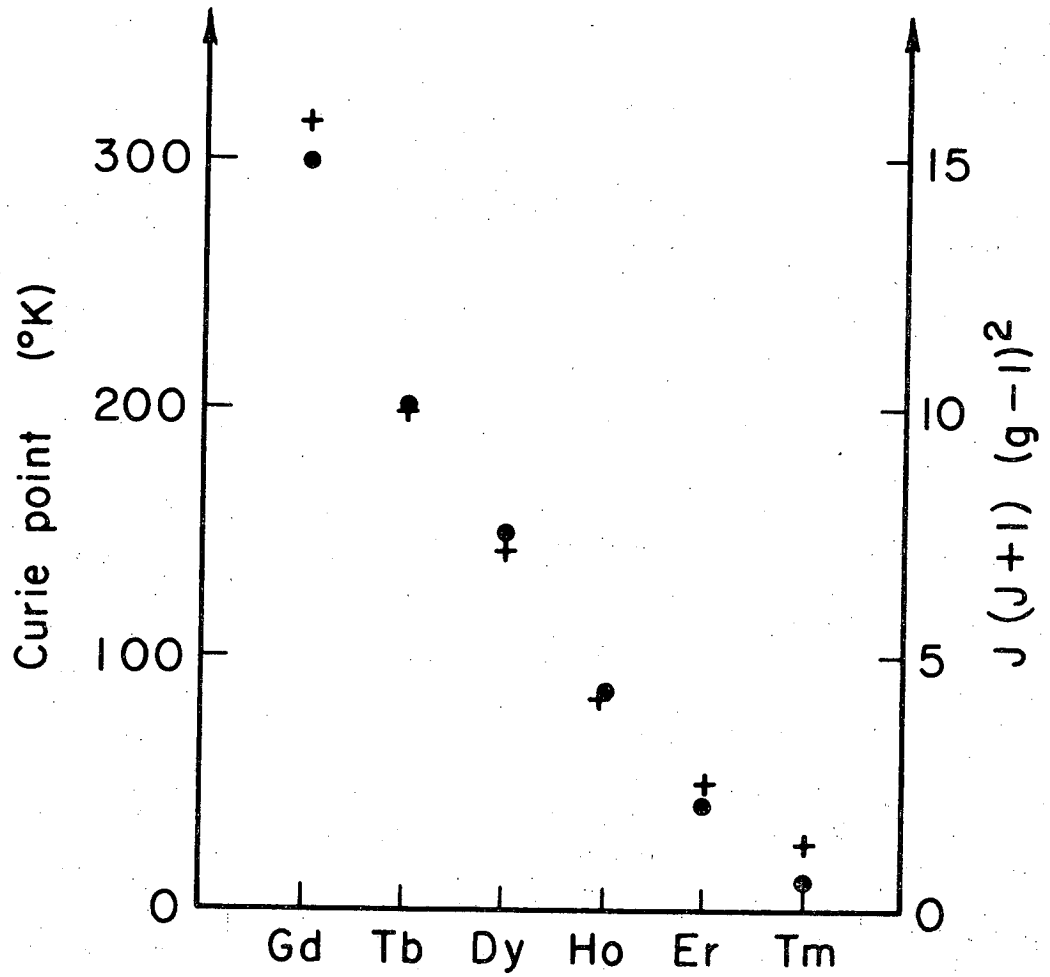

Figure 25. Ferromagnetic transition temperatures of the heavy rare earth metals, and the proportionality to the de Gennes factor, $J(J+1)(g-1)^2$.

● experimentally determined Curie point

\+ proportionality to de Gennes factor, $J(J+1)(g-1)^2$.

to whether this difference is due to mechanical deformation or just the uncertainty in Δ value.

We have seen that at low temperatures the linear relationship between $1/\chi$ and T does not hold in many cases. The deviations from the Curie law have two causes:

a) The field of the surrounding ions (in salts) or conduction electrons splits the levels of the free atomic system into a number of sublevels, each of which has another magnetic behavior, expressed by the Landé g factor. These sublevels are occupied according to the Boltzmann law: at $T = 0$ only the lowest level is occupied and already at moderate temperature the sublevels are occupied nearly equally, in which case—according to the theorem of spectroscopic stability—the magnetism comes out as if no splitting would exist.

b) This splitting would never give ferromagnetism. Heisenberg, using the principles of quantum theory, found that there is an exchange energy between neighboring magnetic ions, which can be either so that the parallel orientation of the moments is favored (ferromagnetism) or the antiparallel (antiferromagnetism). This exchange coupling gives the explanation of the inner field of Weiss, the magnitude of which cannot be derived by simple classical magnetostatic considerations.

In the iron group the effects a) and b) are difficult to separate, because the electronic shell responsible for the magnetism is the outside shell 3d, which is very much modified by the surrounding atoms. So there is no possibility of quantitative comparison between theory and experiment. Better objects are the rare earths and actinides because the shell that is the carrier of the magnetism, the 4f and 5f shell respectively, is protected by the closed group of the two 5s or 6s and the six 5p or 6p electrons respectively, so that the 4f or 5f electrons have no immediate contact with the surrounding ions or the conduction electrons.

The salts show only the splitting effects; the sublevels can be taken from optical measurements, and—e.g., in the case of Nd and Cm—

there is good agreement between the spectroscopic g values and the magnetic behavior, as was shown in the beautiful paper of Dieke and Heroux[50] (for the Nd case) and by us[4,51] (for the Cm case).

The measurements made by Leipfinger[52] prove that in the salts the exchange effects are vanishing.

In contrast to the splitting effects, it is well known that some of the metals are ferromagnetic, a sign of exchange coupling. So one can hope to get information about the still rather "dark" exchange integrals by studying the behavior of these metals at low temperatures. However, qualitatively one can say that apparently the mobile or unbound conduction electrons give a much smaller field than the ions of a salt, so in most cases the magnetism of these metals would probably give the pure exchange effects. In most of the rare earth metals like Ce, Pr, Nd, Dy, Yb, etc., the Δ values are small. However in case of Gd metal the Δ value is very high, -310°K,[47] and such is the case with Cm metal. Both Gd and Cm metals show ferromagnetism; the only difference is that Gd is ferromagnetic with T_c of 16-18°C whereas Cm is ferromagnetic with T_c of 131±10°K.

One other striking similarity between Cm and Gd is the large value of Δ in the metal and the decrease of this value with increasing dilution of the magnetic ions in the compound. This can be shown by comparing the results of some of the compounds of Gd and Cm:

Compound	Δ value[45] (°C)	Compound	Δ value[51,4] (°K)
Gd_2O_3	18±2	CmOCl	24±3
$GdCl_3$	14	$CmF_3 \cdot 1/2(H_2O)$	5±3
$Gd_2(SO_4)_3 \cdot 8H_2O$	2 (or zero)	$(Cm\text{-}La)F_3$*	5±3

*5.6 mole % curium trifluoride diluted with lanthanum trifluoride.

The order of the compounds written is almost certainly the order of increasing "magnetic dilution"; that is, Gd^{+3} and Cm^{+3} are getting farther apart. Gadolinium is the only element in which this value approaches zero, because Δ arises solely from the Heisenberg exchange interaction, due to the presence of gadolinium in the S state. The same trend is very clear in Cm, indicating that the ground state of Cm is mainly an S state ($^8S_{7/2}$).

The melting point of curium has been observed[24] to be $1340\pm40^{\circ}C$, similar to that of Gd.

This clearly indicates that Cm metal is similar in its properties to its rare earth analog, gadolinium.

It is worthy of note that the magnetic transitions—and hence the coupling effects—are sensitive, both to chemical impurities (e.g., oxygen) and to particle size. As reported by Leipfinger,[52] metals like dysprosium, well known to be ferromagnetic, did not show this property in powders.

Not only the magnetic susceptibility of the curium, as presented above, is markedly different from those of the preceding elements in the actinide series, but some of the other physical properties of curium also show such deviation. For example, the curium metal melts at a temperature 345° higher than that of its preceding element, americium. The presence of double hexagonal close-packed structure has been shown to exist in this series for americium[2,3] and curium.[24] This dhcp structure is commonly exhibited by the earlier members of the rare earth series. The earlier members of the actinide series—e.g., uranium, neptunium, and plutonium—have many allotropic forms, and some of the phases have very complex structure. It may be worth mentioning that among the man-made elements plutonium has the most complex structure. The abrupt change in the crystal structure of the actinides at americium and curium is illustrated in Fig. 26. Magnetic properties of curium have been compared with the other actinide elements in Fig. 27.

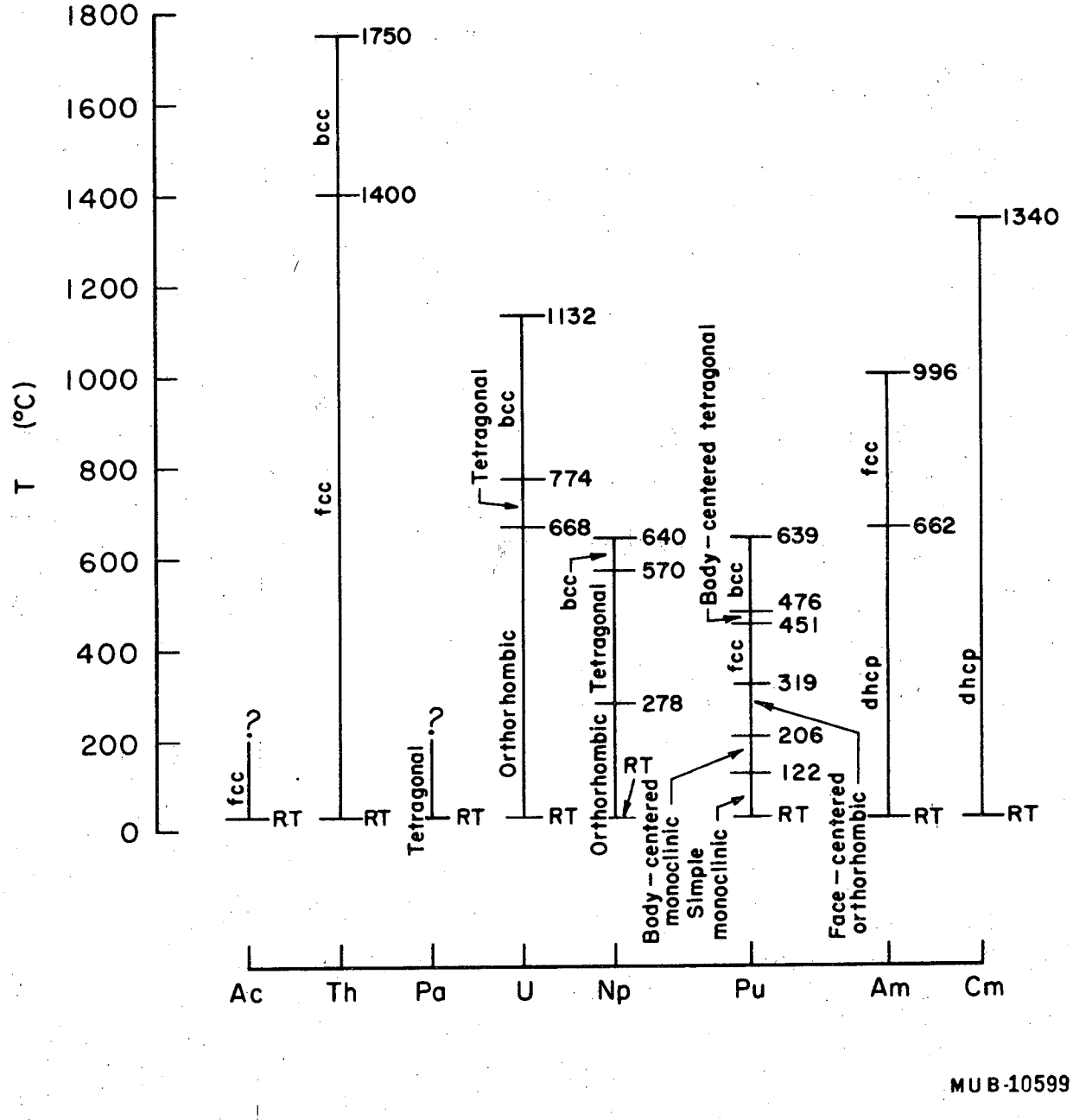

Figure 26. Crystal structures of the actinide metals.

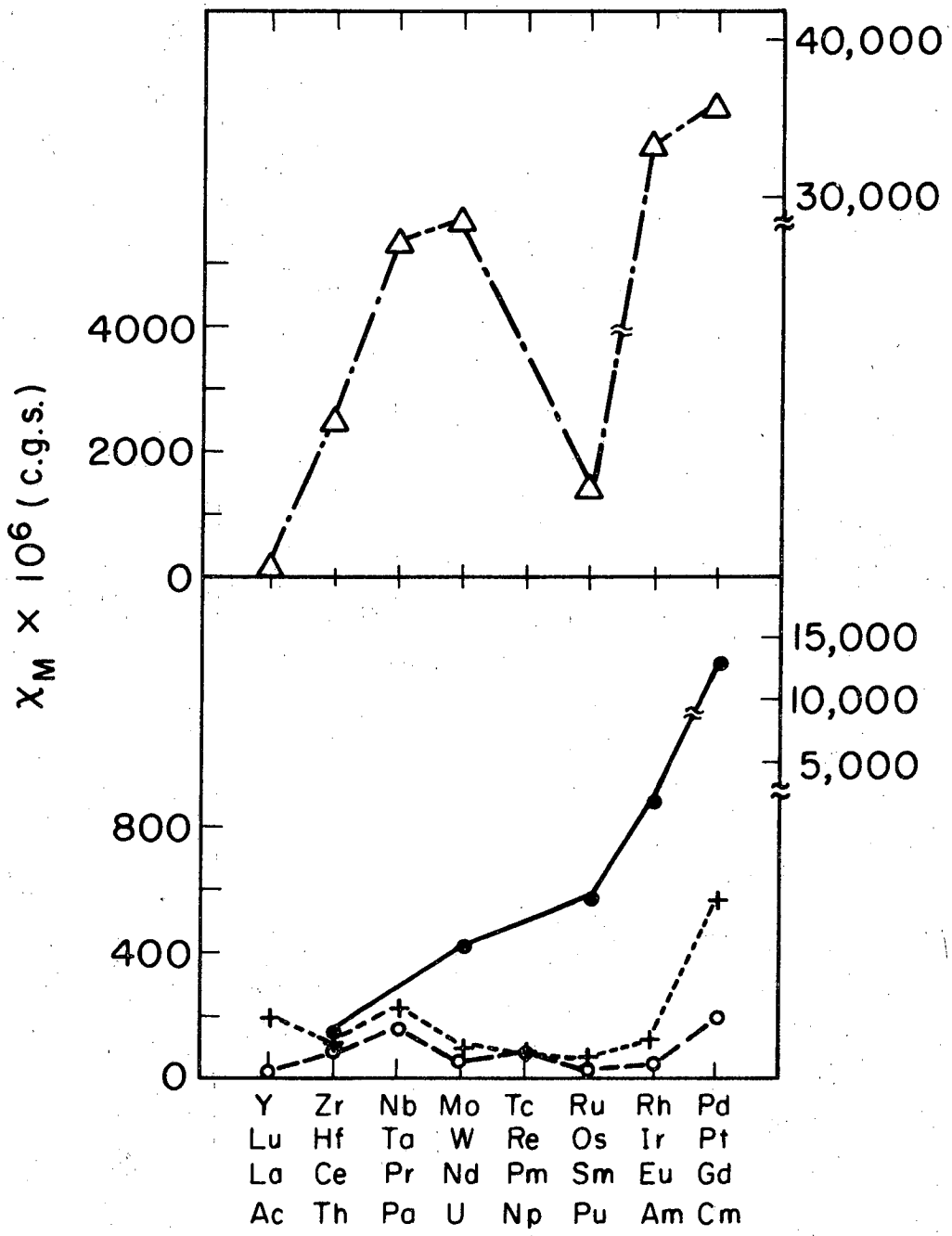

MIIB-5765

Figure 27. Magnetic properties of "d" and "f" transition elements.
+--+ Y, Zr, Nb: 4d transition series
o--o lu, Hf, Ta: 5d transition series
Δ-·-·-Δ La, Ce, Pr: 4f transition series
●—● Ac, Th, Pa: 5f transition series

The same figure shows the comparison of the magnetic properties of the actinide metals with those of the lanthanides as well as second and third "d" transition series elements.[47,53,54,55] A comparison of the atomic volumes and melting points of the actinide metals with those of "4f" and "d" series elements[3,54,55] is presented in Fig. 28. These graphs show that actinium, americium, and curium are very similar to the rare earth elements, but that thorium, protactinium, and uranium—the earlier members of the actinide series—have properties intermediate between those of the lanthanide and "d" transition series. Nevertheless for the elements neptunium, plutonium, americium, and curium the magnetic evidence provides some of the strongest evidence for the actinide concept.

Qualitatively, therefore, the complex nature of the early actinide metals can be understood by considering the electronic configuration of the gaseous atoms of the actinides and lanthanides as determined by atomic beam resonance studies. These are presented in Table X. (The configurations show the electrons above the radon and xenon cores respectively.) The 6d electrons are bound more tightly than the 5f electrons, and, as a result of this, there is a d electron in the gaseous atoms up to plutonium. The relative binding energies of the last competing electron in the lanthanides and the actinides are presented in Fig. 29 (taken from Cabezas[56]). In the lanthanide elements the f band is lower in energy and more internal, thus leading to normal physical properties and simple crystal structures. In the actinides the d and f bands are very close in energy and probably overlap, giving rise to a much more complicated structure which is the cause of the abnormal physical properties and the complex crystal structures observed between protactinium and plutonium. This also leads to more than the "normal" three binding electrons, which probably accounts for the smaller atomic volumes and high heats of vaporization in this region of the periodic table.

The results obtained by us[51,4] for Cm^{+3} ion in various curium compounds along with those obtained from paramagnetic resonance studies

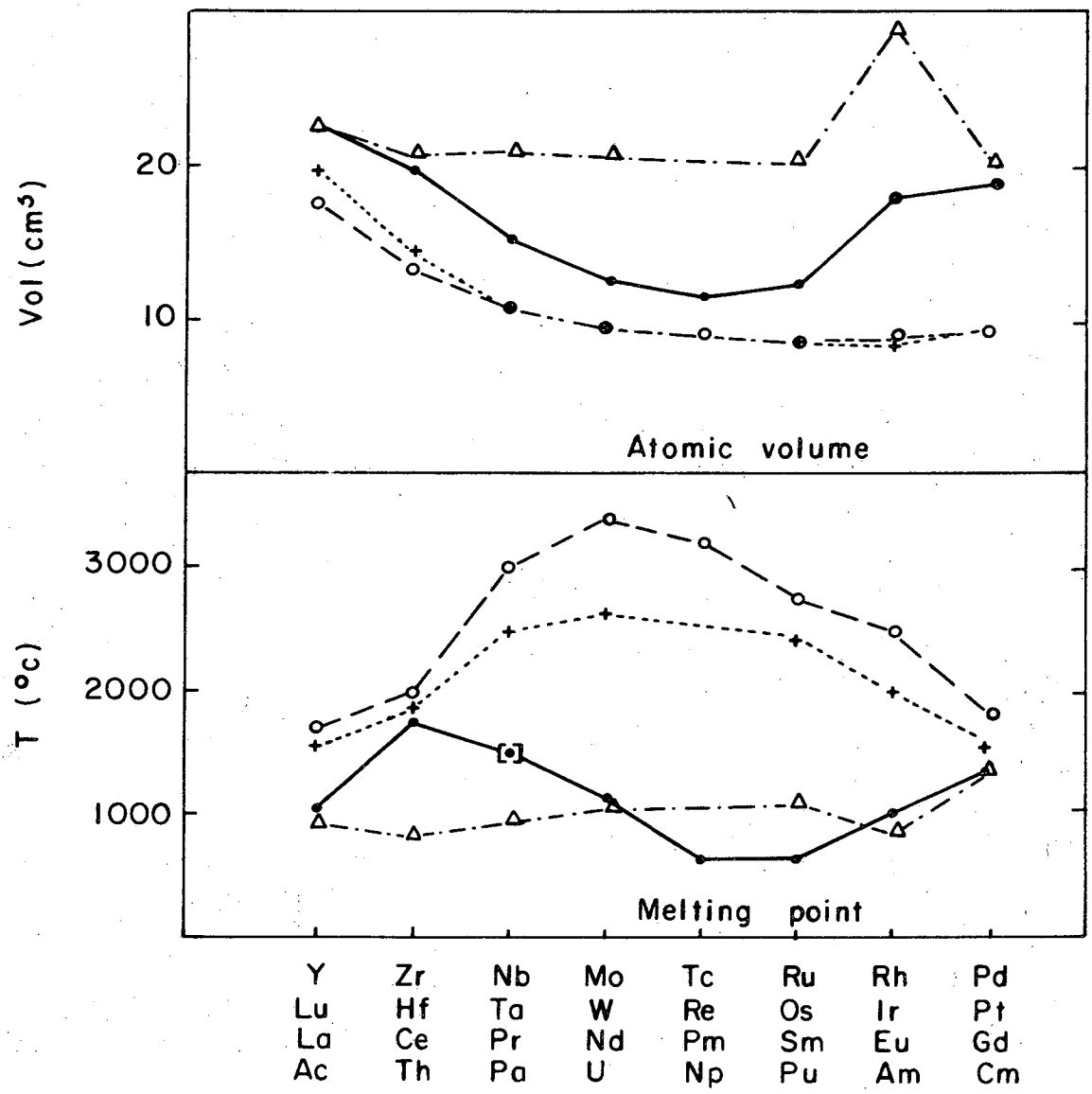

MU-23701

Figure 28. Comparison of various properties of the transition elements, lanthanides, and actinides.

+------+ Y, Zr, Nb: 4d transition series
o------o Lu, Hf, Ta: 5d transition series
Δ-·-·-Δ La, Ce, Pr: lanthanide series
●———● Ac, Th, Pa: actinide series

Table X. Ground state electronic configuration of neutral gaseous atoms (outside closed shells and filled sub-shells).[a]

Actinide element	Configuration	Lanthanide element	Configuration
Ac	$6d$	La	$5d$
Th	$6d^2$	Ce	$4f\ 5d$
Pa	$5f^2\ 6d$	Pr	$4f^3$
U	$5f^3\ 6d$	Nd	$4f^4$
Np	$5f^4\ 6d$	Pm	$4f^5$
Pu	$5f^6$	Sm	$4f^6$
Am	$5f^7$	Eu	$4f^7$
Cm	$5f^7\ 6d$	Gd	$4f^7\ 5d$

[a]For the actinides the filled sub-shells are $6s^2$, $6p^6$ and $7s^2$; for the lanthanides, $5s^2$, $5p^6$, and $6s^2$.

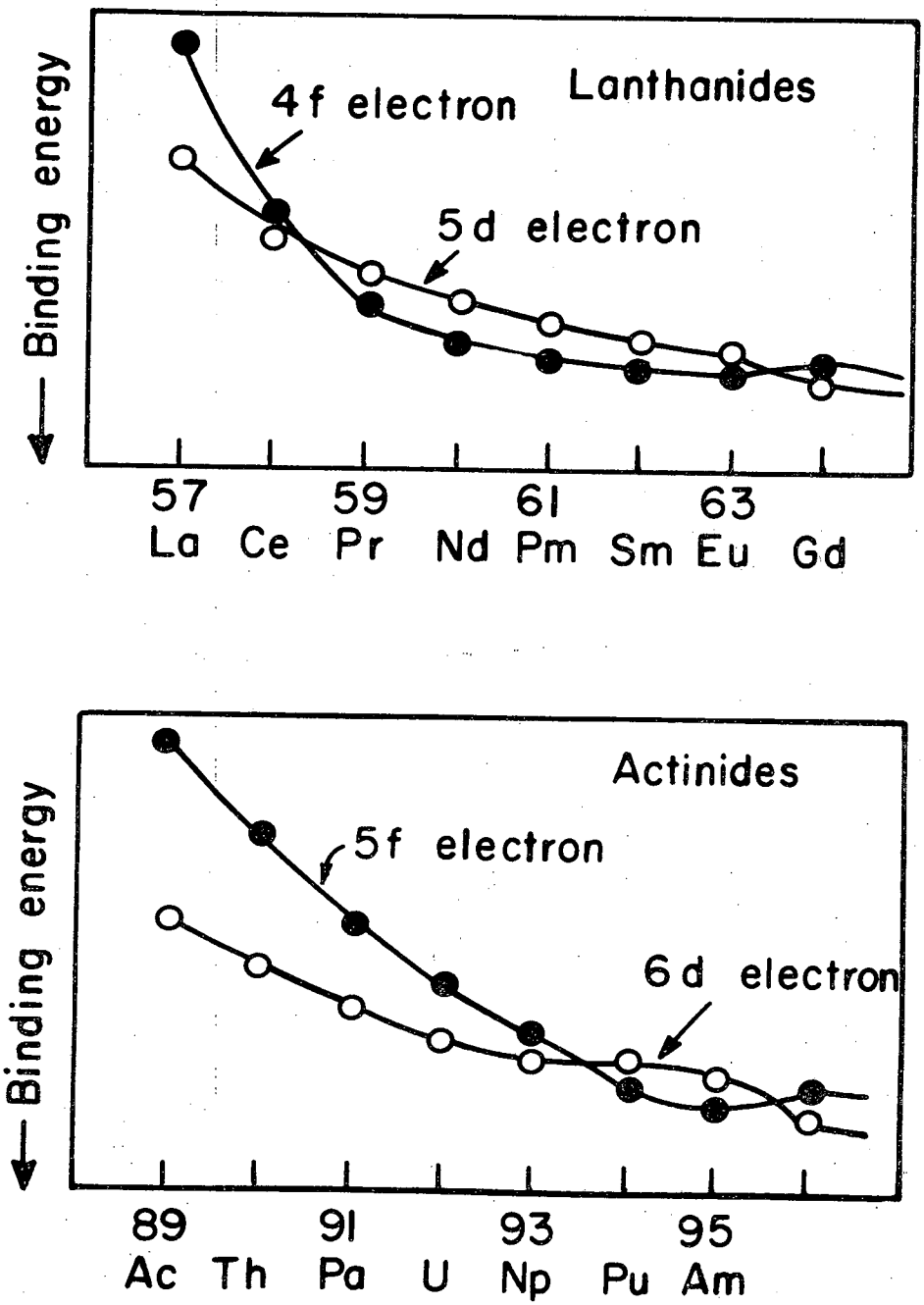

Figure 29. Qualitative comparison of the binding energies of the last competing electron in the lanthanides and actinides.

on single crystals[57] clearly show that there is a considerable departure from Russell-Saunders coupling, with a pronounced tendency towards jj coupling in the actinide region. The actual coupling will be intermediate between the two. In the rare earth region the susceptibility calculated from the Van Vleck formula[46] for a configuration of equivalent 4f electrons in Russell-Saunders coupling agrees very well with the experimental results. The spin orbit coupling which splits the LS terms into J levels also couples together states of the same J but different S and L, causing departure from Russell-Saunders coupling.[58] The spin orbit coupling parameters of the actinides are approximately two thirds as large as those of the corresponding lanthanides.[59] As a result, the energy level structure of the actinides exhibits a considerable departure from Russell-Saunders coupling. Consequently, due to mixing of the ground state with the states of the same J values because of the large spin orbit coupling constant, the g value in curium is expected to be smaller than in gadolinium. The value of g (1.93 ± 0.03) we[51,4] obtained for the curium ion in different curium compounds by susceptibility studies agrees within experimental error reasonably well with that obtained by Abraham et al.[57] ($g = 1.925\pm0.002$) by measuring the paramagnetic resonance spectrum of Cm^{+3} at low concentration in lanthanum ethyl sulfate and lanthanum trichloride crystals. Both these values are smaller than the g value for Gd^{+3} ion. Our g value is higher than that calculated by Wybourne[59] who assumed 5f hydrogenic ratios for the Slater integrals F_2, F_4, and F_6. The best fit to the solution spectra of Cm^{+3} in 1.0 M $HClO_4$ was obtained with $|X| = \xi/F_2 = 10.6$ and $F_2 = 280\ cm^{-1}$, where ξ is the spin orbit coupling constant. The agreement, however, was not very good. Conway[60] has calculated the eigenvalues, the eigenvectors, and the g values corresponding to different values of the parameter $|X|$. From the graph of g vs $|X|$ constructed from Conway's calculations, our g value would correspond to $|X|$ of 11. This $|X|$ value corresponds to an eigenvector of the ground state of curium ion of the form

$$0.879|^8S\rangle + 0.4321|^6P\rangle - 0.097|^6D\rangle + 0.24|^6F\rangle$$
$$+ 0.109|^4{}_3D_{20}\rangle + 0.110|^4{}_2D_{22}\rangle \quad .$$

(Only those components greater than 0.1 are listed. The lower subscripts are the seniority numbers and the Racah U quantum numbers. These are indicated only where there is more than one state with the same L and S.) From the results presented here about curium metal and our magnetic susceptibility results[51,4] for curium ion in several compounds, it is clear that curium has the same configuration as gadolinium. This would be supported by the comparison of the magnetic susceptibility of the various actinide ions with those of the lanthanide ions. This comparison is shown in Fig. 20.[3,4,61]

The qualitative similarity of the actinide curve to the lanthanide can be interpreted as evidence for $5f^n$ electronic configuration for the magnetic electrons in the actinide series. The fact that the experimental magnetic moments are generally lower than the theoretical values can be interpreted as resulting from a stark effect produced by electric fields of anions or water dipoles in case of solutions. This effect will be more pronounced in the case of 5f than in the 4f because of less electrostatic shielding by outer electrons in the case of 5f than with 4f electrons. Partial failure of the Russell-Saunders approximation could also account for some of the discrepancy.

Selwood[45] has contradicted the conclusion regarding the similarity of the actinide and lanthanide curves. He has pointed out that by selecting certain magnetic susceptibility data and excluding others it is possible to construct a curve for several elements of the first transition series with two maxima resembling that shown by the rare earths and the actinides (Fig.30). Since there are no f electrons present in the first transition series, this contradicts the validity of the analogy between actinide and lanthanide elements as derived from Fig. 30. The construction of this Selwood curve

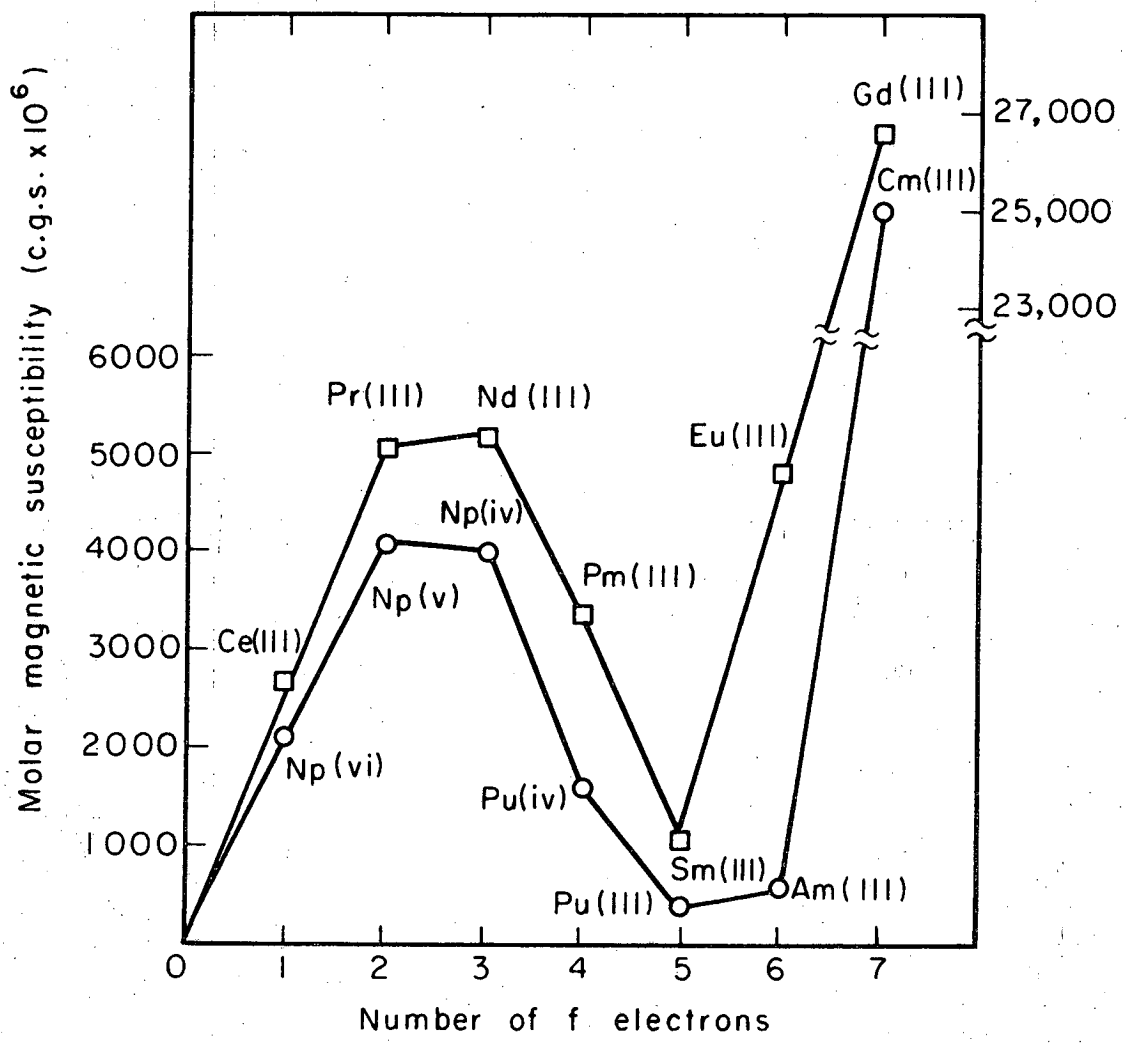

Figure 30. Molar magnetic susceptibility of some actinide and lanthanide ions.

is, however, extremely enlightening, for it shows that even by selecting certain anomalous cases and special conditions, presumably in order to make it resemble Fig. 30 as much as possible, the basic difference in the magnetic behavior of d and f electrons cannot be erased. For instance, the susceptibility of Fe(III) in dilute aqueous solution at pH 2 is $\approx 6600 \times 10^{-6}$ c.g.s. units. This value is close to the spin-only value for five unpaired electrons and shows beyond doubt the presence of unpaired 3d electrons in Fe(III). The susceptibility of Pu(IV) and Sm(III) on the other hand are quite small ($\approx 1000 \times 10^{-6}$ c.g.s. units) and can only be interpreted on the basis of five unpaired f electrons. Similarly, Crane, Wallmann, and Cunningham[62] and later McWhan[3] made susceptibility measurements of AmF_3 and found for the molar susceptibility 566×10^{-6} and 848×10^{-6} c.g.s. units at 295 and 77°K respectively. Here also once again the values obtained are much smaller than expected for the d electrons.

For ions with five or six unpaired electrons the multiplet intervals are not large compared to kT, and therefore in order to calculate their susceptibilities the general formula (which holds for multiplet intervals comparable to kT) should be used. In general, however, there are three cases to be considered:

a) Multiplet intervals large compared to kT.

$$\chi_M = \frac{N g^2 \beta^2 J(J+1)}{3kT} + N\alpha$$

where

g = Landé splitting factor,

β = Bohr magneton,

N = Avagadro's number,

k = Boltzmann constant,

T = absolute temperature,

and J is the vector sum of S and L (the resultant spin and orbital angular momentum of the atom respectively). $N\alpha$ is the high frequency term, or temperature-independent term due to the second-order Zeeman effect:

$$N\alpha = \frac{N\beta^2}{6(2J+1)}\left[\frac{F(J+1)}{h\nu\ (J+1;J)} - \frac{F(J)}{h\nu\ (J;J-1)}\right] ,$$

where

$$F(J) = \frac{1}{J}\,[(S+L+1)^2 - J^2][J^2 - (S-L)^2] \quad .$$

b) Multiplet intervals small compared to kT.

In this case the high frequency term is absent (neglecting the diamagnetic part). The susceptibility arises solely from the low frequency part. Therefore the susceptibility can be expressed by the formula

$$\chi_M = \frac{N\beta^2}{3kT}\,[4S(S+1) + L(L+1)] \quad .$$

c) Multiplet intervals comparable to kT.

This is the general case from which the previous two limiting cases can be easily derived. It involves the summation of the contribution of atoms with different values of J. The number N_J, that is the number of atoms in a mole with a given value of J, is determined by a Boltzmann temperature factor:

$$\chi_M = \frac{N \sum_{J=|L-S|}^{J=|L+S|} \left\{\left[g_J^2\,\beta^2\,J(J+1)/3kT\right] + \alpha_J\right\}(2J+1)\,e^{-W_J^0/kT}}{\sum_J (2J+1)\,e^{-W_J^0/kT}}$$

The functions g_J and α_J [with the same definition as in a)] are derived from the matrix elements $\langle J\ M|L_z+2S_z|J'M'\rangle$. The susceptibility calculations for the case of samarium and europium were done by Van Vleck and Frank,[63] using the general formula given in section c) above, and the discrepancy between theoretical and experimental values was resolved. In the case of Pu(III) and Am(III) McWhan[3] calculated the susceptibilities, using the same general formula as in section c) and taking into account the departure from Russell-Saunders coupling. He obtained values agreeing

rather well with the experimental results. From Van Vleck calculations, the susceptibility of samarium should pass through a temperature minimum in the neighborhood of 400°K; such a minimum has in fact been observed experimentally. Elliot and Lewis[64] made measurements on PuF_3 and $Pu_2(C_2O_4)_3 \cdot 9H_2O$ from 76-300°K. Dawson, Mandleberg, and Davies[65] extended measurements on PuF_3 and $PuCl_3$ up to about 600°K and found a minimum in the susceptibility-temperature curve at about 500-550°K. This is good qualitative evidence that Pu(III) has $5f^5$ electronic configuration.

Susceptibility measurements have been made on a large number of uranium(IV) compounds by many authors.[66-80] The results lie in the range of (3200 to 3800) $\times 10^{-6}$ c.g.s. units (at room temperature), which is closer to the $6d^2$ spin-only value of 3333 than to the limiting $5f^2$ value of 5390, although a number of these investigators have interpreted their experimental results in terms of $5f^2$ configuration. However, paramagnetic exchange interaction (Δ) may be the reason for the low values. This is supported by the results of Hutchinson and Elliot[66] where the Weiss constant for uranium sulfate, oxalate, and acetyl acetonate is found to be 113, 168, and 101°K respectively. The measurements of Handler and Hutchinson[81] on UCl_3 diluted with isomorphous diamagnetic matrix $LaCl_3$ also support this conclusion. It was found that the values for UCl_3 at infinite dilution are very similar to those of $Nd(C_2H_5SO_4)_3 \cdot 9H_2O$. Dawson[82] also made measurements on PuF_4 and PuO_2 diluted with the isostructural diamagnetic compounds ThF_4 and ThO_2 respectively. The magnetic susceptibilities were found to increase with dilution, and the extrapolated value at infinite dilution for room temperature (3020×10^{-6} c.g.s. units) corresponds essentially to the value predicted (3010×10^{-6} c.g.s. units) for the $5f^4$ configuration.

Several measurements and theoretical analyses[83-88] have been made on compounds containing NpO_2^{++} and NpO_2^{+} ions. The results confirm the presence of f^1 and f^2 configuration respectively. From the results presented above, and the survey of the magnetic measurements made on the

actinides, the indicated number of 5f electrons are present in the following ions: $Cm^{+3}(5f^7)$; $Am^{+3}(5f^6)$; $Pu^{+3}(5f^5)$; $Pu^{+4}(5f^4)$; NpO_2^+, $PuO_2^{++}(5f^2)$; $NpO_2^{++}(5f^1)$; $UO_2^{++}(5f^0)$; $U^{+3}(5f^3)$ and $U^{+4}(5f^2)$. In the case of Th^{+3} (one unpaired electron) and Th^{+2} (two unpaired electrons) the evidence strongly favors a 6d assignment.[55]

The magnetic data obtained by Cunningham[13] on Bk^{+3} and Cf^{+3} ions indicate that their electronic configurations are $5f^8$ and $5f^9$ respectively.

It is worthy of note that Cunningham[13] reported μ_{eff} of 8.7 and 9.2 Bohr magnetons for Bk^{+3} and Cf^{+3} ions respectively. The ground state of Bk^{+3} and Cf^{+3} are $^7F_6$ and $^6H_{15/2}$ respectively. These effective moments correspond to g values of 1.34 and 1.15 for Bk^{+3} and Cf^{+3} respectively. Recently Fields and Wybourne[89] reported the g values of 1.445 and 1.285 for Bk^{+3} and Cf^{+3} respectively. The discrepancy is quite big. However, there is still some question about the purity of Bk and Cf used by Cunningham for his measurements with respect to rare earth background contamination. Therefore before coming to final conclusions regarding the coupling scheme in the case of Bk and Cf, these measurements need to be repeated with high purity Bk and Cf.

These results are consistent with many of the conclusions reached about the physical and chemical properties of the actinides and also with the chemical evidence in indicating that although the 6d and 5f levels are of nearly equivalent energy in the first few elements of the series, the f electron levels definitely lie lower once these elements are passed and the rare-earth-like properties predominate.

C. Magnetic Susceptibility of Protactinium Metal

The magnetic susceptibility of several samples of protactinium metal has been investigated within the temperature range 298-20°K. The results are tabulated in Table XI.

Sample no. 1 was obtained by the reduction of a PaF_4 chunk, which in turn was obtained from the 10 mg batch of oxide.

Sample no. 2 was obtained by the reduction of powdered tetrafluoride, using a small thoria crucible. This sample showed field dependence, which is attritubed to contamination with some ferromagnetic impurities due to handling of the metal piece. Therefore the measured susceptibility was corrected for ferromagnetic impurities by plotting the measured susceptibility vs 1/i and extrapolating to 1/i = 0 to get the corrected value as shown in Figs. 31 and 32. Table XII gives the susceptibility of sample no. 2 at various fields together with the corrected susceptibility.

Another attempt was made to measure the susceptibility of a Pa metal sample (1.57 mg) obtained by the reduction of a PaF_4 pellet. This sample unfortunately showed a tremendous amount of ferromagnetic impurity and hence its results were rejected.

Both sample no. 1 and no. 2 showed the magnetic susceptibility of Pa metal to be virtually temperature-independent, within an experimental uncertainty of about 5%, over the temperature region investigated (298-20°K).

The magnetic behavior of protactinium metal thus appears to be similar to that of tantalum, which also exhibits temperature-independent magnetism. The susceptibility of protactinium metal arises then almost entirely from the temperature-independent alpha terms of the Van Vleck equation.[46]

A brief description of the quantum mechanical origin of Van Vleck temperature-independent paramagnetism is given as follows:

Table XI. Magnetic susceptibility of Pa metal at room temperature.

Sample number	Weight of sample (μg)	$\chi_g \times 10^6$	$\chi_M \times 10^6$
1	245.91	1.172 ± 0.06	270.7
2	100.7	1.150 ± 0.08	265.6
		Average χ_M = 268.2 ± 14	

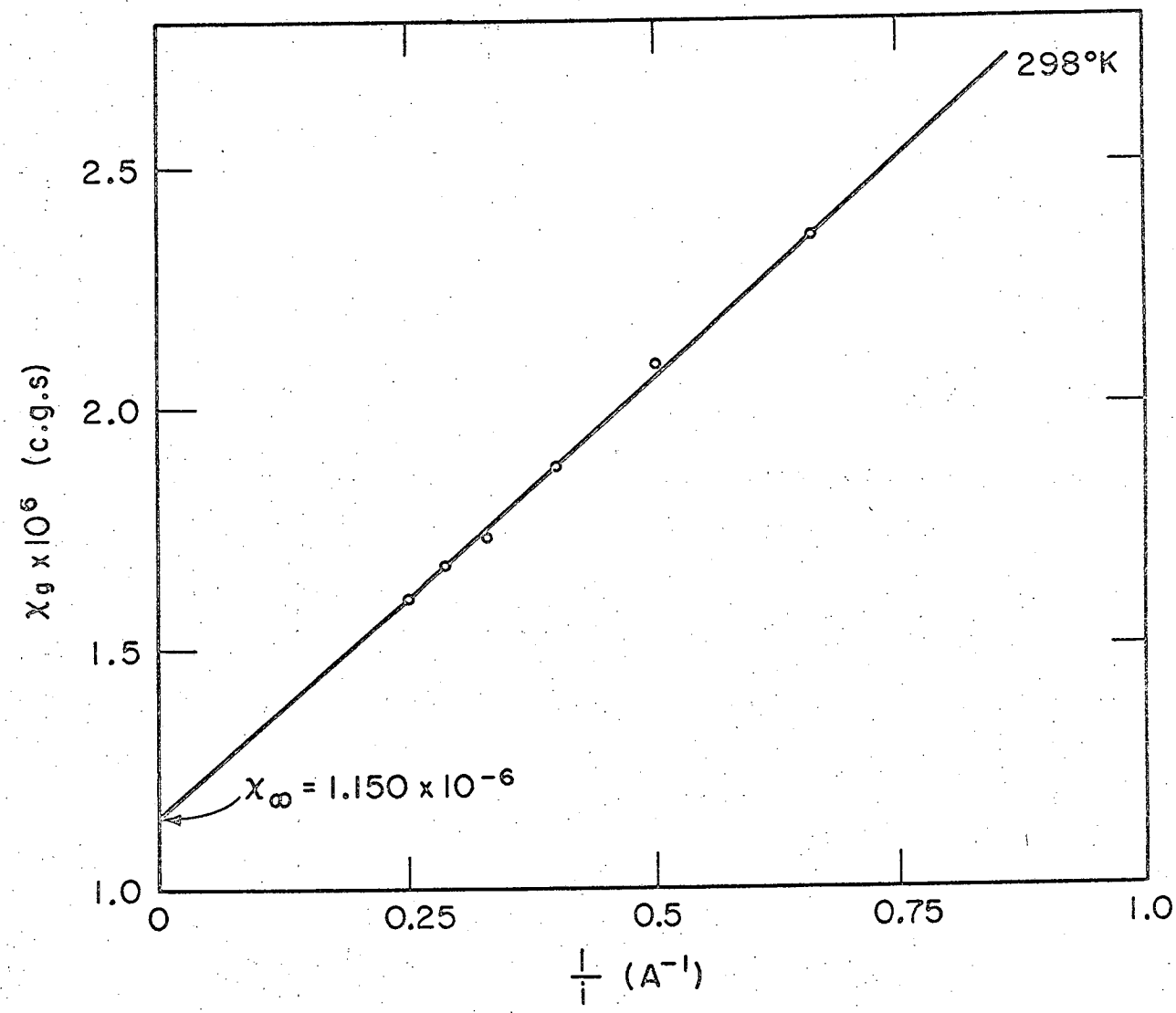

Figure 31. Correction for ferromagnetic impurities at room temperature (sample no. 2).

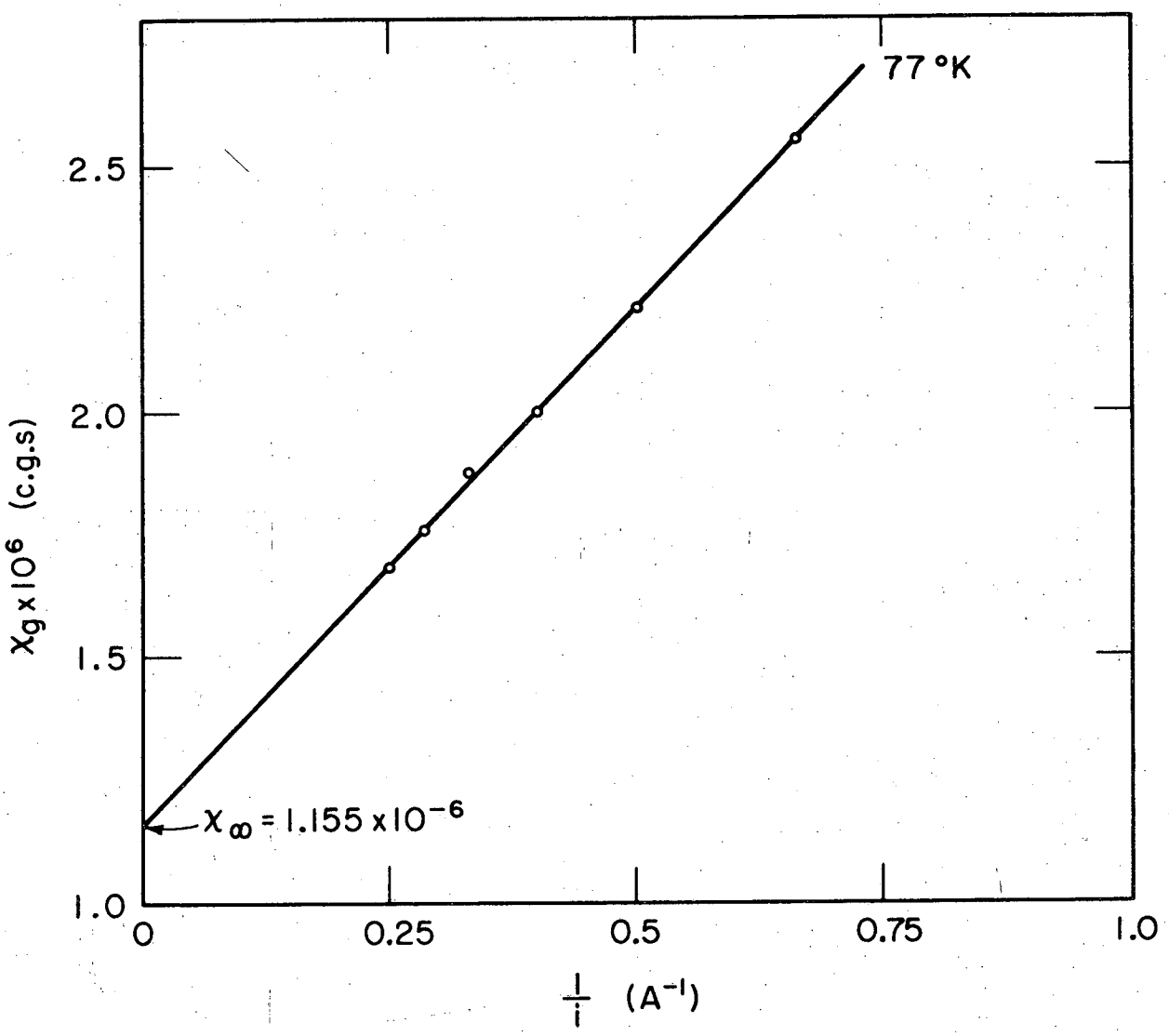

Figure 32. Correction for ferromagnetic impurities at 77°K (sample no. 2).

Table XII. Magnetic susceptibility of Pa metal (sample no. 2).

T(°K)	$\chi_g \times 10^6$						
	1.5 A	2.0 A	2.5 A	3.0 A	3.5 A	4.0 A	χ_∞
298	2.350	2.085	1.871	1.710	1.670	1.602	1.150
77	2.548	2.211	1.999	1.872	1.755	1.680	1.155

We consider a molecular system which has no magnetic moment in the ground state, by which we mean that the diagonal matrix element of the magnetic moment operator μ_z is zero.

Suppose that there is a non-diagonal matrix element $(m|\mu_z|n)$ of the magnetic moment operator, connecting the ground state n with the excited state m of energy $\Delta = E_m - E_n$ above the ground state. Then by standard perturbation theory we see that the wave function of the ground state in a small field ($\mu_z H \ll \Delta$) becomes

$$\psi_n' = \psi_n + \frac{H(m|\mu_z|n)}{\Delta} \psi_m \quad ,$$

and the wave function of the excited state

$$\psi_m' = \psi_m - \frac{H(m|\mu_z|n)}{\Delta} \psi_n \quad .$$

The ground state now has a moment

$$(n'|\mu_z|n') = \frac{2H|(m|\mu_z|n)|^2}{\Delta} \quad ,$$

and the upper state has a moment

$$-\frac{2H|(m|\mu_z|n)|^2}{\Delta} \quad .$$

The two interesting cases to consider are:

Case a): $\Delta \ll kT$ (low frequency matrix elements).

The surplus population in the ground state is approximately equal to $N\Delta/2kT$, where N is the total number of atoms. (For derivation of this equation one can refer to any solid state physics book[90,91].) So the resultant magnetization is

$$M = \frac{2H|(m|\mu_z|n)|^2}{\Delta} \frac{N\Delta}{2kT} \quad ,$$

which gives for the susceptibility

$$\chi = \frac{N\Sigma|(m|\mu_z|n)|^2}{kT} .$$

This contribution is of the usual Curie form, although the mechanism of magnetization here is through polarization of the states of the system, whereas with free spins the mechanism of magnetization is the redistribution of ions among the spin states.

Note that the splitting Δ does not enter in the final equation for χ, on the assumption $\Delta \ll kT$.

Case b): $\Delta \gg kT$ (high frequency matrix elements).

Now the population is nearly all in the ground state, so that

$$M = \frac{2NH_z|(m|\mu_z|n)|^2}{\Delta} ,$$

and the susceptibility is, summed over all suitable states m,

$$\chi = 2N \sum_m \frac{|(m|\mu_z|n)|^2}{E_m - E_n} ,$$

independent of temperature. This type of contribution is known as Van Vleck paramagnetism.

The molar susceptibility of protactinium metal so measured gives an effective moment of about 0.8 Bohr magneton. This piece of evidence indicates that presumably less than one electron per protactinium atom is used in bonding.

Finally as mentioned earlier, Fowler et al.[8] have observed superconductivity in protactinium metal below 1.4°K, and thus filled the last vacant spot in the center of the periodic system, the region in which every element becomes either superconducting, ferromagnetic, or antiferromagnetic. They have further shown the position of Pa in relation to its surrounding elements with their superconducting transition temperatures (as shown in the following table):

Hf	0.1	Ta	4.4	W	0.011
Th	1.4	Pa	1.4	U	0.7 (o), 1.8 (c)*

*The two polymorphic modifications of uranium are orthorhombic and cubic. They have different transition temperatures. See B. S. Chandrasekhar and J. K. Hulm, J. Phys. Chem. Solids 7, 259 (1958).

Any lines of induction present in a metal in the normal state are expelled in the superconducting state; this important experimental result is known as the Meissner effect.[92] Since inside the specimen B = 0, the susceptibility of a superconductor is given by

$$\chi = -1/4\pi$$

This equation is derived very easily as follows.

If a substance is placed in a magnetic field of strength H, then the magnetic induction is given by B, where

$$B = H + 4\pi M.$$

The quantity M is the intensity of magnetization, and $M/H = \kappa$ is the magnetic susceptibility per unit volume. The magnetic susceptibility per unit mass $(\chi) = \kappa/\rho$, where ρ is density.

Therefore

$$B/H = 1 + 4\pi M/H = 1 + 4\pi\chi;$$

since B = 0,

$$\chi = -1/4\pi .$$

This is the maximum negative value of gram susceptibility possible; consequently, a superconducting metal is said to exhibit diamagnetism.

With this in view we thought that if Pa metal could be made to become superconducting then we might be able to see the increase in diamagnetic susceptibility; consequently, we tried to measure sample no. 2 near liquid helium temperature. However, we failed to see any such effect because of a) ferromagnetic contamination of sample no. 2, b) our limitations in trying to get down to such low temperatures, and c) our inability to go to low enough H. The lowest temperature we are able to attain at present ($\approx 6^{\circ}K$) is very high compared to the transition temperature of Pa ($1.4^{\circ}K$).

D. Magnetic Susceptibility of Protactinium Tetrafluoride

The PaF_4 obtained from a 50 mg batch of Pa gave an extremely complex x-ray powder pattern, which was not similar to that of ThF_4. It seems probable that such a comparison shows our product to be non-isostructural with ThF_4, and hence not a single phase of PaF_4.

It is worth mentioning that the Pa-fluorine system, like the U-fluorine system, is very complex. Three possibilities are very likely:

a) Formation of an oxyfluoride, Pa_2OF_8, which is reported by Stein[36] to be isomorphous with U_2F_8 (body-centered cubic structure).

b) Formation of an intermediate protactinium fluoride compound such as Pa_2F_9 or Pa_4F_{17}. The corresponding uranium fluorides are known and reported by Agron et al.[93] to be U_2F_9 (body-centered cubic structure) and U_4F_{17} [x-ray data listed under the heading SAM No. 448 (from a Debye-Scherrer picture of the sample "run Vc", see reports M-2205 and DIF-M-78)].

c) Mixture of PaF_4, which is isomorphous with UF_4 (monoclinic crystal structure), and one or more of the above mentioned phases.

It seems probable to assume that if compounds such as Pa_2F_9 and Pa_4F_{17} exist, though not yet known to the best of our knowledge, they

will be isostructural with the corresponding uranium fluorides. The isomorphism will not be surprising in view of the nearness in size of protactinium and uranium.

The product that we ended up with while preparing PaF_4 was of dark brown color. Although Pa_2OF_8 has been reported by Stein[36] to be white, one cannot exclude the possibility of this phase in our product simply on the basis of color. Asprey[94] from Los Alamos Scientific Laboratory has obtained a dark brown product many times, while preparing PaF_4, which gives a beautiful x-ray pattern of Pa_2OF_8. He thinks that the presence of oxyfluoride can be attributed to oxygen impurity in tank-grade hydrogen, producing the reaction

$$2\ PaF_4(s) + 1/2\ O_2(g) \xrightarrow[600^oC]{HF} Pa_2OF_8(s)$$

With this in mind we treated our dark brown product in a quartz capillary at 550-575°C with pure hydrogen for about 1 - $1\frac{1}{2}$ hr. The pure hydrogen was obtained by the thermal decomposition of uranium hydride, UH_3. The product after reduction with pure hydrogen gives a completely different x-ray powder pattern. The film, as expected, is extremely complex. Although we can match all the 12 lines of PaF_4 which were reported by Stein,[36] we have many strong and moderate lines left unaccounted for.

At present it seems that we do not have an authentic well-established single phase of PaF_4. Unless we are completely sure of our PaF_4, there is not much point in making any susceptibility measurements. However, at this state of the game suffice to say that one can calculate the expected value of χ_M for PaF_4 from the Landé g value and the J quantum number of the ground state of Pa. This is accomplished as follows.

Axe[95] performed some paramagnetic resonance experiments on the $PaCl_4$ - Cs_2ZrCl_6 crystals and reported a Landé g value of 1.141±0.003 for Pa(IV). The Pa(IV) has an electronic configuration of 5f which corresponds to a ground state of $^2F_{5/2}$. It is worth indicating that in atomic spectroscopy the stages of ionization are labeled by indicating the neutral

(or un-ionized) atom, which gives rise to the first spectrum, by the Roman numeral I and by increasing numerals for the successive stages of ionization, whereas we chemists usually assign roman numerals according to the valence of the element rather than to the order of the spectrum. Thus we indicate tetravalent Pa by Pa(IV), whereas in describing the spectra of tetravalent protactinium spectroscopists write Pa(V).

Knowing the g value and the J quantum number for the ground state, we can calculate the effective magnetic moment (μ_{eff}) from the following well-known relation:

$$\mu_{eff} = g\sqrt{J(J+1)} = 1.141\sqrt{5/2.7/2}$$

$$= 1.141 \times 2.958 = 3.375 \text{ B.M.}$$

Now, using the following relation one can calculate χ_M:

$$\mu_{eff} = 2.84\sqrt{\chi_M^{corr}.T}$$

$$3.375 = 2.84\sqrt{\chi_M^{corr}.T}$$

$$\left(\frac{3.375}{2.84}\right)^2 = \chi_M^{corr}.T \quad .$$

At room temperature ($T = 298^{\circ}K$),

$$\chi_M^{corr} = \frac{1.411}{298} = \frac{1.411}{2.98} \times 10^{-2} = \frac{14.11}{2.98} \times 10^{-3} = 4.735 \times 10^{-3} \quad ,$$

or $\chi_M^{corr} = 4735 \times 10^{-6}$ c.g.s. units,

$$\therefore \chi_g^{corr} = \frac{4735 \times 10^{-6}}{307} \text{ c.g.s. units}$$

$$= 15.42 \times 10^{-6} \text{ c.g.s. units.}$$

These molar and gram susceptibility values are the calculated ones only. It remains open to confirm them experimentally. Further work on this is in progress and will be reported elsewhere when completed.

ACKNOWLEDGMENTS

It is with great pleasure that I express my sincere thanks to Professor Burris B. Cunningham. Our discussions and his many suggestions were often instrumental in the solution of the problems at hand, while his personal interest and infectious enthusiasm were constantly encouraging. His thoughtful guidance made my work here an educational experience unequalled in my career.

I would like also to take this opportunity to express my thanks to the late Dr. James C. Wallmann. It was largely through Jim that I was introduced to the fascinating micro-techniques in general, and metal production on micro-scale in particular, involved in this study. I will always consider the time spent under his tutelage to be of primary importance to my professional development.

Special thanks must go to Dr. Sayed A. Marei for his careful assistance during many phases of the work, to Dr. Hermann Haug for his help in calorimetric measurements, to Mr. Tom Parsons for his help in designing and building the low temperature apparatus, to Mr. George Shalimoff and Mr. Ralph D. McLaughlin for making the numerous spectrographic analyses, to Dr. Jere Green and Mr. Ray Dod for their assistance and for our useful discussions, to Mr. Bert Watkins and Mr. Hap Hagopian for their expert engineering advice, and to Mr. Harry Powell for making some of the susceptibility tubes and glass apparatus used in this work.

I am indebted to several of my colleagues for their great help in typing the first draft of many sections of this thesis. It is only owing to the generosity of my colleagues that this thesis was ever typed.

The laboratory assistance of Miss Lilly Goda and Mrs. Lillian White is greatly appreciated, as are the efforts of the Health Chemistry Division in general, and Mrs. Gertrude Bolz in particular.

I would also like to record my indebtedness to the Government of India, Atomic Energy Establishment, Trombay, for granting me leave facilities to complete my Ph.D. studies here.

My greatest debt, however, is to my wife, whose moral support kept my spirits high and whose understanding and patience made my work possible.

This work was performed under the auspices of the United States Atomic Energy Commission.

REFERENCES

1. G. T. Seaborg and A. R. Fritsch, Sci. Am. 208, 68 (1960).
2. D. B. McWhan, B. B. Cunningham, and J. C. Wallmann, J. Inorg. Nucl. Chem. 24, 1025 (1962).
3. D. B. McWhan, Ph.D. Thesis, University of California, Berkeley, Lawrence Radiation Laboratory Report UCRL-9695 (1961).
4. Sayed A. Marei, Ph.D. Thesis, University of California, Berkeley, Lawrence Radiation Laboratory Report UCRL-11984 (1965).
5. P. A. Sellers, S. M. Fried, R. E. Elson, and W. H. Zachariasen, J. Am. Chem. Soc. 76, 5935 (1954).
6. W. H. Zachariasen, Acta. Cryst. 5, 19 (1952).
7. B. B. Cunningham, "Some Properties of Protactinium Metal," paper presented at the conference on Physico-Chemistry of Protactinium, France, 1965.
8. R. D. Fowler, B. T. Matthias, L. B. Asprey, H. H. Hill, J. D. G. Lindsay, C. E. Olsen, and R. W. White, Phys. Rev. Letters 15, 860 (1965).
9. J. C. Wallmann, J. Fuger, Hermann Haug, Sayed A. Marei, and Brij M. Bansal, to be published in J. Inorg. Nucl. Chem.
10. John L. Burnett, Ph.D. Thesis, University of California, Berkeley, Lawrence Radiation Laboratory Report UCRL-11850 (1964).
11. S. R. Gunn, Ph.D. Thesis, University of California, Berkeley, Lawrence Radiation Laboratory Report UCRL-2541 (1954).
12. C. H. Shomate and E. H. Huffman, J. Am. Chem. Soc. 65, 1625 (1943).
13. B. B. Cunningham, J. Chem. Ed. 36, 31 (1959).
14. P. Cosse, J. Inorg. Nucl. Chem. 14, 127 (1960).
15. L. Jackson, Phil. Trans. Roy. Soc. London, A224, 1 (1924).
16. G. Foex, Tables de constantes et donnees numeriques-7: Constantes Selectionnees, diamagnetisme et paramagnetisme (Masson et Cie., Paris, 1957).
17. L. J. Schoem and H. P. Broida, Rev. Sci. Instr. 33, 470 (1962).
18. J. R. Clement and E. H. Quinnell, Rev. Sci. Instr. 23, 213 (1962).

19. F. Trombe, Rev. Met. 52, 2 (1956).
20. S. Fried, E. F. Westrum, Jr., H. L. Baumback, and P. L. Kirk, J. Inorg. Nucl. Chem. 5, 182 (1958).
21. J. C. Wallmann, W. T. Crane, and B. B. Cunningham, J. Am. Chem. Soc. 73, 493 (1951).
22. S. Fried and N. R. Davidson, J. Am. Chem. Soc. 70, 3539 (1948).
23. J. C. Wallmann and B. B. Cunningham, University of California, Lawrence Radiation Laboratory Report UCRL-8369 (1958).
24. B. B. Cunningham and J. C. Wallmann, J. Inorg. Nucl. Chem. 26, 271 (1964).
25. Harris Lowenhaupt and B. B. Cunningham, Lawrence Radiation Laboratory (private communication, 1964).
26. A. C. Demildt, Anal. Chem. 35, 1228 (1963).
27. V. A. Ryan, J. L. Green, and E. H. Lowenhaupt, University of California, Lawrence Radiation Laboratory Report UCRL-11618 (1964).
28. S. G. Thompson and M. L. Muga, Proceedings of the Second International Conference on the Peaceful Uses of Atomic Energy, Geneva, 1958 (United Nations, Geneva, 1959), P/825.
29. G. H. Higgins, University of California, Lawrence Radiation Laboratory, Livermore Report UCRL-6134 (1960).
30. R. C. Petterson, Lawrence Radiation Laboratory Report UCRL-11074 (1963).
31. J. L. Green, Ph.D. Thesis, University of California, Berkeley, Lawrence Radiation Laboratory Report UCRL-16516 (1965).
32. J. K. Dawson and R. M. Elliot, AERE Report, C/R-1207 (1953).
33. Melvin H. Mueller and LeRoy Heaton, Argonne National Laboratory Report ANL-6176 (1961).
34. D. K. Smith, Lawrence Radiation Laboratory Report UCRL-7196 (1963).
35. A. V. Grosse and M. Agruss, J. Am. Chem. Soc. 56, 2200 (1934).
36. L. Stein, Inorg. Chem. 3, 995 (1964).
37. W. H. Zachariasen, Acta. Cryst. 12, 698 (1959).
38. D. F. Peppard, G. W. Mason, W. J. Driscoll, and S. McCarty, J. Inorg. Nucl. Chem. 12, 141 (1959).

39. A. Chetham-Strode, Jr., and O. L. Keller, Jr., "Ion Exchange of Protactinium(V) in HF Solutions and Some Applications," paper presented at Colloques Internationaux du Centre National de la Recherche Scientifique, Paris, France (1965).

40. D. Metta, H. Diamond, R. F. Barnes, J. Milsted, J. Gray, Jr., D. J. Henderson, and C. M. Stevens, J. Inorg. Nucl. Chem. 27, 33 (1965).

41. "Table of Specific Activities of Selected Isotopes," NCS-973-57, August 1957; Rev. November 1962 (RJB).

42. E. F. Westrum, Jr., and H. P. Robinson, Radiochemical Studies: The Transuranium Elements (Edited by G. T. Seaborg, J. J. Katz and W. M. Manning) Plutonium Project Record NNES, Div. IV, Vol. 14-B, p. 922, (McGraw-Hill Book Co., Inc., New York, 1949).

43. J. Fuger and B. B. Cunningham, J. Inorg. Nucl. Chem. 25, 1423 (1963).

44. H. R. Lohr and B. B. Cunningham, J. Am. Chem. Soc. 73, 2025 (1951).

45. Pierce W. Selwood, Magneto Chemistry (Interscience Publishers, Inc., New York, 1956).

46. J. H. Van Vleck, The Theory of Electric and Magnetic Susceptibilities, (Oxford University Press, Amer. House, London, 1932).

47. S. Arajs and R. V. Colvin, "Paramagnetism of Polycrystalline Rare Earth Metals," Rare Earth Research, Ed. by Eugene V. Kleber, (The Macmillan Co., New York, 1961).

48. K. A. Gschneidner, Jr., and B. T. Matthias, "Electrical and Magnetic Properties of the Rare Earth Metals and Their Alloys and Compounds," Rare Earth Research, Ed. by Eugene V. Kleber, (The Macmillan Co., New York, 1961).

49. P. G. deGennes, Compt. rend. 247, 1836 (1958).

50. G. H. Dieke, and L. Heroux, Phys. Rev. 103, 1227 (1956).

51. B. B. Cunningham, Sayed A. Marei, and Brij M. Bansal, to be published in J. Inorg. Nucl. Chem.

52. Hugo Leipfinger, "Magnetic Properties of Rare Earth Metals at Very Low Temperatures," Technical Report, AFOSR-TN-57-561 (1957).

53. J. C. Kriessman and H. B. Callen, Phys. Rev. 94, 837 (1954).
54. K. A. G. Schneidner, "Critical Review of the Alloy Systems of Rare Earth, Scandium, and Yttrium Metals," Preprint of AEC-LA Report.
55. J. J. Katz and G. T. Seaborg, The Chemistry of the Actinide Elements, (Methuen and Co., London, 1957).
56. A. Y. Cabezas, Ph.D. Thesis, University of California, Berkeley, Lawrence Radiation Laboratory Report UCRL-9346 (1960).
57. M. Abraham, B. R. Judd, and H. H. Wickman, Phys. Rev. 130, 611 (1963).
58. B. R. Judd and I. P. K. Lindgren, Phys. Rev. 122, 1802 (1961).
59. W. T. Carnall and B. G. Wybourne, J. Chem. Phys. 40, 3428 (1964).
60. J. G. Conway, Lawrence Radiation Laboratory, (private communication).
61. J. J. Howlander, Jr., and M. Calvin, J. Chem. Phys. 18, 239 (1950).
62. W. W. Crane, J. C. Wallmann, and B. B. Cunningham, University of California, Lawrence Radiation Laboratory Report UCRL-846 (1950).
63. J. H. Van Vleck and A. Frank, Phys. Rev. 34, 1494 (1929).
64. N. Elliot and W. B. Lewis, Report, AECD-29100 (1950).
65. J. K. Dawson, C. J. Mandleberg, and D. Davies, J. Chem. Soc. 2047 (1951).
66. C. A. Hutchinson, Jr., and N. Elliot, J. Chem. Phys. 16, 920 (1948); Phys. Rev. 73, 1229 (1948).
67. J. K. Dawson and M. W. Lester, J. Chem. Soc. 2181 (1950).
68. W. Trzebiatowski and P. W. Selwood, J. Am. Chem. Soc. 72, 4504 (1950).
69. J. K. Dawson, J. Chem. Soc. 2889 (1951).
70. N. Elliot, Phys. Rev. 76, 431 (1949).
71. J. K. Dawson, J. Chem. Soc. 429 (1951).
72. L. Sacconi, Atti accad. naz. Lincei, 6, 639 (1949).
73. H. Haraldsen and R. Bakken, Naturwissen-schaften 28, 127 (1940).
74. H. Bommer, Z. anorg. Chem. 247, 249 (1941).
75. N. Elliot, L. Corliss and Y. Delabarre, Brookhaven National Laboratory Report BNL-39 (AS-3) p. 47, December 1949.
76. R. Stoenner and N. Elliot, J. Chem. Phys. 19, 950 (1951).

77. N. Elliot and W. B. Lewis, U. S. Atomic Energy Commission Document, AECD-2910 (1950).

78. E. Slowinski and N. Elliot, Brookhaven National Laboratory Report BNL-1199.

79. J. K. Dawson and M. W. Lister, J. Chem. Soc. 5041 (1952).

80. C. A. Hutchinson, Jr., and C. M. Herzfeld, J. Chem. Phys. 23, 1650 (1955).

81. P. Handler and C. A. Hutchinson, Jr., J. Chem. Phys. 25, 1210 (1956).

82. J. K. Dawson, J. Chem. Soc. 1882 (1952).

83. D. M. Gruen, Argonne National Laboratory Report ANL-4469 (1950).

84. D. M. Gruen and C. A. Hutchinson, Jr., J. Chem. Phys. 22, 386 (1954).

85. R. J. Elliot, Phys. Rev. 89, 659 (1953).

86. J. C. Eisenstein and M. H. L. Pryce, Proc. Roy. Soc. (London) A229, 20 (1955); A238, 31 (1956).

87. J. K. Dawson, Nucleonics 10, 39 (1952).

88. J. K. Dawson and G. R. Hall, Proceedings of International Conference on the Peaceful Uses of Atomic Energy, Geneva, 1955 (United Nations, Geneva, 1956), P/440, p. 231.

89. P. R. Fields, B. G. Wybourne, Argonne National Laboratory Report ANL-6911 (1964).

90. Charles Kittel, Introduction to Solid State Physics, (John Wiley and Sons, Inc., New York, 1963).

91. Allan H. Morrish, The Physical Principles of Magnetism, (John Wiley and Sons, Inc., New York, 1965).

92. W. Meissner, and R. Ochsenfeld, Naturwiss. 21, 787 (1933).

93. P. Agron, A. Grenall, R. Kunin, and S. Weller, "The Intermediate Uranium Fluoride Compounds," Paper 62, Chemistry of Uranium, (Collected papers, and Ed. by J. J. Katz, and E. Rabinowitch, TID-5290, Book 2, 1958).

94. L. B. Asprey, Los Alamos Scientific Laboratory, (private communication, 1966).

95. John D. Axe, Ph.D. Thesis, University of California, Lawrence Radiation Laboratory Report UCRL-9293 (1960).